Thesis Title

Mathematical Study on Biodiesel Production Considering Ultrasound Effect and Special Emphasis on Ecological Issues

Submitted by
Sk Mosaraf Ahammed
Registration No.: SMATH1405722

in
fulfilment of the requirements
for the degree of *Doctor of Philosophy in Science*

Department of Mathematics
Jadavpur University
Jadavpur, Kolkata - 700032
West Bengal, India

September, 2025

যাদবপুর বিশ্ববিদ্যালয়

FACULTY OF SCIENCE
DEPARTMENT OF MATHEMATICS

JADAVPUR UNIVERSITY
Kolkata - 700 032, India
Telephone : 91 (33) 2457 2269

CERTIFICATE FROM THE SUPERVISOR

This is to certify that the thesis entitled "**Mathematical Study on Biodiesel Production Considering Ultrasound Effect and Special Emphasis on Ecological Issues**" Submitted by Sri / Smt. **Sk Mosaraf Ahammed** who got his name registered on **21.02.2022** For the award of **Ph. D. (Science)** degree of **Jadavpur University**, is absolutely based upon his / her own work under my supervision and that neither this thesis nor any part of it has been submitted for either any degree/diploma or any other academic award anywhere before.

Priti Kumar Roy
02/09/2025

(Signature of the Supervisor with date and official seal)

Prof. (Dr.) Priti Kumar Roy
Professor
Department of Mathematics
Jadavpur University
Kolkata-700 032, West Bengal

This thesis is dedicated to my parents,

Mr. Sk Alenur and Mrs. Tanjira Begam,

who, despite not even passing the eighth grade,

have made me worthy of this achievement.

Acknowledgements

I am deeply grateful to the many individuals whose guidance, advice, support, and encouragement made this journey possible. It is both an honor and a pleasure to extend my heartfelt thanks to all who contributed in various ways to the success of this work.

Firstly, I want to express my heartfelt gratitude to my supervisor, **Prof. Priti Kumar Roy**, for his outstanding guidance during my research. His energy and enthusiasm in research, his inspiring and creative support, and fruitful discussions have motivated me. In addition, he is always available and eager to help in research. As a result, research life has become smooth and successful. I have been highly inspired by his tremendous academic feats, which make him a role model to follow in my scholarly days.

I convey my special thanks of gratitude to Prof. Siddhartha Datta, Department of Chemical Engineering, Jadavpur University, Kolkata, Prof. Nandadulal Bairagi, Department of Mathematics, Jadavpur University, for their immense and valuable advice on the improvement of my research work and Prof. Lakshmi Narayan Guin, Department of Mathematics, Visva Bharati, Santiniketan, for his endless motivation towards my Ph.D. Words are not enough to express my gratitude for their endless co-operation.

I express my gratefulness to Prof. Xianbing Cao, School of Mathematics and Statistics, Beijing Technology and Business University, China, Prof. Oluwole D. Makinde, Faculty of Military Science, Stellenbosch University, South Africa, Prof. Shu Wang, School of Mathematics, Statistics and Mechanics, Beijing University of Technology, China, Dr. Jahangir Chowdhury, Department of Applied Science, RCC Institute of Information Technology, India, for their immense and valuable advice on the improvement of my research work.

It has been a great privilege to spend several years in the Department of Mathematics at Jadavpur University. I would like to express my heartiest gratitude to all of my former and present Departmental Heads, each and every respected teacher, and official staff in my department for making those times like a joyful ride.

My heartfelt thanks to my fellow lab-mates- Salil Da, Amit Roy Da, Subhankar, Sanju, Tushar, Tarun Da, Amit Bag Da, Satyajit, and Homagnic for the stimulating discussions and for all the fun we have had in the last four years. These are really

memorable to me. My acknowledgement will never be completed without the special mention of my lab seniors: Dr. Salil Ghosh, Dr. Amit Kumar Roy, who have taught me the lab culture and the disciplines and dedication required in research. I extend my sincere thanks to Tushar Ghosh for his support in a specific aspect of my research work.

I would also like to thank Dr. Mainul Hossain, who helped me perform several mathematical experiments required in my research work. I am grateful to him for answering all of my research queries, his endless efforts, patience, and for his precious time shared with me during my Ph.d work. Furthermore, I thank Dr. Fahad Al Basir, one of the lab's seniors, for his support with my thesis work.

My acknowledgment would be incomplete without expressing gratitude to the most significant source of my strength—my family. I am deeply thankful to my parents, Mr. Sk Alenur and Mrs. Tanjira Begam, my brothers, Mr. Sk Majaffar Ahammed and Mr. Sk Mudashwer Ahammed, and my sister, Mrs. Rijia Sultana. Their constant encouragement, unconditional love, and unwavering support have been the foundation of my journey. This work would not have been possible without their blessings and sacrifices.

I want to take this opportunity to thank the Swamy Vivekananda Merit-Cum-Means Scholarship and the West Bengal Govt. Departmental Fellowship for financial support.

Sk Mosaraf Ahammed
02/09/2025

September, 2025

Sk Mosaraf Ahammed

Contents

List of Figures

List of Tables

1 Introduction

1.1 General Overview

The global dependence on fossil fuels, coal, petroleum, and natural gas has powered human progress for over a century. However, these conventional energy sources are finite, heavily polluting, and major contributors to environmental degradation and climate change. The escalating energy demand, combined with the geopolitical and ecological consequences of fossil fuel usage, has intensified the search for cleaner, more sustainable alternatives. Among the promising alternatives, biofuels have emerged as renewable energy carriers capable of reducing greenhouse gas emissions and alleviating dependence on imported oil.

Biofuels are derived from biological materials and encompass a range of energy-rich products, including biogas, bioethanol, and biodiesel. Biodiesel, in particular, has gained attention as a viable substitute for diesel fuel due to its compatibility with existing engines, biodegradability, and lower emission profile. In recent years, biodiesel has emerged as a promising and viable alternative to conventional fossil fuels, particularly in the context of increasing global concern over environmental degradation and the finite nature of petroleum resources. As a renewable and biodegradable fuel, biodiesel is often recognized as a clean energy source, capable of significantly reducing harmful emissions and contributing to environmental protection. One of the most notable advantages of biodiesel lies in its ability to lower the emission levels of major pollutants such as carbon dioxide (CO_2), carbon monoxide (CO), sulfur dioxide (SO_2), and unburned hydrocarbons (HC) when compared to traditional petroleum-based diesel (Ogunkunle and Ahmed, 2021). The reduction of sulfur dioxide emissions, in particular, is attributed to the inherently low sulfur content present in biodiesel. This makes it a cleaner-burning alternative, thereby

helping to curb acid rain and other forms of atmospheric pollution that are often linked to high-sulfur fossil fuels. Unlike diesel derived from crude oil, biodiesel combustion produces minimal SO_2, making it a more environmentally sustainable option.

1.2 Feedstocks for Biodiesel Synthesis

Biodiesel can be produced from a variety of renewable feedstocks, making it both versatile and adaptable to regional resource availability. The feedstock used for biodiesel production plays a crucial role in determining its cost, environmental impact, and sustainability. Over the years, raw materials for biodiesel have been broadly classified into three generations, first, second, and third generation, based on their origin, availability, and implications for food security and land use. Each generation represents a step forward in the search for more sustainable and eco-friendly biofuel alternatives.

- **First-Generation Feedstocks:** First-generation biodiesel feedstocks primarily include edible oils derived from food crops. Common examples include: Soybean oil (widely used in North and South America), Rapeseed oil (popular in Europe), Sunflower oil, Palm oil (abundant in Southeast Asia), Coconut oil, etc..

- **Second-Generation Feedstocks:** These feedstocks are more sustainable, as they do not directly compete with food crops and often make use of materials that would otherwise be discarded. Key second-generation feedstocks include non-edible vegetable oils such as: *Jatropha curcas* oil, *Pongamia pinnata* (karanja) oil, Castor oil, Neem oil, Waste Cooking oils (WCO) from restaurants and households, Animal fats (tallow, lard, poultry fat), Grease trap oils and yellow grease.

- **Third-Generation Feedstocks:** Third-generation biodiesel feedstocks are derived from microalgae and other photosynthetic microorganisms, representing a breakthrough in renewable fuel technology. Some species of algae, like Chlorella, Spirulina, and Nannochloropsis, are extensively studied for biodiesel production.

In our study, we focused on three specific feedstocks, Jatropha curcas oil, rapeseed oil, and waste cooking oil, due to their relevance and potential for sustainable biodiesel production. A concise overview of each is presented below.

1.2.1 *Jatropha curcas* Oil as Feedstock

Among various non-edible oilseed crops, *Jatropha curcas* has attracted significant attention as a sustainable and environmental friendly feedstock for biodiesel production, especially in tropical and subtropical regions. *Jatropha curcas* is a hardy perennial shrub belonging to the Euphorbiaceae family. It can grow on marginal lands with minimal input requirements, making it an ideal resource for cultivation in regions unsuitable for food crops (Contran *et al.*, 2013). The seed contains 35–40% oil, and the kernel of Jatropha curcas contains 50–60% oil (Achten *et al.*, 2008), which can be extracted and converted into biodiesel through transesterification.

It requires relatively low maintenance and has a life span of over 30 years, making it a long-term solution for renewable energy production. Moreover, being a non-edible oil crop, it does not compete directly with food production, thereby addressing one of the key concerns associated with first-generation biodiesel feedstocks. The oil is rich in unsaturated fatty acids like oleic and linoleic acids, resulting in biodiesel with satisfactory ignition quality and acceptable cold flow properties. Additionally, Jatropha-based biodiesel generally meets international fuel quality standards, including ASTM D6751 and EN 14214. The inclusion of *Jatropha curcas* in this study offers an opportunity to assess the potential of non-food biodiesel feedstocks.

Despite its potential, several challenges hinder the commercial scalability of *Jatropha curcas* cultivation. Similar to any other crops, Jatropha plantations are also vulnerable to pest infestations, which significantly impact crop yield. More than 40 insect species have been reported to attack Jatropha plant (Anitha and Varaprasad, 2012). Among them, *Pempelia morosalis*, a lepidopteran pest, is particularly damaging, especially during the second year of plantation when the plant is most vulnerable (Terren *et al.*, 2012). This pest feeds on the leaves and stems, causing extensive damage. A single female *P. morosalis* can lay $41 - 60$ eggs in its lifetime. The eggs hatch within $5 - 7$ days into larvae, which consume plant tissues for $25 - 30$ days before the mature stage. The larval stage is considered the most destructive (Sabi-Sabi, Nacro, *et al.*, 2016). The increasing global demand for biofuels has brought

Jatropha into the spotlight, especially in developing countries. However, despite its huge potential to serve as an alternative to standard fuel sources, there is a lack of comprehensive knowledge about pest control strategies and agronomic management practices for Jatropha cultivation (Chowdhury *et al.*, 2016; Ranga Rao *et al.*, 2010).

Various pest control methods have been explored previously to address this issue. Chemical control remains one of the most commonly applied strategies due to its rapid effectiveness against pest populations (Smith, 1962). However, prolonged use of these techniques is harmful in cultivation because these can degrade soil quality, contaminate water sources, disrupt beneficial insect populations, and ultimately destabilize the agro-ecosystem. In contrast, biological control methods offer a more sustainable alternative, using natural enemies such as predators, parasitoids and pathogens to reduce the pest populations (Bhattacharyya and Bhattacharya, 2006; Ghosh and Bhattacharya, 2010). Additionally, integrated pest management (IPM) strategies have also garnered considerable attention from researchers lately. IPM is a holistic and comprehensive pest management approach which aims to achieve effective and long-term pest control by working with nature and utilizing a range of strategies. It reduces dependence on synthetic pesticides, lowering potential risks to human health and the environment and encourages a more sustainable and ecologically balanced approach to pest control (Chowdhury *et al.*, 2019). Among the emerging strategies, the sterile insect technique (SIT) stands out as an innovative, eco-friendly and highly targeted approach to pest management. While SIT can be operated independently, it is widely classified as a compatible and primary component under the IPM umbrella.

SIT requires mass-rearing and sterilizing insects using radiation. These sterile insects are then released into the wild population to interrupt the reproductive cycle of the pest. When sterile males mate with wild females, no viable offspring are produced. This ultimately leads to a decline in the pest population over successive generations (Dame, 1984). Thus, as a biological control method, SIT works by suppressing wild pest populations through reproductive interference, which ultimately drives the target population toward a complete collapse over time. The synergy between biological control agents and SIT was first emphasized by Knipling (Knipling, 1979) and Barclay (Barclay, 1987), who suggested that merging these two methods enhances the overall effectiveness of the combined strategy. In recent times, SIT

has been successfully implemented against various pest populations which include plant pests such as fruit fly *Drosophila suzukii* (Sassù *et al.*, 2019; Lanouette *et al.*, 2017), red palm weevil *Rynchophorus ferrugineus Olivier* (Liu *et al.*, 2021; Dembilio and Jaques, 2015), livestock pests e.g. sheep blow fly *Lucilia caprina* (Yan *et al.*, 2020; Kotze and James, 2022) and numerous vectors associated with human disease for instance, mosquitoes (Gato *et al.*, 2021; Bourtzis and Vreysen, 2021; Patinvoh and Susu, 2014). Despite the successful trials of SIT, certainly, many challenges are still to be explored by the researchers in the domain of mathematical modeling and experimental studies. In this context, key focus areas remain developing more cost-effective mass-rearing techniques, improving strain competitiveness of sterile insects, integrating SIT with other established control methods and most importantly, expanding the application of SIT to new pest species.

Several mathematical frameworks have been developed earlier to address pest management in Jatropha plantations (Roy *et al.*, 2015; Al-Basir *et al.*, 2017, 2018, 2023). Roy and collaborators proposed and analyzed biological control strategies by incorporating viruses as pest-suppressing agents in Jatropha sp. ecosystems (Roy *et al.*, 2015; Chowdhury *et al.*, 2016). In particular, Roy et al. (Roy *et al.*, 2015) investigated the application of bio-pesticides in a periodic impulsive framework. Chowdhury et al. (Chowdhury *et al.*, 2019) formulated a mathematical model based on integrated pest management using an optimal control approach, demonstrating its cost-effectiveness and rapid pest suppression. Basir et al. (Al Basir *et al.*, 2023) introduced a dual-impulse technique involving the combined release of chemical and biological pesticides for enhanced pest control. Although several mathematical models have explored pest control strategies in Jatropha cultivation using chemical and bio-pesticides, various significant drawbacks and limitations have been observed in recent experimental literature. This certainly demands innovation and investigation of a novel pest control strategy such as SIT by stepping outside the box instead of existing conventional techniques experimented with so far for pest control in Jatropha plantation.

In this thesis, we present a chapter that develops three mathematical models incorporating the release of sterile male insects to disrupt the mating dynamics of wild pest populations, specifically targeting *Pempelia morosalis*. Considering these models we explore how different strategies for releasing sterile males at various time

intervals can effectively control pest populations while ensuring ecological sustainability.

1.2.2 Rapeseed Oil as Feedstock

In the quest for sustainable energy alternatives, rapeseed oil has emerged as one of the most promising feedstocks for biodiesel production, particularly in Europe and parts of Asia. Rapeseed (*Brassica napus*) is an oilseed crop belonging to the Brassicaceae family. It is primarily cultivated in temperate climates and has become the second most important source of vegetable oil globally after soybean. The seeds of the plant contain a high oil content, ranging from 40% to 45%, making it highly suitable for biofuel applications. Rapeseed is well-suited for large-scale biodiesel production due to its adaptation to different climate conditions, relatively short growth cycle, and high yield per hectare, identifying it as an efficient and desirable feedstock.

Despite its benefits, rapeseed cultivation poses certain challenges, including competition for arable land with food crops and vulnerability to pests and diseases, which require careful management. Ongoing research focuses on improving rapeseed cultivars with higher oil yield and resistance to biotic stresses. The inclusion of rapeseed oil as a biodiesel feedstock in this study provides a comparative perspective with other sources, such as Jatropha curcas. This comparison offers valuable insights into how the choice of feedstock, along with technological interventions and control-based optimization, can influence the future of renewable fuel production.

1.2.3 Waste Cooking Oil as Feedstock

Among the various feedstocks considered for biodiesel production, waste cooking oil (WCO) has gained significant attention due to its abundance, low cost, and contribution to waste reduction. Waste cooking oil is a by-product generated in large quantities from households, restaurants, food processing units, and the hospital industry. Improper disposal of WCO poses serious environmental hazards, including water pollution and sewer blockages. Utilizing WCO for biodiesel production provides an environmentally sustainable solution by transforming a problematic waste into a valuable fuel. Chemically, waste cooking oil is composed of triglycerides, free fatty acids (FFA), and degradation products resulting from repeated

heat generation during cooking. These thermal alterations often increase the FFA content and introduce impurities, making WCO a challenging but viable feedstock for biodiesel production. Conventional transesterification methods are less effective when the FFA content is high, as it leads to soap formation. Therefore, pretreatment processes such as acid esterification are often employed to reduce FFAs before the base-catalyzed transesterification step. The major advantages of using WCO include cost-effectiveness, non-competitiveness with food sources.

Although waste cooking oil is widely recognized for its potential as a biodiesel feedstock, its practical use is limited by challenges such as complex collection logistics, variability in quality, and the high costs associated with pretreatment processes. However, with proper infrastructure for collection and quality assessment, along with efficient processing technologies, WCO stands out as one of the most sustainable and economical options for biodiesel production. The inclusion of WCO as a biodiesel feedstock in this study emphasizes the role of waste-to-energy conversion in promoting circular economy principles. This thesis evaluates WCO alongside both conventional and non-edible plant-based sources, such as rapeseed oil and Jatropha oil. The comparative assessment highlights how the choice of feedstock can substantially improve the economic and environmental sustainability of biodiesel production systems.

1.3 Transesterification Reaction for Biodiesel Production

The production of biodiesel is fundamentally a chemical transformation process in which triglycerides, the primary constituents of fats and oils, are converted into mono-alkyl esters (biodiesel) through a reaction with short-chain alcohols, most commonly methanol or ethanol. This process is known as *transesterification* and can be catalyzed chemically or, in some cases, biologically (Ma and Hanna, 1999; Leung *et al.*, 2010). The most widely adopted route for biodiesel production is chemical transesterification using acid or base catalysts. In the base-catalyzed method, sodium hydroxide (NaOH) or potassium hydroxide (KOH) is dissolved in methanol to form alkoxide ions. These ions attack triglyceride molecules, releasing one mole of fatty acid ester and forming diglycerides, which subsequently react until full conversion. In contrast, acid catalysts such as sulfuric acid are used when feedstocks

contain high free fatty acid (FFA) content, which would otherwise lead to soap formation under alkaline conditions (Ma and Hanna, 1999). Despite its slower kinetics, acid-catalyzed transesterification effectively facilitates the esterification of free fatty acids (FFAs) as well as the transesterification of triglycerides. Beyond these, enzymatic catalysts (lipases), either free or immobilized, offer an eco-friendly and selective alternative, eliminating soap formation and easing purification.

1.3.1 Reaction Schema for Base-Catalyzed Transesterification

The overall stoichiometric reaction for base-catalyzed transesterification is represented as:

$$\text{Triglyceride (TG)} + 3\,\text{ROH} \xrightarrow{\text{Catalyst}} 3\,\text{R'-COOR} + \text{Glycerol},$$

where **ROH** denotes the alcohol (typically methanol or ethanol), and **R'-COOR** represents the corresponding fatty acid methyl or ethyl ester, which constitutes the biodiesel. This transformation occurs through a sequence of three consecutive and reversible reactions, each involving the stepwise conversion of glyceride intermediates: In the first step, the triglyceride reacts with one mole of alcohol to form a diglyceride (DG) and one mole of fatty acid ester:

$$\text{TG} + \text{ROH} \rightleftharpoons \text{DG} + \text{R'-COOR}.$$

In the second step, the diglyceride undergoes transesterification with another mole of alcohol to yield monoglyceride (MG) and an additional mole of ester:

$$\text{DG} + \text{ROH} \rightleftharpoons \text{MG} + \text{R'-COOR}.$$

In the final step, the monoglyceride reacts with a third mole of alcohol to produce glycerol and the third mole of ester:

$$\text{MG} + \text{ROH} \rightleftharpoons \text{Glycerol} + \text{R'-COOR}.$$

The reversibility of these steps underscores the need for optimized reaction conditions to ensure complete conversion and high yield of biodiesel. Catalysts such as

NaOH or KOH are commonly used to accelerate the reaction under mild temperature and pressure conditions.

1.3.2 Reaction Schema for Enzyme-Catalyzed Transesterification

In enzymatic transesterification, the production of biodiesel from Jatropha oil primarily involves the conversion of triglycerides (TG) and free fatty acids (F) into biodiesel (BD) through a two-step mechanism, catalyzed by a lipase enzyme (E). This process is particularly advantageous due to its mild reaction conditions, substrate specificity, and the ability to process high free fatty acid content without soap formation. The overall enzymatic pathway can be described as follows: In the first step, the enzyme (E) reacts with triglyceride (TG) to form a complex $[E \cdot TG]$. This intermediate subsequently breaks down to produce free fatty acid (F), glycerol (GL), and regenerates the free enzyme (E). In the second step, the free fatty acid (F) reacts with methanol (AL) to form a second complex $[F \cdot AL]$. This complex further dissociates to yield biodiesel (BD) and releases the free enzyme (E) for reuse. These reversible reactions can be schematically represented as:

$$E + TG \rightleftharpoons [E \cdot TG] \rightleftharpoons F + GL,$$
$$F + AL \rightleftharpoons [F \cdot AL] \rightleftharpoons E + BD.$$

The enzyme functions catalytically and is regenerated at the end of each cycle, enabling sustained reaction progression.

1.3.3 Mass Transfer Resistance in Transesterification Reaction

Biodiesel production through transesterification is a complex physicochemical process involving the conversion of triglycerides into fatty acid methyl esters (FAME) in the presence of alcohol and a catalyst. While this reaction appears simple in stoichiometric terms, its efficiency is deeply influenced by several interrelated physical and chemical phenomena, among which mass transfer plays a central role. Particularly, the mass transfer resistance between alcohol and triglyceride phase emerges as a critical barrier during the reaction, significantly impacting reaction kinetics, conversion rates, and overall process yield.

Nonpolar triglycerides and polar alcohol are immiscible or partially miscible under reaction conditions, resulting in the formation of a two-phase system. The reaction primarily occurs at the interface between the alcohol-rich and oil-rich phases, meaning that the effective interaction between these two liquids is essential for a smooth transesterification process. In such biphasic systems, mass transfer resistance arises due to the limited solubility of methanol in the oil phase and the relatively sluggish diffusion of reactants across the phase boundary. The presence of this resistance restricts the contact between methanol and triglyceride molecules, thereby slowing the reaction rate, especially in the early stages. This issue is even more pronounced when methanol is used in low molar ratios, as the available alcohol is quickly depleted near the interface, necessitating additional diffusion from the bulk phase to sustain the reaction.

Several studies have emphasized that enhancing mass transfer is crucial for achieving higher biodiesel yields, particularly during the initial phase of the reaction. Various factors collectively contribute to reduce mass transfer resistance between alcohol and triglyceride. By increasing agitation or mixing, the alcohol is dispersed into finer droplets, which promotes better contact between the immiscible phases and increases the interfacial area. The application of ultrasound induces cavitation and microturbulence, which disrupts the phase boundary and accelerates mass transfer. The molar ratio of alcohol to oil also plays a key role in reducing mass transfer resistance. Higher alcohol concentrations increase the driving force for diffusion and increase the saturation level of alcohol in the oil phase, thereby improving the reaction rate. Reaction temperature is another important factor influencing mass transfer. Higher temperatures lower oil viscosity, enhance diffusion, and improve alcohol solubility in triglycerides, and so, mass transfer resistance is diminished. Additionally, the size of the reactor vessel plays a non-negligible role in determining the overall efficiency of mass transfer.

A detailed explanation of the role of ultrasound frequency in the biodiesel production process, along with a comparison to mechanical stirring, has been given below.

1.4 Role of Ultrasound in Biodiesel Production

The production of biodiesel through the transesterification of triglyceride-rich oils with alcohol often suffers from inherent limitations due to slow reaction kinetics,

phase immiscibility, and mass transfer resistance between the reactants. Traditionally, mechanical stirring has been employed to address these challenges by promoting macro-level mixing. However, in recent years, the application of ultrasound (US) technology, particularly in the form of ultrasonic cavitation, has gained prominence as a highly efficient method to intensify the transesterification process. The frequency of ultrasound plays a vital role in determining the cavitational dynamics, mixing efficiency, and consequently, the reaction rate and biodiesel yield. Ultrasound refers to sound waves with frequencies above 20 kHz, beyond the upper limit of human hearing. In biodiesel synthesis, ultrasound is applied through a probe (direct) or bath (indirect) that delivers high-frequency acoustic energy into the reaction mixture. This acoustic energy causes the formation, growth, and sudden collapse of microbubbles in the liquid medium, a phenomenon known as acoustic cavitation. When these cavitation bubbles collapse, they generate localized hot spots with transient temperatures reaching up to 5000 K and pressures over 1000 atm. This intense micro-environment enables efficient micromixing, breaks interfacial resistance, and boosts both mass transfer and reaction rates. As a result, it is significantly reduce reaction time and the amount of catalyst needed for high conversion. Such effects are particularly beneficial in overcoming the limitations posed by mechanical stirring and enabling more sustainable, high-yield biodiesel production.

1.4.1 Mass Transfer Coefficient in terms of Ultrasound Frequency

To evaluate the impact of ultrasound on the process, the mass transfer coefficient is mathematically modeled, as it directly reflects how efficiently reactants reach the reaction site. This coefficient is governed by both hydrodynamic and diffusional transport phenomena, which are typically characterized using two dimensionless numbers: the Reynolds number (Re) and the Schmidt number (Sc). The Reynolds number represents the ratio of inertial to viscous forces in the fluid and is given by

$$Re = \frac{d^2 \rho H}{\mu},$$

where d is the characteristic length scale (e.g., vessel diameter), ρ is the fluid density, μ is the dynamic viscosity, and H is the applied ultrasound frequency (analogous to

a velocity term in this context). The Schmidt number expresses the ratio of momentum diffusivity to mass diffusivity and is defined as

$$Sc = \frac{\mu}{\rho D},$$

where D is the molecular diffusivity of the fluid. The mass transfer coefficient r_c under ultrasonic agitation can be estimated using a semi-empirical correlation analogous to the Dittus-Boelter correlation (Dittus and Boelter, 1985):

$$r_c = 0.023 \, \frac{D}{d} \, (Re)^{0.8} \, (Sc)^{0.33}, \tag{1.1}$$

where all variables retain their previously defined meanings. This correlation reflects how ultrasound-induced turbulence and acoustic streaming enhance interfacial transport. Since the inverse of the mass transfer coefficient indicates the resistance that the reactants face in reaching the reaction site, it follows that both the vessel diameter and sonication conditions significantly influence this resistance. A useful formulation is to express the overall mass transfer rate constant M_c as the mass transfer coefficient per unit vessel diameter is:

$$M_c = \frac{r_c}{d} = 0.023 \, \frac{D}{d^2} \, (Re)^{0.8} \, (Sc)^{0.33} = 0.023 \, \frac{D}{d^2} \left(\frac{d^2 \rho H}{\mu} \right)^{0.8} \left(\frac{\mu}{\rho D} \right)^{0.33}. \tag{1.2}$$

This final expression illustrates how the mass transfer performance in ultrasound-assisted biodiesel production depends not only on the physical properties of the fluid (density, viscosity, diffusivity), but also on the design parameters of the system (vessel diameter) and most importantly, on the applied ultrasound frequency. Such mathematical modeling facilitates a more comprehensive understanding of reactor behavior and promotes the advancement of ultrasound technology for large-scale biodiesel production.

1.4.2 Mathematical Modeling Approach for Biodiesel Production

Biodiesel production through transesterification is a complex multiphase process influenced by reaction kinetics, mass transfer phenomena, and mixing dynamics.

Mathematical modeling plays a vital role in understanding, analyzing, and optimizing this process by formulating a nonlinear set of equations that describe the evolution of reactants concentrations over time. Conventionally, biodiesel models are constructed based on mass balance equations that consider both chemical reaction rates and transport processes. In this study, reaction kinetics are typically modeled using a set of ordinary differential equations (ODEs), accounting for sequential conversion of triglycerides into diglycerides, monoglycerides, and ultimately glycerol and biodiesel. By developing such models for transesterification reactions, biodiesel production can become more cost-effective. These models assist in optimizing reaction parameters while also forecasting biodiesel yield and quality under various conditions. Several mathematical model-based studies on base-catalyzed transesterification reactions in biodiesel synthesis have been documented in the literature.

1.5 Literature Review and Motivation

Ultrasound has been effectively used to enhance both mass transfer and reaction rates in homogeneous (Berlan *et al.*, 1994; Cum *et al.*, 1988) and heterogeneous (Jie and Lam, 1995; Luche, 1994) systems. Its application in biodiesel production offers notable advantages over mechanical stirring. Stavarache et al. (Stavarache *et al.*, 2003) showed that low-frequency ultrasound (40 kHz) accelerates transesterification and improves biodiesel yield. Similarly, Colucci (Colucci *et al.*, 2005) found that ultrasound increases apparent rate constants in alkaline transesterification. Georgogianni et al. (Georgogianni *et al.*, 2007, 2009) demonstrated that ultrasound, with both catalyst types, enhanced soybean oil conversion compared to mechanical stirring. In another study, a 98% ester yield from sunflower oil was achieved in 40 minutes using a 24 kHz ultrasonic probe (200 W), while mechanical stirring yielded only 88% in 4 hours (Georgogianni *et al.*, 2008). Lifka et al. (Lifka and Ondruschka, 2004) reported 87% biodiesel conversion from canola oil in 30 minutes under ultrasound (24 kHz, 200 W) using a 6:1 molar ratio and 0.5–1% NaOH. Santos et al. (Santos *et al.*, 2010) achieved 98.2% yield from Nile Tilapia fish oil in 90 minutes at 40 kHz.

Several mathematical model-based studies on base-catalyzed transesterification reactions in biodiesel synthesis have been documented in the literature. Benavides and Diwekar showed the effects of both deterministic control (Diwekar and Benavides, 2012) and stochastic control (Benavides and Diwekar, 2012) mathematically

for biodiesel production in a batch reactor. The effect of stirring profile on mass transfer resistance is studied by Roy et al. (Roy *et al.*, 2014) through mathematical modeling, combined with control theory, using Jatropha seed oil as a feedstock. Chowdhury et al. (Chowdhury *et al.*, 2017) demonstrated the influence of temperature and catalyst loading on biodiesel production, and in a subsequent study (Chowdhury *et al.*, 2020), conducted a comparative analysis between chemical catalytic and supercritical methods for biodiesel synthesis. The literature contains a limited number of studies on kinetic modeling for enzymatic biodiesel production. Al-Zuhair et al. (Al-Zuhair *et al.*, 2007) formulated a kinetic model for producing biodiesel catalyzed by lipase from waste cooking oil. Liu et al. (Liu *et al.*, 2014), Basir et al. (Al Basir *et al.*, 2015; Al Basir and Roy, 2017; Al Basir *et al.*, 2017), Kartika et al. (Juan *et al.*, 2011) have investigated mathematical models for enzymatic biodiesel production from various feedstocks.

Recently, fractional-order derivatives have attracted growing interest in mathematical modeling for their ability to capture memory and time-dependent reactive behavior in dynamic systems (Patnaik *et al.*, 2020). Unlike traditional integer-order derivatives, fractional derivatives account for the influence of past states on present behavior through their integral-based formulation. Various fractional operators exist, defined by different kernel functions that determine the extent and nature of memory influence (Uchaikin, 2013). Among these, the Caputo–Fabrizio (CF) and Atangana–Baleanu in Caputo sense (ABC) derivatives have gained prominence due to their non-singular kernel structures. Several studies have applied fractional derivatives to heat and mass transfer, chemical kinetics, and fluid dynamics. Khan et al. (Khan *et al.*, 2017) compared CF and ABC derivatives in modeling second-grade fluids and observed that ABC predicts faster flow. Singh et al. (Singh *et al.*, 2017) used the ABC derivative in chemical kinetics, noting its superior representation of memory effects. Edessa (Edessa, 2022) showed that CF derivatives offer a more accurate representation of enzyme kinetics compared to classical models.

In the context of biodiesel production, particularly transesterification, memory effects, where the system's current state depends on its history, are significant. This memory effect influences reaction rates and system stability, making fractional-order models highly suitable for describing the complex kinetics involved. Among the limited studies applying this framework to biodiesel, Basir et al. (Al Basir *et al.*, 2017) used a fractional-order model for enzymatic biodiesel synthesis under mechanical stirring. Their findings revealed improved biodiesel yield at a fractional

order of 0.9, suggesting the benefit of incorporating memory effects.

Despite extensive research on biodiesel production, several critical gaps remain unaddressed. While many studies have examined mass transfer limitations in mechanically stirred systems (Chowdhury *et al.*, 2020; Al Basir *et al.*, 2015), there remains a notable gap in mathematical modeling focused specifically on ultrasound-induced mass transfer in biodiesel production. After exploring the effect of ultrasound in reducing mass transfer limitations in biodiesel production, it becomes necessary to conduct a mathematical comparison with mechanical stirring to determine which approach is superior and cost-efficient for biodiesel production. Furthermore, the influence of key factors like reaction rates and mass transfer coefficients in determining the yield across these mixing techniques remains poorly understood. This opens up important questions regarding the fundamental nature of the transesterification process: does it exhibit memory-dependent behavior, and if so, which fractional derivative formulation, Caputo–Fabrizio or Atangana–Baleanu, best captures the underlying dynamics? Lastly, while enzymatic biodiesel production under ultrasound has been experimentally studied, no predictive, model-based mathematical framework has yet been proposed to describe this process. Addressing these gaps can significantly advance the optimization and scalability of biodiesel production process.

1.6 Objective of this Thesis

The objective of this thesis is to maximize biodiesel yield while minimizing production time and cost through the use of mathematical modeling and optimal control techniques, with a focus on improving its environmental sustainability. A central focus of this thesis is the in-depth analysis of the role of ultrasound frequency in enhancing mass transfer dynamics and reaction kinetics in the biodiesel production process. To achieve this, mathematical models are formulated and analyzed to examine the influence of ultrasound frequency on various feedstocks, such as Jatropha oil, rapeseed oil, and waste cooking oil. Special emphasis is placed on a comparative analysis between ultrasound frequency and mechanical stirring using rigorous mathematical modeling; on examining memory-dependent behavior in the transesterification process through fractional-order derivatives, particularly the Caputo–Fabrizio and Atangana–Baleanu formulations; and on exploring enzymatic biodiesel production. These models aim to provide deeper insights into how

the use of ultrasound affects biodiesel yield and conversion efficiency. In addition, the thesis addresses a key ecological constraint in biodiesel feedstock cultivation by proposing a novel pest management framework based on the sterile insect technique (SIT). This study focuses on controlling populations of *Pempelia morosalis*, a major pest affecting *Jatropha curcas*, to ensure stable and sustainable biomass availability. Together, the mathematical and ecological modeling approaches constitute an integrated pathway to enhance the efficiency, scalability, and sustainability of biodiesel production systems.

1.7 Orientation

The thesis is organized in the following manner:

- In Chapter 2, a mathematical model is formulated to study ultrasound-assisted biodiesel production from *Jatropha curcas* oil. The model incorporates the modified Dittus-Boelter correlation to calculate the mass transfer rate under varying ultrasound frequencies and vessel diameters. A control theoretic approach is applied to ultrasound frequency for optimizing biodiesel yield by minimizing mass transfer resistance. Numerical analysis reveals that over 97% biodiesel yield is achievable within 50 minutes at 50 kHz frequency using a 6:1 methanol-to-oil molar ratio in a 1-meter vessel, demonstrating the potential for industrial scalability.

- In Chapter 3, an extension has been done of earlier work to examine biodiesel production from rapeseed oil at three different temperatures: 30°C, 50°C, and 65°C. A comparative study between mechanical stirring (MS) and ultrasound (US) mixing is conducted using mass transfer coefficients and molar ratios. Sensitivity and uncertainty analyses using the LHS-PRCC method are employed to assess parameter influence. Optimal control theory is applied to both mixing strategies, revealing that ultrasound-assisted transesterification yields higher conversion rates in less time compared to mechanical stirring, making it a superior method for biodiesel production from rapeseed oil.

- Chapter 4 focuses on capturing memory effects in biodiesel production by developing two fractional-order models using the Caputo–Fabrizio (CF) and Atangana–Baleanu (ABC) operators. These models describe the transesterification process of waste cooking oil (WCO), with analytical and numerical

solutions validated against experimental data. Existence and uniqueness of solutions are proven, and sensitivity analysis identifies key parameters influencing biodiesel yield. An optimal control strategy based on the ABC formulation is proposed for ultrasound frequency, significantly enhancing biodiesel production efficiency under fractional dynamics.

- In Chapter 5, a novel mathematical model is introduced to predict enzymatic biodiesel production under ultrasound exposure, a topic that has been experimentally explored but lacks predictive modeling. The model incorporates ultrasound frequency as a control variable and applies Pontryagin's Minimum Principle to derive an optimal frequency profile for cost-effective biodiesel synthesis. Simulation results exhibit strong agreement with experimental outcomes, validating the model's predictive accuracy and utility for optimizing enzymatic transesterification process.

- Chapter 6 addresses the ecological limitations of *Jatropha curcas* cultivation by presenting a mathematical model that incorporates the Sterile Insect Technique (SIT) to control *Pempelia morosalis*, a major pest species affecting the Jatropha plant. Three different scenarios are examined: (i) a pest-infested system without any sterile males, (ii) a system with continuous release of sterile males, and (iii) a system with periodic impulsive release of sterile males. The key purpose of this study is to explore how SIT can be utilized to effectively control the pest populations in Jatropha plantation while maintaining ecological sustainability. Our proposed mathematical framework rigorously evaluates two principal release modalities, continuous and impulsive (periodic) introductions to identify cost-effective protocols that maximize pest eradication while minimizing resource expenditure. Analytical and numerical results show that both continuous and periodic sterile male releases effectively suppress pest populations and promote sustainable growth of the Jatropha plant biomass.

- Finally, Chapter 7 outlines avenues for future research in biodiesel production through the combined application of ultrasound and mechanical stirring. In addition, potential directions for pest management in *Jatropha curcas* plantations are discussed, particularly the integration of pesticides with the sterile insect technique (SIT).

2 Enhancement of Biodiesel Production via Ultrasound Technology: A Mathematical Study

Mechanical stirring has long been employed at the industrial scale for effective mixing of reactants and the reduction of mass transfer resistance between triglyceride and methanol in biodiesel production process. However, ultrasound frequency has emerged as a promising alternative, offering higher biodiesel yield in shorter reaction times while consuming less energy than traditional stirring methods. This chapter[1] develops a mathematical model for analyzing the transesterification reaction mechanism with the help of ultrasound frequency. The study examines how ultrasound influences the immiscible interaction between methanol and Jatropha curcas oil, particularly in overcoming mass transfer limitations to improve biodiesel production efficiency.

2.1 The Mathematical Model

In order to depict a basic mathematical model for the transesterification reaction of alcohol (methanol) and Jatropha curcas oil (triglyceride), we have relied on the following assumptions:
(a1): Biodiesel production through transesterification of Jatropha oil with methanol is a chemical process that involves three stepwise and reversible reactions (Freedman *et al.*, 1986).
(a2): The reaction mixture of methanol and oil includes a very small amount of water (0.2% w/w), so the hydrolysis reaction has been neglected (Xu *et al.*, 2005).

[1]The majority of this chapter has been published in *ACS Omega*, American Chemical Society, Vol. 9, Issue 18, pp. 20502–20511, 2024.

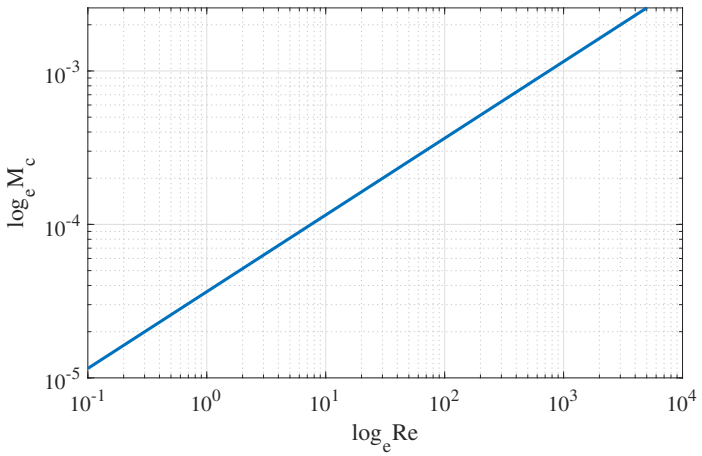

Figure 2.1: *Correlation of mass transfer rate constant and Reynolds number.*

(a3): Due to the presence of free fatty acid (FFA, 1% w/w) in Jatropha oil, triglyceride, FFA and produced biodiesel will participate in the saponification reaction with KOH catalyst (Komers *et al.*, 2001).
(a4): The mass transfer coefficient r_c due to ultrasound is given by

$$r_c = 0.023 \, \frac{D}{d} \, (Re)^{0.8} \, (Sc)^{0.33} \, , \tag{2.1}$$

where $Re = \frac{d^2 \rho H}{\mu}$ and $Sc = \frac{\mu}{\rho D}$ are called the Reynolds number and Schmidt number respectively (Subramanian, 2014). Here D, ρ, and μ are the mass diffusivity, density, and viscosity of Jatropha oil respectively. H is the applied ultrasound frequency and d is the diameter of the production vessel. The inverse of the mass transfer coefficient denotes the mass transfer resistance for the molecules to reach the reaction site which depends not only on the creation of turbulence inside the vessel but also on the diameter of the vessel. That is why $\frac{r_c}{d}$ denotes total mass transfer rate coefficient. In this case, the total mass transfer resistance depends on the sonicator frequency as well as the size of the vessel. Thus the total mass transfer rate constant (M_c) becomes

$$M_c = \frac{r_c}{d} = 0.023 \, \frac{D}{d^2} \, (Re)^{0.8} \, (Sc)^{0.33} = 0.023 \, \frac{D}{d^2} \left(\frac{d^2 \rho H}{\mu} \right)^{0.8} \left(\frac{\mu}{\rho D} \right)^{0.33} . \tag{2.2}$$

Here, Figure 2.1 represents the log-log plot of M_c and Reynolds number Re using parameter values from Table 2.1. The figure demonstrates how the mass transfer

Parameter	Definition	Value
D	diffusivity of *Jatropha* oil	$5.49 \times 10^{-6} - 1.16 \times 10^{-5}$ m^2s^{-1}
ρ	density of *Jatropha* oil	896.51 kg m^{-3}
μ	viscosity of *Jatropha* oil	24.8646 kg $m^{-1}s^{-1}$
d	diameter of the tube	1–2 m
H	ultrasound frequency	30–70 kHz

Table 2.1: *Some Liquid Properties of Jatropha curcas Oil and Input Range of Ultrasound and Vessel Size Used in the Reaction at 50 °C*

reaction constant increases as Reynolds number increases. The creation of turbulence in the reaction system enhances with the increase of Reynolds number. Consequently, the mass transfer resistance, which is inversely proportional to the mass transfer coefficient between J oil and methanol, decreases, and the mass transfer reaction constant increases. Table 2.2 shows the values of the mass transfer coefficient found from the correlation defined above at various ultrasound frequencies and vessel diameters.

H (kHz)	D ($m^2 \cdot s^{-1}$)	d (m)	ρ ($kg \cdot m^{-3}$)	μ ($kg \cdot m^{-1} \cdot s^{-1}$)	M_c ($m \cdot s^{-1}$)
40	9.1×10^{-6}	1	896.51	24.8646	1.0×10^{-3}
50	9.1×10^{-6}	1	896.51	24.8646	1.2×10^{-3}
60	9.1×10^{-6}	1	896.51	24.8646	1.4×10^{-3}
70	9.1×10^{-6}	1	896.51	24.8646	1.6×10^{-3}
40	9.1×10^{-6}	2	896.51	24.8646	8.0×10^{-4}
50	9.1×10^{-6}	2	896.51	24.8646	9.0×10^{-4}
60	9.1×10^{-6}	2	896.51	24.8646	1.0×10^{-3}
70	9.1×10^{-6}	2	896.51	24.8646	1.2×10^{-3}

Table 2.2: *Mass transfer coefficient (M_c) for different ultrasound frequencies and vessel sizes at* $50°C$.

(a5): Though there is a slight temperature elevation when using ultrasound, we keep the temperature constant at 50°C throughout this work, as viscosity and density change with respect to temperature. Moreover, Jahangir et al. (Chowdhury *et al.*, 2017) demonstrated that the saponification reaction accelerates and biodiesel conversion decreases when the temperature exceeds 50°C.

(a6): The transesterification reaction for biodiesel synthesis occurs through three stepwise reversible reactions in presence of KOH catalyst (Freedman *et al.*, 1986). In the first reversible step, 1 mole of triglyceride (TG) reacts with 1 mole of methanol (AL), yielding 1 mole of biodiesel (BD) and 1 mole of diglyceride (DG). During the second reversible step, 1 mole of diglyceride (DG) reacts with 1 mole of methanol (AL) to produce 1 mole of biodiesel (BD) and 1 mole of monoglyceride (MG). In

the final reversible step, 1 mole of monoglyceride (MG) reacts with another 1 mole of methanol (AL), resulting in 1 more mole of biodiesel (BD) and 1 mole of glycerol (GL) as by-product. In total, 1 mole of triglyceride reacts with 3 moles of methanol to produce 3 moles of biodiesel and 1 mole of glycerol. The stepwise reaction scheme is shown as:

$$\begin{aligned} \boldsymbol{TG} + \boldsymbol{AL} &\underset{r_2}{\overset{r_1}{\rightleftharpoons}} \boldsymbol{DG} + \boldsymbol{BD}, \\ \boldsymbol{DG} + \boldsymbol{AL} &\underset{r_4}{\overset{r_3}{\rightleftharpoons}} \boldsymbol{MG} + \boldsymbol{BD}, \\ \boldsymbol{MG} + \boldsymbol{AL} &\underset{r_6}{\overset{r_5}{\rightleftharpoons}} \boldsymbol{GL} + \boldsymbol{BD}. \end{aligned} \tag{2.3}$$

Also, there will be some soap formation of potassium by the side reaction of catalyst KOH with triglyceride, diglyceride, monoglycerides, biodiesel, and free fatty acid (FFA). Due to slow reaction rate we have neglected soap formation from diglycerides and monoglycerides (Zhang *et al.*, 2009; Chowdhury *et al.*, 2017). This saponification reaction will happen in three steps as below:

$$\begin{aligned} \boldsymbol{TG} + \boldsymbol{K} &\overset{r_7}{\rightarrow} \boldsymbol{S} + \boldsymbol{GL}, \\ \boldsymbol{BD} + \boldsymbol{K} &\overset{r_8}{\rightarrow} \boldsymbol{S} + \boldsymbol{AL}, \\ \boldsymbol{F} + \boldsymbol{K} &\overset{r_9}{\rightarrow} \boldsymbol{S} + \boldsymbol{W}, \end{aligned} \tag{2.4}$$

where, r_1, r_3, r_5 are the rate constants for forward reaction, r_2, r_4, r_6 are the rate constants for backward reaction of main reaction and r_7, r_8, r_9 are the rate constants for forward reaction of side saponification reaction. All these rate constants follow the Arrhenius equation by the relation $r_i = A_i e^{\frac{-E_{A_i}}{RT}}$ (Benavides and Diwekar, 2012), where A_i, T, R and E_{A_i} are the frequency factor, the reaction temperature, the universal gas constant and the activation energy for each component $i = 1, 2, ..., 9$. The values of r_1 to r_9 are shown in Table 2.3 obtained by using the values of A_i and others in (Benavides and Diwekar, 2012) with the help of the Arrhenius equation.

Parameter	Definition	Value
r_1	forward reaction constant	$0.0500\ \text{mol}^{-1}\text{L}\,\text{min}^{-1}$
r_2	backward reaction constant	$0.1099\ \text{mol}^{-1}\text{L}\,\text{min}^{-1}$
r_3	forward reaction constant	$0.1220\ \text{mol}^{-1}\text{L}\,\text{min}^{-1}$
r_4	backward reaction constant	$0.2147\ \text{mol}^{-1}\text{L}\,\text{min}^{-1}$
r_5	forward reaction constant	$0.2420\ \text{mol}^{-1}\text{L}\,\text{min}^{-1}$
r_6	backward reaction constant	$0.0070\ \text{mol}^{-1}\text{L}\,\text{min}^{-1}$
r_7	forward reaction constant	$0.00281\ \text{mol}^{-1}\text{L}\,\text{min}^{-1}$
r_8	forward reaction constant	$0.00279\ \text{mol}^{-1}\text{L}\,\text{min}^{-1}$
r_9	forward reaction constant	$0.2817\ \text{mol}^{-1}\text{L}\,\text{min}^{-1}$
$B_{\max}$	maximum biodiesel production	$3\ \text{mol L}^{-1}$

Table 2.3: *Values of various reaction constants at* $50°C$ *and the maximum biodiesel that can be produced under ideal conditions.*

Based on the above assumptions, the governing differential equations of the main reaction and side reaction scheme can be written as:

$$\begin{cases} \frac{dY_B}{dt} = & r_1Y_TY_A - r_2Y_DY_B + r_3Y_DY_A - r_4Y_MY_B + r_5Y_MY_A - r_6Y_GY_B - r_8Y_BY_K + M_cY_B\left(1 - \frac{Y_B}{B_{\max}}\right), \\ \frac{dY_T}{dt} = & -r_1Y_TY_A + r_2Y_DY_B - r_7Y_TY_K, \\ \frac{dY_D}{dt} = & r_1Y_TY_A - r_2Y_DY_B - r_3Y_DY_A + r_4Y_MY_B, \\ \frac{dY_M}{dt} = & r_3Y_DY_A - r_4Y_MY_B - r_5Y_MY_A + r_6Y_GY_B, \\ \frac{dY_A}{dt} = & -r_1Y_TY_A + r_2Y_DY_B - r_3Y_DY_A + r_4Y_MY_B - r_5Y_MY_A + r_6Y_GY_B + r_8Y_BY_K, \\ \frac{dY_G}{dt} = & r_5Y_MY_A - r_6Y_GY_B + r_7Y_TY_K, \\ \frac{dY_K}{dt} = & -\frac{dY_S}{dt} = -\left(r_7Y_TY_K + r_8Y_BY_K + r_9Y_KY_F\right), \\ \frac{dY_F}{dt} = & -\frac{dY_W}{dt} = -r_9Y_FY_K, \end{cases} \tag{2.5}$$

where Y_B, Y_T, Y_D, Y_M, Y_A, Y_G, Y_K, Y_S, Y_F and Y_W are the concentration of biodiesel, triglyceride, diglyceride, monoglyceride, methanol, glycerol, potassium hydroxide, soap, free fatty acid and water respectively with initial condition $Y_B(0) = 0$, $Y_T(0) = Y_{T_0}$, $Y_D(0) = 0$, $Y_M(0) = 0$, $Y_A(0) = Y_{A_0}$, $Y_G(0) = 0$, $Y_K(0) = Y_{K_0}$, $Y_S(0) = 0$, $Y_F(0) = Y_{F_0}$ and $Y_W(0) = 0$. We have designed our model with a logistic approach, incorporating the term $M_cY_B\left(1 - \frac{Y_B}{B_{\max}}\right)$ during its development. Here Y_B denotes biodiesel concentration at any time t and B_{max} represents maximum biodiesel production in the transesterification reaction. Both have the same unit $moles/L$. This expression has been utilized in a logistical sense, since the total mass transfer rate goes up as mass transfer resistance diminishes and after reaching a specific ultrasound frequency and vessel diameter, the mass transfer resistance becomes insignificant.

2.2 The Optimal Control Problem for Chemical Reaction System

Optimal control technique focuses on determining control parameters that guide a dynamical or chemical system over time to optimize a given objective function (Ross, 2015). In this work, we have applied optimal control theoretic approach to optimize ultrasound frequency over time in biodiesel production process. Initially, the reaction proceeds slowly due to high mass transfer resistance between methanol and Jatropha oil. Due to the application of ultrasound, this resistance is reduced and the reaction is accelerated. However, once the reaction is underway, ultrasound is no longer needed, allowing it to be turned off to reduce costs. Our goal is to determine an optimal range of ultrasound frequency to maximize biodiesel production while minimizing cost. Let the control variable z represent the ultrasound input at time t, where $0 \leq z \leq 1$; here, the value $z = 1$ denotes the highest utilization of ultrasound frequency, while $z = 0$ indicates the absence of frequency.
Mathematically, the control-induced system corresponding to the System (2.5) is formulated as:

$$\begin{cases} F_1 = & \frac{dY_B}{dt} = r_1 Y_T Y_A - r_2 Y_D Y_B + r_3 Y_D Y_A - r_4 Y_M Y_B + r_5 Y_M Y_A - r_6 Y_G Y_B - r_8 Y_B Y_K + M_c Y_B \left(1 - \frac{Y_B}{B_{\max}}\right) z, \\ F_2 = & \frac{dY_T}{dt} = -r_1 Y_T Y_A + r_2 Y_D Y_B - r_7 Y_T Y_K, \\ F_3 = & \frac{dY_D}{dt} = r_1 Y_T Y_A - r_2 Y_D Y_B - r_3 Y_D Y_A + r_4 Y_M Y_B, \\ F_4 = & \frac{dY_M}{dt} = r_3 Y_D Y_A - r_4 Y_M Y_B - r_5 Y_M Y_A + r_6 Y_G Y_B, \\ F_5 = & \frac{dY_A}{dt} = -r_1 Y_T Y_A + r_2 Y_D Y_B - r_3 Y_D Y_A + r_4 Y_M Y_B - r_5 Y_M Y_A + r_6 Y_G Y_B + r_8 Y_B Y_K, \\ F_6 = & \frac{dY_G}{dt} = r_5 Y_M Y_A - r_6 Y_G Y_B + r_7 Y_T Y_K, \\ F_7 = & \frac{dY_K}{dt} = -\left(r_7 Y_T Y_K + r_8 Y_B Y_K + r_9 Y_K Y_F\right), \\ F_8 = & \frac{dY_S}{dt} = r_7 Y_T Y_K + r_8 Y_B Y_K + r_9 Y_K Y_F, \\ F_9 = & \frac{dY_F}{dt} = -r_9 Y_F Y_K, \\ F_{10} = & \frac{dY_W}{dt} = r_9 Y_F Y_K, \end{cases} \tag{2.6}$$

with initial conditions: $Y_B(0) = Y_{B_0}, Y_T(0) = Y_{T_0}, Y_D(0) = Y_{D_0}, Y_M(0) = Y_{M_0}, Y_A(0) = Y_{A_0}, Y_G(0) = Y_{G_0}, Y_K(0) = Y_{K_0}, Y_S(0) = Y_{S_0}, Y_F(0) = Y_{F_0}$ and $Y_W(0) = Y_{W_0}$.

Our main objective is to maximize biodiesel production with minimum production costs. So, we formulated the cost function as:

$$J[z] = \int_{t_0}^{t_f} \left[W_1 z^2 - W_2 Y_B^2\right] dt, \tag{2.7}$$

where W_1 represents the weight constant for the cost function's benefit with $W_1 > 0$, while W_2 stands for the penalty multiplier. We want to identify the best control z^* such that $J(z^*) = min\{J(z) : z \in Z\}$, Z represents the permissible control set,

defined by

$$Z = \left\{ z(t) : \text{z(t) is measurable with } 0 \leq z(t) \leq 1, \quad t \in [t_0, t_f] \right\}.$$

Here, we employ the Minimum Principle by Pontryagin's (Pontryagin, 1987) to determine z^*.
The Hamiltonian can be written as:

$$\mathcal{H} = W_1 z^2 - W_2 Y_B^2 + \sum_{n=1}^{10} \Psi_i F_i, \tag{2.8}$$

where Ψ_1, Ψ_2,..., Ψ_{10} are adjoint variables and F_1, F_2,..., F_{10} are functions defined in Equation (2.6).

Now, when the optimal control z^* and the solution $(Y_B^*, Y_T^*, Y_D^*, Y_M^*, Y_A^*, Y_G^*, Y_K^*, Y_S^*, Y_F^*, Y_W^*)$ of the corresponding System (2.5) minimize $J(z)$ over Z, there will be adjoint variables $\Psi_1, \Psi_2, ..., \Psi_{10}$ that satisfy the following equations:

$$\begin{cases}
\frac{d\Psi_1}{dt} = & 2W_2 Y_B + \Psi_1(r_2 Y_D + r_4 Y_M + r_6 Y_G + r_8 Y_K) + M_c\left(1 - \frac{2Y_B}{B_{\max}}\right) z - \Psi_2 r_2 Y_D \\
& + \Psi_3(r_2 Y_D - r_4 Y_M) + \Psi_4(r_4 Y_M - r_6 Y_G) - \Psi_5(r_2 Y_D + r_4 Y_M + r_6 Y_G + r_8 Y_K) \\
& + \Psi_6 r_6 Y_G + \Psi_7 r_8 Y_K - \Psi_8 r_8 Y_K, \\
\frac{d\Psi_2}{dt} = & -\Psi_1 r_1 Y_A + \Psi_2 r_1 Y_A + \Psi_2 r_7 Y_K - \Psi_3 r_1 Y_A + \Psi_5 r_1 Y_A - \Psi_6 r_7 Y_K + \Psi_7 r_7 Y_K - \Psi_8 r_7 Y_K, \\
\frac{d\Psi_3}{dt} = & \Psi_1 r_2 Y_B - \Psi_1 r_3 Y_A - \Psi_2 r_2 Y_B + \Psi_3 r_2 Y_B + \Psi_3 r_3 Y_A - \Psi_4 r_3 Y_A - \Psi_5 r_2 Y_B + \Psi_5 r_3 Y_A, \\
\frac{d\Psi_4}{dt} = & \Psi_1 r_4 Y_B - \Psi_1 r_5 Y_A - \Psi_3 r_4 Y_B + \Psi_4(r_4 Y_B + r_5 Y_A) - \Psi_5(r_4 Y_B - r_5 Y_A) - \Psi_6 r_5 Y_A, \\
\frac{d\Psi_5}{dt} = & -\Psi_1(r_1 Y_T + r_3 Y_D + r_5 Y_M) + \Psi_2 r_1 Y_T - \Psi_3 r_1 Y_T + \Psi_3 r_3 Y_D - \Psi_4(r_3 Y_D - r_5 Y_M) \\
& + \Psi_5(r_1 Y_T + r_3 Y_D + r_5 Y_M) - \Psi_6 r_5 Y_M, \\
\frac{d\Psi_6}{dt} = & (\Psi_1 - \Psi_4 - \Psi_5 + \Psi_6) r_6 Y_B, \\
\frac{d\Psi_7}{dt} = & \Psi_1 r_8 Y_B + \Psi_2 r_7 Y_T - \Psi_5 r_8 Y_B - \Psi_6 r_7 Y_T + \Psi_7(r_7 Y_T + r_8 Y_B + r_9 Y_F) - \Psi_8(r_7 Y_T \\
& + r_8 Y_B + r_9 Y_F) + \Psi_9 r_9 Y_F - \Psi_{10} r_9 Y_F, \\
\frac{d\Psi_8}{dt} = & 0, \\
\frac{d\Psi_9}{dt} = & (\Psi_7 - \Psi_8 + \Psi_9 - \Psi_{10}) r_9 Y_K, \\
\frac{d\Psi_{10}}{dt} = & 0.
\end{cases} \tag{2.9}$$

along with the transversality conditions $\Psi_i(t_f) = 0$ for all i=1, 2, ..., 10. From Equation (2.7) we can write the Hamiltonian as:

$$\begin{aligned}
\mathcal{H} =& W_1 z^2 - W_2 Y_B^2 + \sum_{n=1}^{10} \Psi_i F_i, \\
=& W_1 z^2 + \Psi_1 z M_c Y_B \left(1 - \frac{Y_B}{B_{max}}\right) + \text{terms not containing } z.
\end{aligned} \tag{2.10}$$

Now, according to the necessary condition of Pontryagin Minimum Principle (Pontryagin, 1987), optimal control variable z^* will satisfy the condition

$$\frac{\partial \mathcal{H}}{\partial z^*} = 0. \tag{2.11}$$

From the Equation (2.9) and Equation (2.10), we have

$$\frac{\partial \mathcal{H}}{\partial z^*} = 2W_1 z^* + M_c Y_B \left(1 - \frac{Y_B}{B_{max}}\right)(\Psi_1) = 0. \tag{2.12}$$

Which implies that

$$z^* = \frac{M_c Y_B \left(1 - \frac{Y_B}{B_{max}}\right)(-\Psi_1)}{2W_1}. \tag{2.13}$$

Since the standard control is bounded $(0 \leq z \leq 1)$, we can write

$$z^* = \begin{cases} 0, & \frac{M_c Y_B \left(1-\frac{Y_B}{B_{\max}}\right)(-\Psi_1)}{2W_1} \leq 0; \\ \frac{M_c Y_B \left(1-\frac{Y_B}{B_{\max}}\right)(-\Psi_1)}{2W_1}, & 0 < \frac{M_c Y_B \left(1-\frac{Y_B}{B_{\max}}\right)(-\Psi_1)}{2W_1} < 1; \\ 1, & \frac{M_c Y_B \left(1-\frac{Y_B}{B_{\max}}\right)(-\Psi_1)}{2W_1} \geq 1. \end{cases} \tag{2.14}$$

or in compact form, we can write z^* as

$$z^* = max\left(0, min\left(1, \frac{M_c Y_B \left(1 - \frac{Y_B}{B_{max}}\right)(-\Psi_1)}{2W_1}\right)\right). \tag{2.15}$$

Based on the Minimum Principle by Pontryagin's (Pontryagin, 1987), adjoint variables satisfy the following equations:

$$\frac{d\Psi_j}{dt} = -\frac{\partial \mathcal{H}}{\partial Y_j}, \quad j = 1, 2, ..., 10, \tag{2.16}$$

where $Y_j \equiv \left(Y_B^*, Y_T^*, Y_D^*, Y_M^*, Y_A^*, Y_G^*, Y_K^*, Y_S^*, Y_F^*, Y_W^*\right)$ and the necessary conditions that satisfy the optimal control z^* are

$$\mathcal{H}(Y_j, z^*, \Psi_j, t) = min\big(Y_j, z, \Psi_j, t\big), \quad j = 1, 2, ..., 10. \tag{2.17}$$

Utilizing the relations (2.16), we obtain the whole adjoint system denoted by Equation (2.9).

2.3 Numerical Validation

In this section, numerical simulations using the ode45 solver have been performed to examine the system dynamics and gain deeper insight into the transesterification reaction in the presence of a KOH catalyst. Due to the immiscibility of methanol and Jatropha oil, significant mass transfer resistance arises from their differing polarities. To reduce this mass transfer limitation, we have used ultrasound frequency and compared the biodiesel yield with and without control through the Minimum Principle by Pontryagin's with Hamiltonian. In the biodiesel production process, we employ the molar ratio of Jatropha oil-to-methanol, along with ultrasound, to investigate their respective effects. Also, we have analyzed the biodiesel yield dependency on the size of the reaction vessel. Figure 2.2 represents the concentration

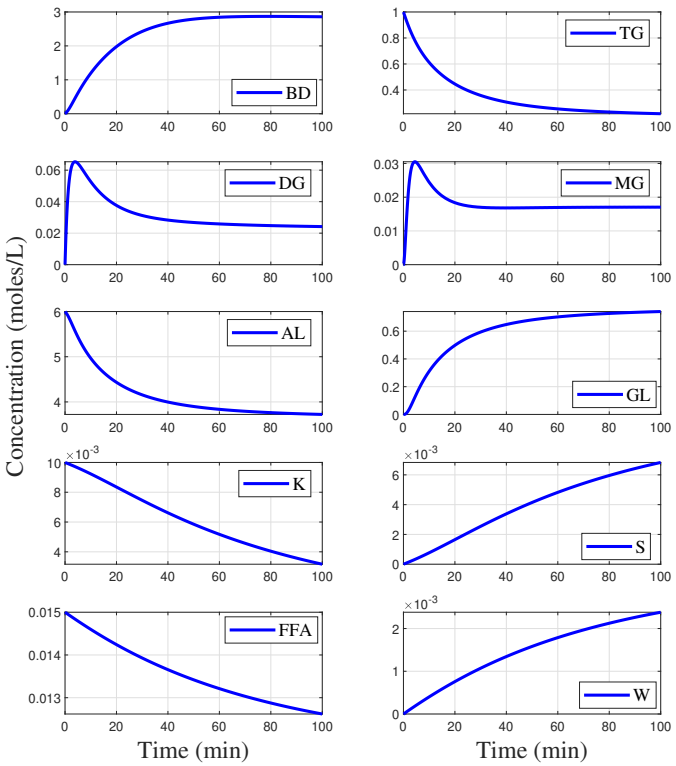

Figure 2.2: *Variation of concentration over time at a fixed temperature in base-catalyzed transesterification, utilizing parameters outlined in Table-2.1. Here ultrasound frequency H = 50 kHz, vessel diameter d = 1 meter, and methanol-to-oil ratio 6:1.*

trajectories of biodiesel, soap, glycerol and some other intermediates of transesterification reaction utilizing 50 kHz ultrasound frequency, 1 meter vessel diameter and

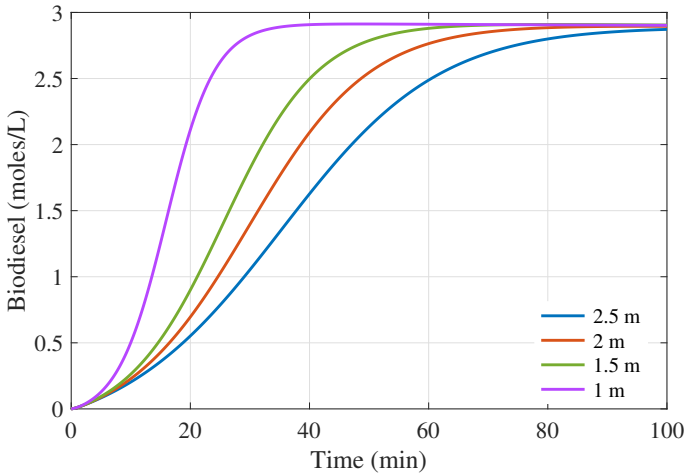

Figure 2.3: *Concentration profile of biodiesel production for different diameters of the reaction vessel with ultrasound frequency H = 50 kHz and AL : TG is 6 : 1.*

$6:1$ methanol-to-Jatropha oil molar ratio. Various reaction constants and B_{max} are taken from Table 2.3. It is evident from the figure that the production of biodiesel and glycerol gradually increased from 0 to 40 minutes, and after 40 minutes, the production remained constant until the end of the reaction. Also a small amount of soap is produced with increasing time.

Figure 2.3 represents the effect of the length of the vessel diameter in the reaction kinetics. Based on this figure, it is evident that reducing the vessel diameter results in an enhanced biodiesel production, holding the ultrasonic frequency at 50 kHz and the methanol-to-oil molar ratio at 6:1. Because increasing the vessel diameter for a fixed ultrasound frequency will produce less turbulence between methanol and jatropha oil, and decreasing the diameter will produce more turbulence. Therefore, a reduction in vessel diameter leads to a decrease in mass transfer resistance, resulting in an increased biodiesel production yield. Hence, the vessel's diameter plays a pivotal role in biodiesel production. In this case, the considerable diameter of the vessel is 1 meter.

The molar ratio of methanol to Jatropha oil is one of the key factor in determining biodiesel production (Sengupta *et al.*, 2019). In Figure 2.4, the influence of methanol-to-Jatropha oil molar ratio has been shown for $4:1$, $5:1$, $6:1$ and $7:1$. At $6:1$, we get 90% of biodiesel in less than 60 minutes at 50 kHz frequency of ultrasound. Initially, the biodiesel production increases at 7:1 molar ratio with 50 kHz ultrasound frequency but after 50 minutes, the yield conversion is almost the same as $6:1$ molar ratio. It can also be observed from Figure 2.6(b) that there is no need to increase

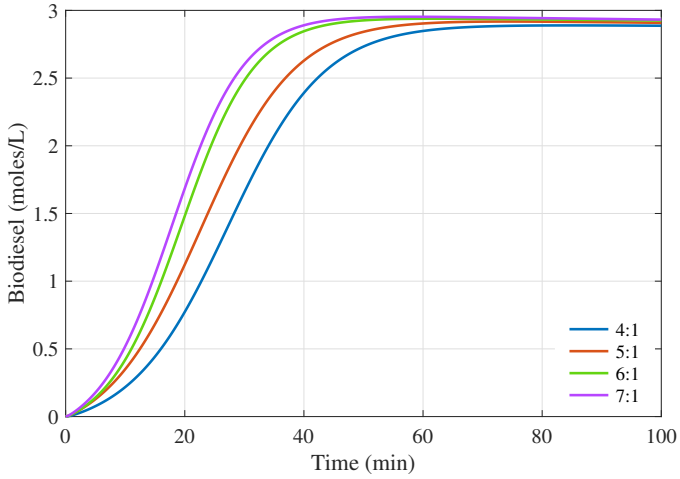

Figure 2.4: *Biodiesel concentration profiles with varying methanol-to-triglyceride molar ratios. Here ultrasound frequency H = 50 kHz and the vessel diameter d = 1 meter.*

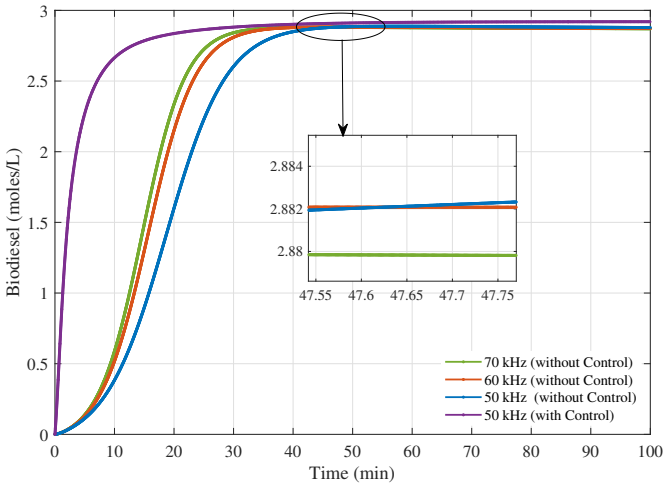

Figure 2.5: *Variation in biodiesel yield concentration with ultrasound frequencies at a fixed methanol-to-oil molar ratio of 6:1 and vessel diameter of 1 meter with and without control.*

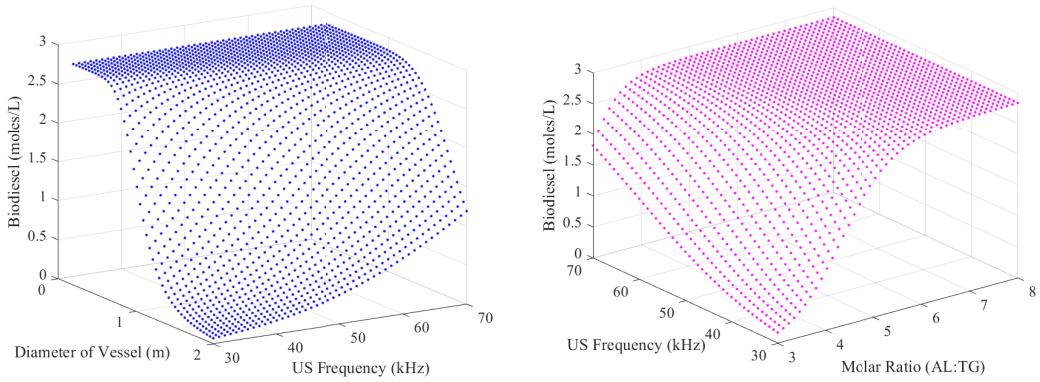

(a) (b)

Figure 2.6: *Biodiesel yield concentration for different (a) vessel diameters and ultrasound frequencies and (b) molar ratio of methanol-to-triglyceride and ultrasound frequencies*

the molar ratio of methanol to oil beyond 6:1, as there is no further increase in production. To reduce costs, we have chosen $6:1$ molar ratio of methanol and Jatropha oil for the synthesis of biodiesel in our research work.

Figure 2.5 shows how biodiesel production varies with ultrasound frequency. The reaction rate increases significantly when the frequency of ultrasound is increased up to 50 kHz. For a further increment of frequency of ultrasound concentration of biodiesel decreases over time. Elevating the ultrasound frequency to 60 kHz or 70 kHz initially boosts biodiesel production. However, after 47 minutes of reaction time, biodiesel yields start to decrease, leading to an undesirable drop in biodiesel concentration over time. This occurs as a result of the fact that a higher frequency of ultrasound increases the volatility of reacting methanol. The vaporization of methanol from the reaction vessel leads to a reduction in the quantity of one of the reactants and also interferes with the desired methanol-to-triglycerides ratio. According to the figure, achieving the highest biodiesel output requires a 50 kHz ultrasonic frequency in conjunction with a 6:1 methanol-to-Jatropha oil ratio and 1 meter of vessel diameter.

Figure 2.6(a) depicts the mutual effect of ultrasound frequency and vessel diameter, whereas Figure 2.6(b) depicts the mutual effect of molar ratio and ultrasound frequency for biodiesel synthesis. These figures demonstrate how biodiesel conversion varies on ultrasound frequency, molar ratio of methanol and Jatropha oil and vessel diameter.

Although mixing intensity plays a crucial role in biodiesel synthesis together with molar ratio of reactants and vessel size, the control on ultrasound frequency holds

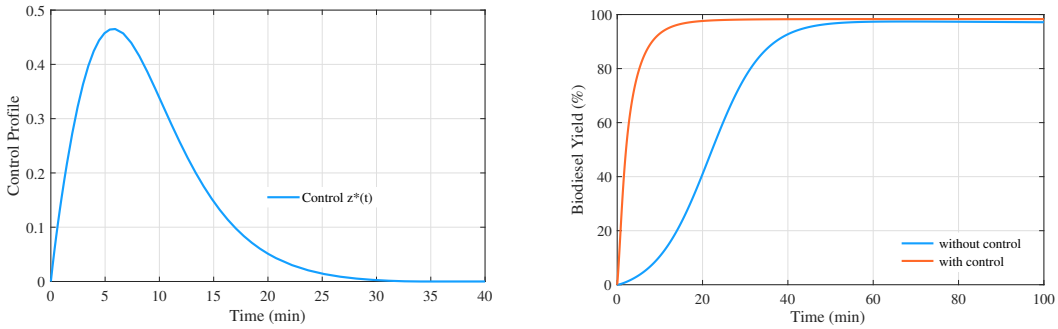

(a) (b)

Figure 2.7: *(a) Time-dependent optimal control profile for ultrasound frequency. (b) Biodiesel yield conversion with respect to time with and without control at 50 kHz ultrasound frequency, 6:1 methanol-to-Jatropha oil molar ratio, and 1 meter of vessel diameter.*

substantial importance for the optimization of the intended outcomes. As triglyceride and methanol are incapable of mixing because of their non-polar and polar properties, initially a greater ultrasound frequency is required to overcome the mass transfer limitation in the transesterification reaction. Figure 2.7(a) clearly shows that, after 8 minutes, less control over ultrasound is necessary. This is because the biodiesel, which is created after 8 minutes will serve as a medium for the mixture of the two reactants, functions as a continuous state for reactants, and minimizes mass transfer limitation. Eventually, at almost 40 minutes, a very low frequency of ultrasound is needed because, at this point, the reaction has almost finished. Based on the aforementioned discussion, it is apparent that, despite the substantial impact of mixing intensity and other kinetic factors on biodiesel synthesis, controlling the ultrasound frequency throughout the reaction process has a crucial role in optimizing biodiesel production. Figure 2.5 presents a comparison of biodiesel concentration, both with and without the incorporation of an ultrasound control technique. Through the application of optimal control on ultrasound frequency, the constraint of mass transfer limitation is nearly eradicated, achieving a yield conversion of more than 97% in less than 40 minutes of reaction time. Figure 2.7(b) shows biodiesel yield conversion with respect to time. According to this figure, control operation enhances biodiesel yield by approximately 6%.

2.4 Discussion and Conclusion

This chapter introduces a mathematical model for the transesterification reaction between methanol and Jatropha oil for biodiesel production, based on several fundamental assumptions. It highlights the significant influence of mixing intensity induced by ultrasound, molar ratio, and vessel diameter on the reaction's progress. The formulation of the Reynolds number shows a direct proportional relationship with ultrasound frequency. Mathematically, it is evident that biodiesel production reaches a threshold level with increasing ultrasonic frequency, indicating that higher Reynolds numbers enhance biodiesel yield. Biodiesel concentration is evaluated under different reaction conditions, including varying methanol-to-triglyceride molar ratios and ultrasound frequencies. This study emphasizes the importance of optimizing ultrasonic effects and overcoming mass transfer limitations. Thus, ultrasound application and vessel dimensions, which contribute to turbulence generation, are identified as key parameters influencing mass transfer in the process. It can be demonstrated that delivering ultrasound to the system has a significant effect on the economic production of biodiesel by assuming a control technique on the ultrasound effect.

Through a comparative analysis of biodiesel yield conversion under varying ultrasound frequencies, we achieved 90% biodiesel yield within 60 minutes, when we set ultrasound frequency to 50 kHz, molar ratio of methanol and Jatropha oil to 6:1, and the vessel diameter to 1 meter without any control. But employing control theoretic approach in conjunction with 50 kHz ultrasound frequency, while maintaining the same molar ratio and vessel diameter, we have achieved more than 97% of biodiesel yield within a reduced time-frame of just 50 minutes. The present study demonstrates the effectiveness of ultrasound frequency in significantly reducing mass transfer limitations during biodiesel production, with results comparable to those obtained using mechanical stirring. However, a mathematical comparison between mechanical stirring and ultrasound frequency has not yet been explored, which is addressed in Third Chapter.

3 Optimization of Biodiesel Synthesis using Ultrasound and Mechanical Stirring: A Comparative Study

Several studies have already investigated biodiesel production from *Jatropha curcas* using mechanical stirring. In second chapter, biodiesel synthesis is explored from *Jatropha curcas* employing ultrasound frequency. Building upon these findings, the current chapter[1] aims to perform a comparative analysis of mechanical stirring and ultrasound frequency, using a different feedstock, rapeseed oil. To assess the combined effects of temperature and mixing technique on biodiesel yield, we extend our study across three different operating temperatures, 30°C, 50°C, and 65°C, highlighting the impact of reaction rates under each condition and evaluating the efficiency of both mixing methods.

3.1 The Mathematical Model

In transesterification reaction between rapeseed oil and MeOH to produce biodiesel yield, mass transfer resistance can significantly affect the reaction rate, especially in heterogeneous systems where TG and MeOH are immiscible (Likozar and Levec, 2014). This resistance occurs at the interface between two phases, primarily during the initial stage of the reaction. Mass transfer resistance in transesterification reaction is primarily caused by poor mutual solubility of oil and MeOH, diffusion limitations, high oil viscosity, and limited catalyst accessibility (Su and Guo, 2014). MS and US frequency are the most effective techniques for reducing mass transfer

[1]Maximum portion of this chapter is communicated in a peer-reviewed international journal.

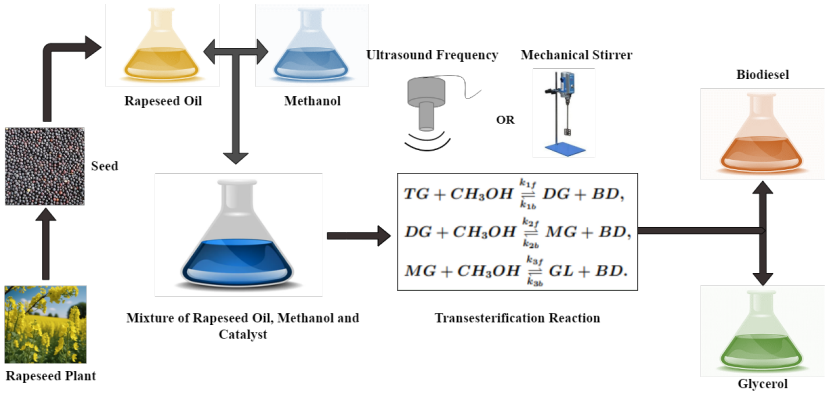

Figure 3.1: *Transesterification of rapeseed oil using MS rotation or US frequency.*

resistance between the oil and alcohol phases (Yin *et al.*, 2012). MS minimizes mass transfer resistance by expanding the contact area between oil and MeOH, while US frequency improves mixing via cavitation, disrupting phase boundaries and facilitating enhanced diffusion. The mass transfer rate due to MS is given by (Roy *et al.*, 2014; Al Basir *et al.*, 2015)

$$K_c = \frac{1}{K_r} = \frac{a}{1 + exp(-b(f - c))}, \tag{3.1}$$

where a, b, c are constants and f is agitation speed which is measured in rpm and K_r is the mass transfer resistance which is opposite to the mass transfer rate. The mass transfer rate due to US frequency using modified Dittus-Boelter correlation is given by (Cao *et al.*, 2024)

$$M_c = \frac{1}{M_r} = 0.023\,\frac{D}{d^2}\,(Re)^{0.8}\,(Sc)^{0.33} = 0.023\,\frac{D}{d^2}\left(\frac{d^2\rho H}{\mu}\right)^{0.8}\left(\frac{\mu}{\rho D}\right)^{0.33}, \tag{3.2}$$

where M_r is the mass transfer resistance, Re is the Reynolds number and Sc is the Schmidt number. D, ρ, μ are the mass diffusivity, density, and viscosity of rapeseed oil respectively. d is the diameter of the reaction vessel and H is the applied US frequency.

Biodiesel production involves the transesterification of rapeseed oil (TG) using MeOH in the presence of potassium hydroxide (KOH) catalyst (see Figure 3.1). Transesterification of triglyceride (TG) consists of three reversible steps. In first step, TG undergo partial methanolysis to form diglycerides (DG). DG is partially methanolyzed to produce monoglycerides (MG) in second step. In the final step,

MG undergoes partial methanolysis to yield glycerol (GL). Each reaction step releases one molecule of biodiesel (BD). The step-wise reaction scheme is shown as:

$$\begin{aligned} \boldsymbol{TG + MeOH} &\underset{k_{1b}}{\overset{k_{1f}}{\rightleftharpoons}} \boldsymbol{DG + BD}, \\ \boldsymbol{DG + MeOH} &\underset{k_{2b}}{\overset{k_{2f}}{\rightleftharpoons}} \boldsymbol{MG + BD}, \\ \boldsymbol{MG + MeOH} &\underset{k_{3b}}{\overset{k_{3f}}{\rightleftharpoons}} \boldsymbol{GL + BD}, \end{aligned} \tag{3.3}$$

where, k_{1f}, k_{2f}, k_{3f} are forward rate coefficient and k_{1b}, k_{2b}, k_{3b} are backward rate coefficient of the transesterification reaction. These reaction rate constants are related with temperature by the Arrhenius equation $k_i = \alpha_i e^{\frac{-E_{\alpha_i}}{RT}}$, where α_i, E_{α_i}, R, and T are the frequency factor, the activation energy, the universal gas constant, and the reaction temperature respectively (Benavides and Diwekar, 2012). To investigate the effect of temperature on biodiesel production, the entire study is conducted at three different temperatures: 30°C, 50°C, and 65°C as temperature significantly influences liquid properties such as viscosity, density, and diffusivity of the reactants. The parameter values of ρ, μ, D of rapeseed oil, along with the reaction rate constants for the transesterification reaction at these three temperatures, are presented in Table 3.1 and Table 3.2. Based on the above assumptions and to show the effect of MS on

Temperature (°C)	**Density ρ (kg m^{-3})**	**Viscosity μ (kg m^{-1}s^{-1})**	**Diffusivity D (m^{2}s^{-1})**
30 (Zongo *et al.*, 2018)	908.117	97.7575	8.9339×10^{-5}
50 (Zongo *et al.*, 2018)	894.735	39.6956	8.7142×10^{-5}
65 (Zongo *et al.*, 2018)	881.353	21.9229	8.3704×10^{-5}

Table 3.1: *Density, viscosity, and diffusivity of rapeseed oil at three different temperatures.*

BD production, a mathematical model corresponding to the reaction Schema 3.3 can be written as:

$$\begin{cases} \frac{dY_A}{dt} = & -k_{1f}Y_TY_A + k_{1b}Y_DY_B - k_{2f}Y_DY_A + k_{2b}Y_MY_B - k_{3f}Y_MY_A + k_{3b}Y_GY_B, \\ \frac{dY_T}{dt} = & -k_{1f}Y_TY_A + k_{1b}Y_DY_B, \\ \frac{dY_D}{dt} = & k_{1f}Y_TY_A - k_{1b}Y_DY_B - k_{2f}Y_DY_A + k_{2b}Y_MY_B, \\ \frac{dY_M}{dt} = & k_{2f}Y_DY_A - k_{2b}Y_MY_B - k_{3f}Y_MY_A + k_{3b}Y_GY_B, \\ \frac{dY_B}{dt} = & k_{1f}Y_TY_A - k_{1b}Y_DY_B + k_{2f}Y_DY_A - k_{2b}Y_MY_B + k_{3f}Y_MY_A - k_{3b}Y_GY_B + K_cY_B\left(1 - \frac{Y_B}{B_{\max}}\right), \\ \frac{dY_G}{dt} = & k_{3f}Y_MY_A - k_{3b}Y_GY_B, \end{cases} \tag{3.4}$$

and similarly, to investigate the effect of US frequency, the mathematical model for same Schema 3.3 can be written as:

$$\begin{cases} \frac{dY_A}{dt} = & -k_{1f}Y_TY_A + k_{1b}Y_DY_B - k_{2f}Y_DY_A + k_{2b}Y_MY_B - k_{3f}Y_MY_A + k_{3b}Y_GY_B, \\ \frac{dY_T}{dt} = & -k_{1f}Y_TY_A + k_{1b}Y_DY_B, \\ \frac{dY_D}{dt} = & k_{1f}Y_TY_A - k_{1b}Y_DY_B - k_{2f}Y_DY_A + k_{2b}Y_MY_B, \\ \frac{dY_M}{dt} = & k_{2f}Y_DY_A - k_{2b}Y_MY_B - k_{3f}Y_MY_A + k_{3b}Y_GY_B, \\ \frac{dY_B}{dt} = & k_{1f}Y_TY_A - k_{1b}Y_DY_B + k_{2f}Y_DY_A - k_{2b}Y_MY_B + k_{3f}Y_MY_A - k_{3b}Y_GY_B + M_cY_B\left(1 - \frac{Y_B}{B_{\max}}\right), \\ \frac{dY_G}{dt} = & k_{3f}Y_MY_A - k_{3b}Y_GY_B, \end{cases} \tag{3.5}$$

where Y_A, Y_T, Y_D, Y_M, Y_B, and Y_G are the concentration of MeOH, TG, DG, MG, BD, and GL respectively with initial condition $Y_A(0) = Y_{A_0}$, $Y_T(0) = Y_{T_0}$, $Y_D(0) = 0$, $Y_M(0) = 0$, $Y_B(0) = 0$, and $Y_G(0) = 0$. Here the effect of MS and US frequency is represented by the terms $K_cY_B\left(1 - \frac{Y_B}{B_{\max}}\right)$ and $M_cY_B\left(1 - \frac{Y_B}{B_{\max}}\right)$ respectively, where $B_{\max}$ denotes the maximum biodiesel conversion achievable in an ideal scenario, meaning a system without mass transfer limitation or resistance. These terms are used in a logistic fashion because increased MS or US frequency reduces mass transfer limitations, which become negligible after a certain point.

Rate Constant $[\mathbf{L \cdot mol^{-1} \cdot min^{-1}}]$	**30°C**	**50°C**	**65°C**
k_{1f} (TG $\rightarrow$ DG)	0.0061	0.0359	0.1784
k_{1b} (TG $\leftarrow$ DG)	0.0358	0.1781	0.8134
k_{2f} (DG $\rightarrow$ MG)	0.0767	0.6157	8.2189
k_{2b} (DG $\leftarrow$ MG)	1.3496	6.4165	30.6887
k_{3f} (MG $\rightarrow$ GL)	0.2181	0.4379	0.4717
k_{3b} (MG $\leftarrow$ GL)	0.0013	0.0014	0.0020

Table 3.2: *Forward and backward reaction rate constants for the transesterification reaction using rapeseed oil at three different temperatures, taken from (Šánek* et al., *2019).*

3.2 Optimal Control Approach

An optimal control problem involves determining a control policy that will optimize a certain performance criterion for a given dynamic system. This type of problem is prevalent in various fields such as engineering, economics, and operations research (Bertsekas, 2012). The optimal control problem is typically represented by a set of differential or difference equations that describe the evolution of the system-state over time (Grass *et al.*, 2008). In this chapter, two mathematical models for biodiesel

production have been addressed under some basic assumptions to determine which is more effective among MS and US frequency in maximizing biodiesel yield and minimizing the cost of production. To reduce the cost of production, we need to regulate or control the MS and US frequency. Here, control $u(t)$ and $z(t)$ are given to the terms K_r and M_r, respectively, to reduce mass transfer resistance by regulating MS and US frequency over time t. We want to identify the theoretical optimal ranges for MS and US frequency while keeping the cost function, as measured by time, as low as possible. The ranges of $u(t)$ and $z(t)$ are $0 \leq u(t) \leq 1$ and $0 \leq z(t) \leq 1$, in which $u(t)$ and $z(t)$ represents control input with values normalized between 0 and 1. $u(t)$ or $z(t)$ equal to 1 represents the maximal use of MS or US frequency, and equal to 0 represents no stirring or frequency.

Mathematically, the control-induced system corresponding to the System (3.4) can be formulated as:

$$\begin{cases} F_1 = & \frac{dY_A}{dt} = -k_{1f}Y_TY_A + k_{1b}Y_DY_B - k_{2f}Y_DY_A + k_{2b}Y_MY_B - k_{3f}Y_MY_A + k_{3b}Y_GY_B, \\ F_2 = & \frac{dY_T}{dt} = -k_{1f}Y_TY_A + k_{1b}Y_DY_B, \\ F_3 = & \frac{dY_D}{dt} = k_{1f}Y_TY_A - k_{1b}Y_DY_B - k_{2f}Y_DY_A + k_{2b}Y_MY_B, \\ F_4 = & \frac{dY_M}{dt} = k_{2f}Y_DY_A - k_{2b}Y_MY_B - k_{3f}Y_MY_A + k_{3b}Y_GY_B, \\ F_5 = & \frac{dY_B}{dt} = k_{1f}Y_TY_A - k_{1b}Y_DY_B + k_{2f}Y_DY_A - k_{2b}Y_MY_B + k_{3f}Y_MY_A - k_{3b}Y_GY_B + \frac{Y_B}{u(t).K_r}\left(1 - \frac{Y_B}{B_{\max}}\right), \\ F_6 = & \frac{dY_G}{dt} = k_{3f}Y_MY_A - k_{3b}Y_GY_B, \end{cases} \tag{3.6}$$

and the control-induced system corresponding to the System (3.5) can be written as:

$$\begin{cases} F_1' = & \frac{dY_A}{dt} = -k_{1f}Y_TY_A + k_{1b}Y_DY_B - k_{2f}Y_DY_A + k_{2b}Y_MY_B - k_{3f}Y_MY_A + k_{3b}Y_GY_B, \\ F_2' = & \frac{dY_T}{dt} = -k_{1f}Y_TY_A + k_{1b}Y_DY_B, \\ F_3' = & \frac{dY_D}{dt} = k_{1f}Y_TY_A - k_{1b}Y_DY_B - k_{2f}Y_DY_A + k_{2b}Y_MY_B, \\ F_4' = & \frac{dY_M}{dt} = k_{2f}Y_DY_A - k_{2b}Y_MY_B - k_{3f}Y_MY_A + k_{3b}Y_GY_B, \\ F_5' = & \frac{dY_B}{dt} = k_{1f}Y_TY_A - k_{1b}Y_DY_B + k_{2f}Y_DY_A - k_{2b}Y_MY_B + k_{3f}Y_MY_A - k_{3b}Y_GY_B + \frac{Y_B}{z(t).M_r}\left(1 - \frac{Y_B}{B_{\max}}\right), \\ F_6' = & \frac{dY_G}{dt} = k_{3f}Y_MY_A - k_{3b}Y_GY_B, \end{cases} \tag{3.7}$$

with initial conditions for both the System (3.6) and System (3.7): $Y_A(0) = Y_{A_0}, Y_T(0) = 1, Y_D(0) = 0, Y_M(0) = 0, Y_B(0) = 0$, and $Y_G(0) = 0$.

We formulated the cost function for both System (3.6) and System (3.7) as:

$$J[g(t)] = \int_{t_0}^{t_f} \left[w_1 g^2(t) - w_2 Y_B^2\right] dt, \quad (g(t) = u(t), z(t)), \tag{3.8}$$

where $w_1 (> 0)$ and w_2 are the weight constant on the benefit of the cost function and the penalty multiplier, respectively. Since both System (3.6) and System (3.7)

are of the same type, we will determine the control profile only for System (3.7). The control profile for System (3.6) can be found similarly. Now, we seek to identify the best control $z^*(t)$ such that

$$J(z^*(t)) = min\{J(z(t)) : z(t) \in Z\},$$

Z is the admissible control set defined by

$$Z = \{z(t) : z(t) \text{ is measurable}, 0 \leq z(t) \leq 1, t \in [t_i, t_f]\}. \tag{3.9}$$

Now, we employ the Minimum Principle by Pontryagin (Pontryagin, 2018) to determine $z^*(t)$.

Theorem 3.2.1. *The control parameter $z^*(t)$ that minimizes $J(z(t))$ over Z are given by*

$$z^*(t) = max\left(0, min\left(1, \left\{\frac{\Psi_B Y_B(B_{max} - Y_B)}{2w_1 M_r B_{max}}\right\}^{\frac{1}{3}}\right)\right),$$

where Ψ_A, Ψ_T, Ψ_D, Ψ_M, Ψ_B, and Ψ_G are the adjoint variables satisfying Equation (3.7) and the following transversality conditions:

$$\Psi_A(t_f) = \Psi_T(t_f) = \Psi_D(t_f) = \Psi_M(t_f) = \Psi_B(t_f) = \Psi_G(t_f) = 0,$$

Proof. The Hamiltonian can be written as:

$$\begin{aligned}
\mathcal{H} &= w_1 z^2(t) - w_2 Y_B^2 + \sum_{i=1}^{6} \Psi_i F_i, \\
&= w_1 z^2(t) - w_2 Y_B^2 + \Psi_A(-k_{1f} Y_T Y_A + k_{1b} Y_D Y_B - k_{2f} Y_D Y_A + k_{2b} Y_M Y_B - k_{3f} Y_M Y_A \\
&+ k_{3b} Y_G Y_B) + \Psi_T(-k_{1f} Y_T Y_A + k_{1b} Y_D Y_B) + \Psi_D(k_{1f} Y_T Y_A - k_{1b} Y_D Y_B - k_{2f} Y_D Y_A \\
&+ k_{2b} Y_M Y_B) + \Psi_M(k_{2f} Y_D Y_A - k_{2b} Y_M Y_B - k_{3f} Y_M Y_A + k_{3b} Y_G Y_B) + \Psi_B\Big(k_{1f} Y_T Y_A \\
&- k_{1b} Y_D Y_B + k_{2f} Y_D Y_A - k_{2b} Y_M Y_B + k_{3f} Y_M Y_A - k_{3b} Y_G Y_B + \frac{Y_B}{z(t).M_r}\left(1 - \frac{Y_B}{B_{\max}}\right)\Big) \\
&+ \Psi_G(k_{3f} Y_M Y_A - k_{3b} Y_G Y_B),
\end{aligned} \tag{3.10}$$

where Ψ_A, Ψ_T,. . ., Ψ_G are adjoint variables and F_1, F_2,..., F_6 are functions defined in Equation (3.6). Differentiating the Hamiltonian (3.10) with respect to $z(t)$ we get:

$$\frac{\partial H}{\partial z^*(t)} = 0 = 2w_1 z^*(t) - \frac{\Psi_B Y_B (B_{max} - Y_B)}{M_r B_{max} z^{*2}},$$

$$\implies z^*(t) = \left\{ \frac{\Psi_B Y_B (B_{max} - Y_B)}{2w_1 M_r B_{max}} \right\}^{\frac{1}{3}}.$$

As $B_{max} \geq Y_B$ for all values of t, thus $z^*(t)$ will always exist and the value of $z^*(t)$ will be

$$z^*(t) = \begin{cases} 0 \quad when \quad \lambda \leq 0, \\ \lambda^{\frac{1}{3}} \quad when \quad 0 < \lambda < 1, \\ 1 \quad when \quad \lambda \geq 1, \end{cases} \tag{3.11}$$

where $\lambda = \frac{\Psi_B Y_B (B_{max} - Y_B)}{2w_1 M_r B_{max}}$, and also by the Pontryagin Minimum Principle, adjoint variables satisfy the following equations:

$$\begin{cases} \frac{d\Psi_A}{dt} = -\frac{\partial H}{\partial Y_A} & = k_{1f} Y_T (\Psi_A + \Psi_T - \Psi_D - \Psi_B) + k_{2f} Y_D (\Psi_A + \Psi_D - \Psi_M - \Psi_B) \\ & \quad + k_{3f} Y_M (\Psi_A + \Psi_M - \Psi_B - \Psi_G), \\ \frac{d\Psi_T}{dt} = -\frac{\partial H}{\partial Y_T} & = k_{1f} Y_A (\Psi_A + \Psi_T - \Psi_D - \Psi_B), \\ \frac{d\Psi_D}{dt} = -\frac{\partial H}{\partial Y_D} & = k_{1b} Y_B (-\Psi_A - \Psi_T + \Psi_D + \Psi_B) + k_{2f} Y_A (\Psi_A + \Psi_D - \Psi_M - \Psi_B), \\ \frac{d\Psi_M}{dt} = -\frac{\partial H}{\partial Y_M} & = k_{2b} Y_B (-\Psi_A - \Psi_D + \Psi_M + \Psi_B) + k_{3f} Y_A (\Psi_A + \Psi_M - \Psi_B - \Psi_G), \\ \frac{d\Psi_B}{dt} = -\frac{\partial H}{\partial Y_B} & = 2w_2 Y_B + k_{1b} Y_D (-\Psi_A - \Psi_T + \Psi_D + \Psi_B) + k_{2b} Y_M (-\Psi_A - \Psi_D + \\ & \quad \Psi_M + \Psi_B) + k_{3b} Y_G (-\Psi_A - \Psi_M + \Psi_B + \Psi_G) - \frac{1}{z(t) M_r} \left(1 - \frac{2Y_B}{B_{max}}\right), \\ \frac{d\Psi_G}{dt} = -\frac{\partial H}{\partial Y_G} & = k_{3b} Y_B (-\Psi_A - \Psi_M + \Psi_B + \Psi_G), \end{cases} \tag{3.12}$$

with the transversality conditions

$$\Psi_A(t_f) = \Psi_T(t_f) = \Psi_D(t_f) = \Psi_M(t_f) = \Psi_B(t_f) = \Psi_G(t_f) = 0.$$

□

In a similar way, we can write the control profile for MS i.e. for system (3.6) as

$$u^*(t) = \begin{cases} 0 \quad when \quad \xi \leq 0, \\ \xi^{\frac{1}{3}} \quad when \quad 0 < \xi < 1, \\ 1 \quad when \quad \xi \geq 1, \end{cases} \tag{3.13}$$

where $\xi = \frac{\Psi_B Y_B (B_{max} - Y_B)}{2 w_1 K_r B_{max}}$.

3.3 Numerical Results

In this section, we have implemented the ode45 solver in MATLAB to visualize the results numerically to understand the chem-dynamical reaction System (3.4) and System (3.5). Here, a comparison is made between MS and US frequency to determine the reduction of mass transfer resistance between MeOH and rapeseed oil (TG) more effectively. The study is performed at three distinct temperatures: 30°C, 50°C, and 65°C, using a vessel with a diameter of 1 m. Biodiesel production is evaluated at each temperature using various MeOH to TG molar ratios, employing both MS and US frequency. Molar ratio of MeOH and TG plays a crucial role in BD production process (Musa, 2016). Figure 3.2 (a), (b), and (c) show the comparison of mixing effect using MS and US frequency for biodiesel production at 50°C in 4:1, 5:1, and 6:1 molar ratios of MeOH and rapeseed oil, respectively. Here, MS speed is set at 600 rpm and US frequency is set at 50 kHz. Figure 3.2(a) shows that US frequency reduces the mass transfer resistance between the reactants more effectively than MS, as a result, higher biodiesel conversion is observed for US frequency. Due to the continuous application of high-intensity MS and US frequency in the system, a certain amount of MeOH gets evaporated, causing the actual MeOH amount in the system to be less than 3 moles, leading to a slight decrease in biodiesel production. From Figure 3.2(b) and Figure 3.2(c), it is clear that US frequency produces more biodiesel compared to MS. The presence of excess MeOH in the system increases the molar conversion of biodiesel for both 5:1 and 6:1 ratios, with the highest production observed at 6:1 molar ratio. In this way, we have achieved almost 93.66% and almost 95.33% biodiesel yields in just less than 60 minutes and 40 minutes, respectively, by the implementation of MS and US frequency, respectively. Hence, the US frequency proves to be more effective than MS for the same amount of molar ratio. Figure

Temp. (°C)	Molar Ratio (MeOH:TG)	MS (rpm)	US (kHz)	BD Yield (%)	BD Yield (Control) (%)	Time (min)
30	4:1	600	–	54.07	60.00	60
30	4:1	–	50	68.72	74.67	60
30	5:1	600	–	61.30	70.05	60
30	5:1	–	50	71.19	78.67	60
30	6:1	600	–	43.33	61.33	20
30	6:1	600	–	71.66	78.67	40
30	6:1	600	–	84.66	87.33	60
30	6:1	–	50	45.33	63.00	20
30	6:1	–	50	76.00	81.67	40
30	6:1	–	50	81.33	85.33	60
50	4:1	600	–	48.00	57.67	20
50	4:1	600	–	58.00	66.00	40
50	4:1	600	–	64.00	78.67	60
50	4:1	–	50	67.33	75.33	20
50	4:1	–	50	80.00	84.25	40
50	4:1	–	50	81.33	87.67	60
50	5:1	600	–	68.66	75.67	20
50	5:1	600	–	83.33	87.33	40
50	5:1	600	–	88.00	91.67	60
50	5:1	–	50	77.33	83.33	20
50	5:1	–	50	90.00	93.00	40
50	5:1	–	50	91.66	94.33	60
50	6:1	600	–	85.00	88.00	20
50	6:1	600	–	91.33	94.06	40
50	6:1	600	–	93.66	95.32	60
50	6:1	–	50	87.33	95.88	20
50	6:1	–	50	94.00	97.67	40
50	6:1	–	50	95.33	97.00	60
65	6:1	600	–	89.00	94.33	20
65	6:1	600	–	91.33	94.67	40
65	6:1	600	–	90.66	95.33	60
65	6:1	–	50	92.66	96.49	20
65	6:1	–	50	92.33	97.00	40
65	6:1	–	50	91.66	97.67	60

Table 3.3: *Percentages of biodiesel yields obtained in 20, 40, and 60 minutes during transesterification reactions at 30°C, 50°C, and 65°C, both with and without optimal control, for different MeOH to rapeseed oil molar ratios, stirrer speeds, and ultrasound frequencies. KOH catalyst concentration is 1 wt%.*

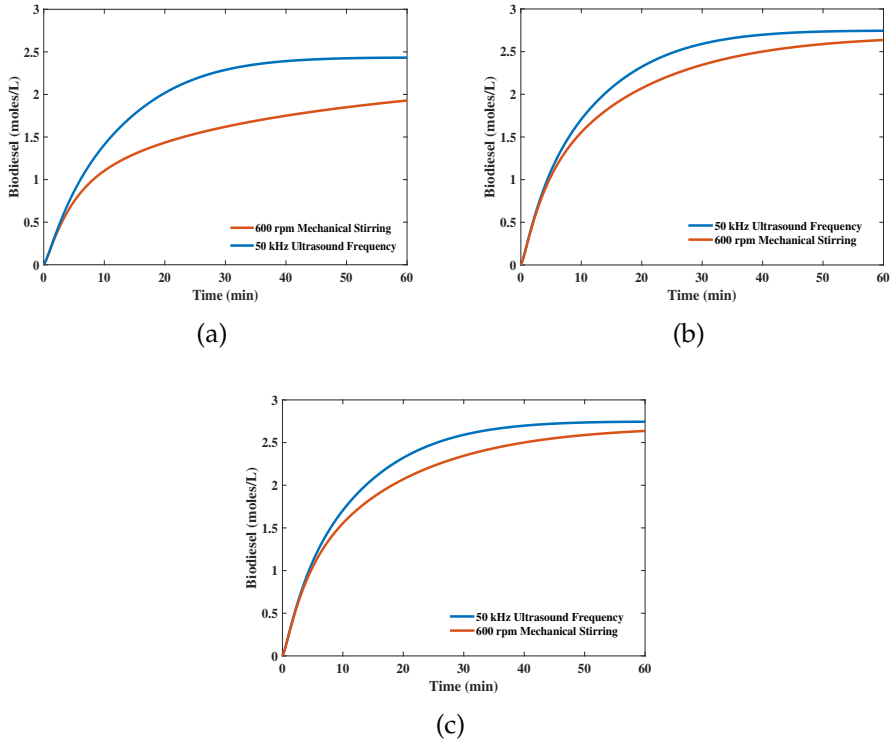

Figure 3.2: ***Comparison effect:*** *Comparison of molar conversion of biodiesel using MS and US frequency at (a) 4:1, (b) 5:1, and (c) 6:1 MeOH-to-TG molar ratio. Here, temperature is fixed at 50°C, stirrer rotation $f = 600$ rpm, and US frequency $H = 50$ kHz, with other parameter values taken from Table 3.1 and Table 3.2.*

3.3 demonstrates how increasing the reaction temperature affects the molar conversion of biodiesel when MS speed, US frequency and molar ratio of MeOH to TG is maintained at 600 rpm, 50 kHz and 6:1 respectively. It is evident from these three figures that biodiesel conversion is more when we have applied US frequency in the system. Figure 3.3(a) shows that it takes about 60 minutes to reduce the mass transfer resistance between MeOH and oil phases. When the temperature is increased from 30°C to 50°C, a higher production is started from 30 minutes. We have considered the reaction temperature in Figure 3.3(c) as 65°C. At this temperature, biodiesel conversion begins rapidly for both MS and US frequency, but production decreases after 30 minutes. Due to the higher temperature and continuous use of high intensity stirring or frequency, some amount of MeOH vaporizes, and TG, produced biodiesel, and free fatty acids (FFA) presence in the oil react with the catalyst to form soap. This leads to a lower final production compared to 50°C. This also proves that for a fixed temperature US frequency is more effective. In Figure 3.4(a), the impact

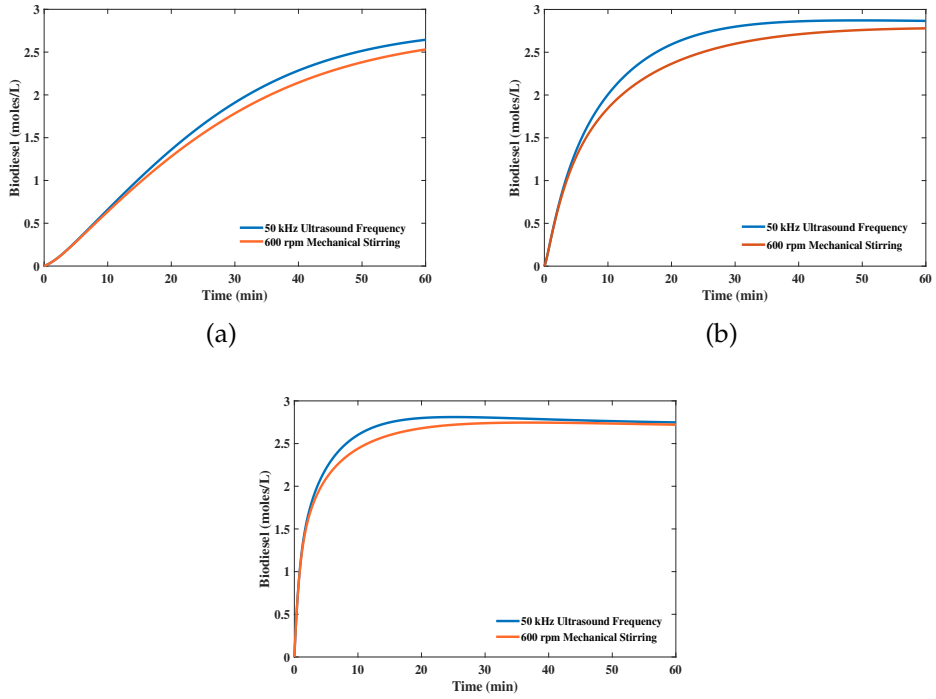

Figure 3.3: ***Comparison plot:*** *these plots depict the molar conversion of biodiesel due to MS and US frequency at three different temperatures: (a) 30°C, (b) 50°C, and (c) 65°C when MeOH:TG = 6:1, MS speed $f = 600$ rpm, US frequency $H = 50$ kHz and other parameter values are taken from Table 3.1 and Table 3.2.*

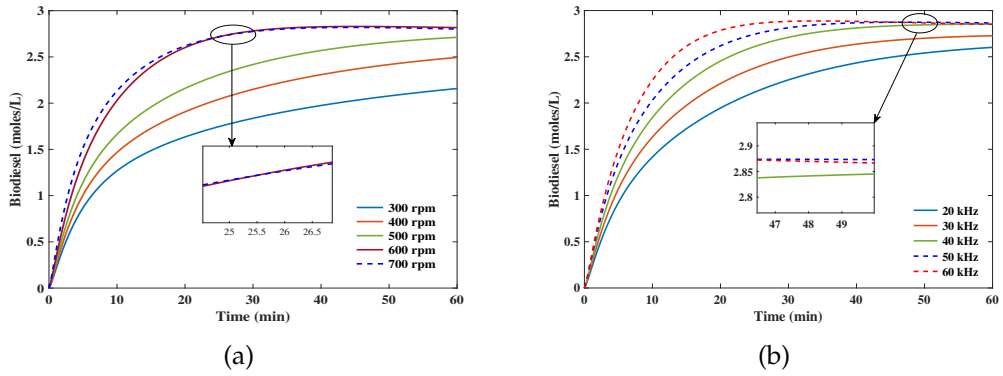

Figure 3.4: *(a)* ***MS effect:*** *BD yield when five different stirrer speeds are applied, (b)* ***US effect:*** *BD yield when five different US frequencies are applied. In both cases, MeOH:TG = 6:1, reaction temperature = 50°C, and other parameter values are taken from Table 3.1 and Table 3.2.*

of MS on biodiesel production is shown with a MeOH to TG ratio of 6:1 at a reaction temperature of 50°C. As the stirrer speed increases from 300 rpm to 600 rpm, biodiesel conversion also increases. At 700 rpm, biodiesel production starts rapidly

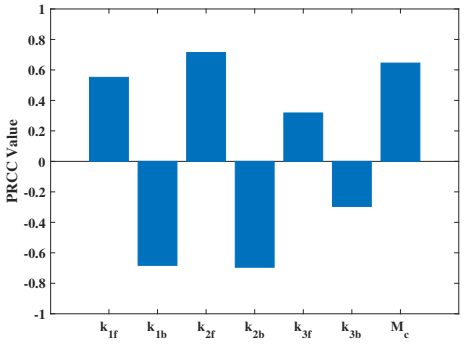

Figure 3.5: ***Sensitivity analysis:*** *Bar diagram displaying the sensitivity indices of the model parameters with the maximum biodiesel production by Partial Rank Correlation Coefficients (PRCCs) using Pearson's correlation coefficient.*

but begins to decrease after about 25 minutes, resulting in lower conversion than at 600 rpm. This reduction occurs because higher rotational speeds cause MeOH to vaporize, disrupting the MeOH to oil molar ratio. In Figure 3.4(b), the effect of US frequency is shown for the same molar ratio and temperature. At 50 kHz frequency, we have achieved the highest biodiesel yield. When frequency increase to 60 kHz, biodiesel production is initially higher but starts to decrease after around 45 minutes of reaction. Higher US frequency leads to a slight increase in reaction temperature, causing MeOH vaporization and saponification reactions, which reduces biodiesel yield conversion. We have conducted uncertainty analysis by considering assign all parameters are in uniform probability distribution. For each parameter, we have taken 1000 random samples by using the Latin hypercube sampling (LHS) technique (for details see (Dutta *et al.*, 2024)). In the bar Diagram (3.5), we have demonstrated the sensitivity index of reaction rates and mass transfer coefficients on final biodiesel yield. This figure allows us to determine the model's robustness to parameter values and identify the parameters that have a significant impact on final biodiesel yield. This figure suggests that M_c and k_{2f} are the most positively significant parameters, while k_{1b} and k_{2b} are the most negatively significant parameters for BD production.

For parameter sensitivity analysis we have implemented the combined LHS-PRCC approach (Marino *et al.*, 2008). In The scatter plots including the regression line (Figure 3.6) described the statistical impact of reaction rates and mass transfer coefficients on final biodiesel yield. The alignment of regression line indicates the qualitative relation between final biodiesel production and individual parameter's range. The p value represents the level of uncertainty related to each PRCC has

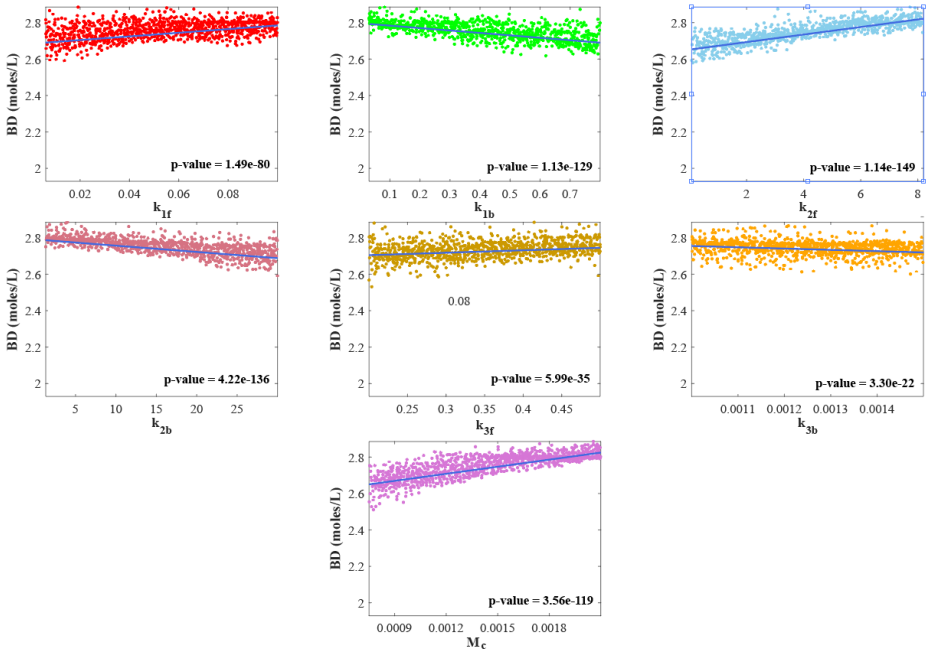

Figure 3.6: ***Scatter plots:*** *Scatter plots represent the different parametric ranges correlated to the biodiesel production with the regression line. Here, the significance level is 0.05 and for each parameter, the sample size is 1000 based on the LHS approach with uniform probability distribution.*

been calculated. For the numerical performance we have considered preassigned minimum allowed certainty or confidence level of 95 ($p \leq 0.05$) on PRCC values. The continuous use of high-intensity MS and US frequency causes some amount of MeOH to vaporize from the reaction vessel. As a result, additional methanol needs to be added to the system to achieve higher biodiesel yield, which increases the production costs. The study aims to maximize biodiesel yield in less time while minimizing production costs as much as possible. To address these requirements, we have applied optimal control on MS and US frequency in the system. Figure 3.7(a) and 3.7(b) represent the control profile for US frequency and MS, respectively. It is seen from Figure 3.7(a) that, initially a higher US frequency of 50 kHz is given in the system to reduce the initial mass transfer resistance between the reactants, after 22 minutes of reaction, the production has reached its equilibrium, so there is no need to apply further US frequency. We have seen from the above analysis that US frequency is more effective in reducing the mass transfer limitation than MS (see Figure 3.5(a)). It is needed to give stirrer rotation of 600 rpm a little bit more duration. After 36 minutes of reaction, there is no need to give higher rotation, so we can gradually decrease the stirring. This phenomenon is plotted in Figure 3.7(b). By regulating the MS and US frequency, MeOH does not vaporize from the system. So,

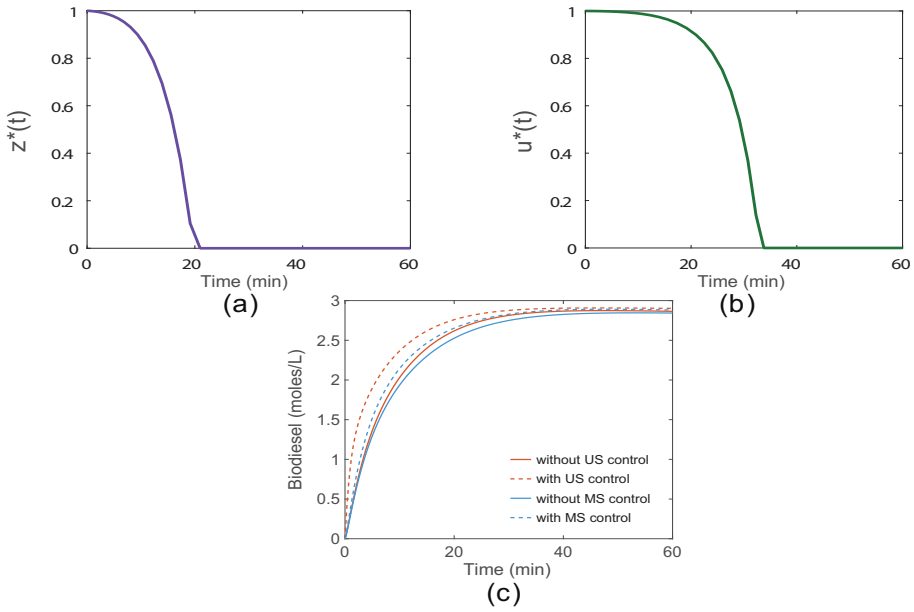

Figure 3.7: *(a)* ***Control profile for US frequency*** *has been plotted. The reaction has been started with 50 kHz of US frequency up to 22 minutes, after that the frequency is cut down to a lower frequency (b)* ***Control profile for MS*** *has been plotted here. 600 rpm of MS has been given up to 36 minutes and then its speed decreased gradually. In both cases, temperature = 50°C and MeOH:TG = 6:1, and (c) corresponding biodiesel molar conversion with respect to time and their comparison when no control is applied.*

there is always an adequate amount of methanol in the reaction vessel, eliminating the need to add extra methanol to the system. This reduces production costs and enables higher biodiesel production (see Figure 3.7(c)). This figure demonstrates that regulating the US frequency for a shorter duration still produces a higher yield compared to MS. From Figure 3.2 - 3.4, it is observed that the highest BD yield can be achieved at a stirring speed of 600 rpm for MS and at a frequency of 50 kHz for US, individually, when the MeOH-to-TG molar ratio is 6:1 and the temperature is 50°C. The bar diagram in Figure 3.8(a) illustrates the yield over various reaction times. The diagram clearly indicates that US frequency is more effective than MS in enhancing mass transfer between the reactants. However, the difference in BD conversion starts to decrease after 30 minutes. Using the same conditions outlined in Figure 3.8(a), the molar conversion of biodiesel was tracked over time with optimal control methods. Figure 3.8(b) visualizes these changes in conversion over time using a bar diagram. Biodiesel yield for these two scenarios and by varying temperature and molar ratio has been illustrated in Table 3.3. Additionally, a comparison is made for both without and with optimal control, and MS and US frequency by providing BD yield in 20 min, 40 min, and 60 min time intervals. Based on the data

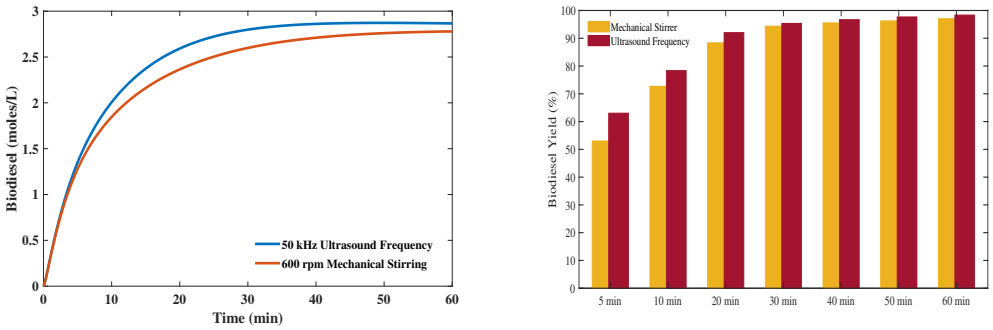

(a) (b)

Figure 3.8: ***Comparison Bar Diagram:*** *(a) Bar diagram has been plotted to show the biodiesel yield to compare the effectiveness of MS and US frequency without any type of regulation when MeOH:oil = 6:1, temperature is 50°C, stirrer speed $f = 600$ rpm and US frequency $H = 50$ kHz, (b) Bar diagram has been plotted when we regulate MS and US frequency over time for the same parameter values.*

provided in Table 3.3, one can produce 4-7% more biodiesel yield from rapeseed oil by controlling or regulating MS or US frequency over time in biodiesel production process, compared to when neither the MS nor the US frequency is controlled.

3.4 Discussions and Conclusions

In this chapter, we have investigated two mathematical models: one is for MS (System (3.4)) and another is for US frequency (System (3.5)) to compare the biodiesel production from the three-step transesterification reaction between methanol and rapeseed oil. To better understand the mixing effect during the reaction period of MeOH and TG, we have formulated mass transfer correlation for both MS and US frequency (see Equation (3.1) and Equation (3.2)) and compared their effect on BD production. Using these correlations of mass transfer, molar conversion of BD has been evaluated for different molar ratios (see Figure 3.2) and for different temperatures (see Figure 3.3). Also BD production has been observed for different MS (see Figure 3.4(a)) and US frequency (see Figure 3.4(b)) to compare the performance efficacy of these two external efforts. The bar Diagram 3.5 demonstrates the qualitative significance of reaction rates, which revealed the model robustness of final BD production against the reaction rates variations. We have also performed uncertainty analysis (Figure 3.6) to exhibit the statistical impacts of the considered reaction rates on the BD production, along with the correlations between the particular range of

reaction rates with the final biodiesel yields. Our uncertainty and PRCC analysis enhance the model's plausibility and indicate that M_c and k_{2f} are the most positively significant parameters, whereas k_{1b} and k_{2b} are the most negatively significant parameters for BD production. Once the initial mass transfer resistance is over-

Feedstocks	Catalyst	MeOH:TG	Temp. (°C)	MS/US	Time (min)	Outcomes (%) & Methods	Ref.
Jatropha Oil	KOH wt% 1.5	8:1	62	US	15	85.2 (ANN)	(Tan *et al.*, 2019)
Beniseed Oil	Mango, wt% 0.9	6:1	57	MS	60	93.6 (ANN)	(Adepoju and Okunola, 2015)
Soybean Oil	KOH wt% 1	9:1	60	MS	60	93.2 (ANN)	(Moradi *et al.*, 2013)
Sunflower Oil	KOH wt% 0.7	7.5:1	30	US	60	89.9 (ANN)	(Rajković *et al.*, 2013)
Fish Oil	KOH wt% 1.55	9.92:1	65	US	32.37	99.2 (RSM)	(Shenbaga Vinayaga Moorthi *et al.*, 2015)
Jatropha Oil	Heteropolyacid wt% 4.23	25:1	65	US	38	96.26 (ANN)	(Badday *et al.*, 2014)
Palm Oil	KOH wt% 2	12:1	50	US	60	92.81 (EXP.)	(Sajjadi *et al.*, 2017)
Ceiba Oil	KOH wt% 1	10:1	60	MS	108	99.80 (ANN)	(Kusumo *et al.*, 2017)
Jatropha+Ceiba Oil	KOH wt% 0.68	40%v/v	60	MS	120	93.70 (ANN)	(Dharma *et al.*, 2017)
Neem Oil	KOH wt% 1.2	7:1	50	US	30	94.47 (RSM)	(Maran and Priya, 2015)
Jatropha Oil	KOH wt% 1	6:1	50	US	50	97.00 (By controlling US frequency)	(Cao *et al.*, 2024)
Rapeseed Oil	KOH wt% 1	6:1	50	US	40	97.67 (By regulating US frequency)	Present study
Rapeseed Oil	KOH wt% 1	6:1	50	MS	60	95.32 (By regulating MS)	Present study

Table 3.4: *Optimal conditions reported in literature for biodiesel production using various transesterification processes.*

come, the reaction proceeds smoothly. After the initial state of reaction, the intense levels of mechanical stirring (MS) and ultrasound (US) frequency are no longer necessary. Therefore, to make the process cost-effective and ensure smooth reaction progression, it is essential to control or regulate both MS and US frequency. Here, we have applied optimal control theory to extend our formulated models by incorporating the suitable control parameters (see System (3.6) and System (3.7)). The control inputs $u(t)$ and $z(t)$ are employed for regulating the MS and US frequency, respectively, to overcome the initial mass transfer resistance between MeOH and TG. Evaluated optimal control parameters $u^*(t)$ and $z^*(t)$ (see Equation (3.11)) ensure the optimum use of MS and US frequency for biodiesel production with the

cost-effective manner. The numerical representations of optimal control profiles (see Figure 3.7) demonstrate that initially a higher efficacy of control input ($z^*(t)$ = 1 (H = 50 kHz)) is required to start the reaction and after 22 minutes no further US frequency is needed. On the other hand, when we are using MS, a higher efficacy of optimal control parameter ($u^*(t)$ = 1 (f = 600 rpm)) is required for a longer time (36 minutes) and then it gradually decreases until the end of the reaction. These results clearly indicate that the US frequency is more suitable for applying as an external effort with optimum manner to reduce the mass transfer resistance during the reaction.

Through our mathematical study along with the application of optimal control theory on MS and US frequency, we have achieved some important results while using significantly lower amounts of methanol and catalyst. We have compared our obtained results with the biodiesel production outcomes and optimal conditions reported in previously published articles (see Table 3.4). The present study depicts the reaction time i.e., 40 minutes for US and 60 minutes for MS, which is notably faster than the reports verified by several other experimental and theoretical studies (see Table 3.4). This also demonstrates that the optimum regulation of US frequency can lead to higher biodiesel production than the use of optimum mechanical stirring. Compared to our previous work using jatropha oil as feedstock (Cao *et al.*, 2024) under identical reaction conditions, the current study with rapeseed oil demonstrates a higher biodiesel yield achieved in a shorter time when ultrasound frequency is regulated over time in an optimum manner. This highlights the advantage of using rapeseed oil over jatropha oil, though jatropha is a second-generation crop.

The concentration of catalyst used for BD production also influences the production (Atadashi *et al.*, 2013), to avoid the mathematical complexity we have used KOH catalyst with fixed 1 wt% concentration. The work can be more improved if we will be able to capture the impact of the catalyst in another modified form. The reaction rates, which have used in this model have been considered from a small experimental study (Šánek *et al.*, 2019), that may not be directly usable for industrial-scale biodiesel production. Though there are few limitations, this model study will be highly beneficial for experimental researchers, and they can utilize its optimization techniques for biodiesel production.

In conclusion, our control-induced System (3.6) and System (3.7) demonstrate that optimally regulating mechanical stirring (MS) and ultrasound (US) frequency over time significantly enhances biodiesel production, with US frequency proving

more production than MS. This study also highlights that, despite being a first-generation crop, rapeseed oil is a more suitable feedstock for biodiesel production than jatropha oil when used optimally. Finally, at 50°C with a MeOH-to-rapeseed oil molar ratio of 6:1, a biodiesel yield of 95.33% can be obtained within 60 minutes at a stirrer speed of 600 rpm and by applying a 50 kHz ultrasound frequency, the yield can be increased to 97.67% in only 40 minutes.

4 Exploring Fractional-Order Nonlinear Dynamics in Biodiesel Production with Optimal Control

Earlier, in Chapter 2 and Chapter 3, we observed that ultrasound frequency is more effective than mechanical stirring in achieving proper mixing and reducing mass transfer resistance between methanol and triglycerides. In both chapters, the mathematical models were developed using ordinary differential equations with integer-order derivatives. However, it is possible that the transesterification reaction exhibits memory effects, which cannot be captured by integer-order models alone. To address this issue, the present chapter[1] develops a mathematical framework based on fractional-order derivatives, using Caputo–Fabrizio (CF) and Atangana–Baleanu in Caputo sense (ABC) operators to describe the transesterification process using another feedstock, Waste cooking oil (WCO). The models are validated against experimental data, highlighting the role of memory effect of transesterification reaction for biodiesel production dynamics.

4.1 Preliminaris

Definition 1 (Caputo, 1969): The Caputo fractional derivative of order $\alpha \in (n-1, n]$ of $f(x)$ is defined as

$$ {}_a^C D_x^\alpha f(x) = \frac{1}{\Gamma(\mathrm{n}-\alpha)} \int_a^x (x-t)^{n-\alpha-1} f^n(t) dt, \quad n = [\alpha] + 1. $$

[1]The maximum portion of this chapter has been published in *CSIAM Transactions on Applied Mathematics*, Global Science Press, doi: 10.4208/csiam-am.SO-2025-0016, (2025).

Definition 2 (Caputo and Fabrizio, 2015): Let $f \in \mathcal{H}'(a,b), b > a, 0 < \phi < 1$. Then, the CF fractional differential operator is defined as follows:

$$^{CF}D_x^{\phi}(f(x)) = \frac{M(\phi)}{1-\phi}\int_0^x \exp\left[-\frac{\phi(x-t)}{1-\phi}\right] f'(t)dt, x \geq 0, \quad 0 < \phi < 1.$$

The function $M(\phi)$ serves as a normalization function, dependent on ϕ and meets the condition $M(0) = M(1) = 1$.

Definition 3 (Atangana and Baleanu, 2016): The ABC fractional derivative in Caputo sense of a function $f(x) \in \mathcal{H}^1(a,b), b > a$ with $\theta \in (0,1]$ is defined as:

$$^{ABC}_{a}D_x^{\theta}f(x) = \frac{\vartheta(\theta)}{1-\theta}\int_a^x \frac{\mathrm{d}f}{\mathrm{d}t}E_{\theta}\left[-\frac{\theta}{1-\theta}(x-t)^{\theta}\right]\mathrm{d}t.$$

where $\mathcal{H}^1(a,b), b > a$ is a space of square-integrable functions and is defined as:

$$\mathcal{H}^1(a,b) = \left\{f(x) \in \mathbb{L}^2(a,b) \mid f'(x) \in \mathbb{L}^2(a,b)\right\}, \quad \text{and} \quad \vartheta(\theta) = 1-\theta+\frac{\theta}{\Gamma(\theta)}.$$

Definition 4 (Atangana and Baleanu, 2016): Let $f \in H^1(a,b)$ and $\theta \in (0,1]$. The θ th ABC fractional integral of the function $f(x)$ is:

$$^{AB}_{a}\mathrm{I}_x^{\theta}f(x) = \frac{(1-\theta)}{\vartheta(\theta)}f(x) + \frac{\theta}{\vartheta(\theta)\Gamma(\theta)}\int_a^x \frac{f(s)}{(x-s)^{1-\theta}}ds, \quad x \in [a,b]$$

where $\vartheta(\theta)$ is as defined in above.

4.2 The Basic Integer-Order Model and The Corresponding CF and ABC Fractional Order Model Formulation

To develop a mathematical model for the transesterification reaction between waste cooking oil (triglycerides) and methanol for biodiesel production, the following key assumptions are considered:

- **[L1]:** The transesterification process consists of three consecutive and reversible reaction steps, where triglycerides react with methanol to produce biodiesel and glycerol as a byproduct (Freedman *et al.*, 1986).

- **[L2]:** The reaction mixture contains a minimal amount of water (0.2% w/w), which is insufficient to significantly influence hydrolysis reactions. Hence, hydrolysis is neglected in this model (Xu *et al.*, 2005).
- **[L3]:** Since free fatty acids (FFAs) and other impurities are removed before transesterification, the saponification reaction is assumed to be negligible.

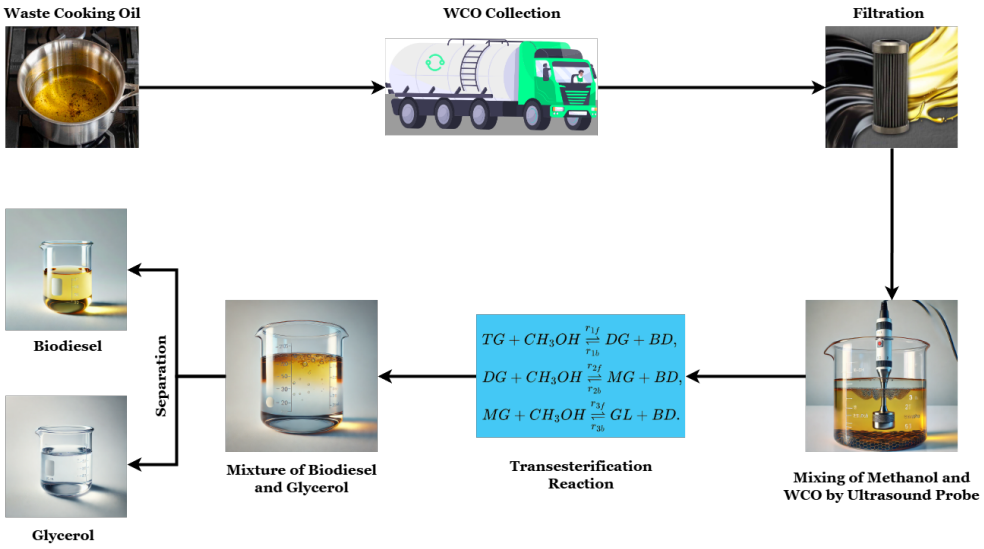

Figure 4.1: *Scheme for WCO collection from various restaurants and households, filtration and transesterification reaction to produce biodiesel using ultrasound frequency.*

In transesterification reaction, mass transfer resistance at the interface between methanol and triglyceride phases plays a crucial role, particularly in heterogeneous reaction systems where the reactants are immiscible. Factors such as high viscosity, poor solubility, and diffusion limitations contribute to mass transfer resistance. Ultrasound application significantly improves mass transfer by reducing phase boundary resistance through cavitation, leading to enhanced diffusion. The mass transfer coefficient, considering ultrasound effects, is estimated using a modified Dittus-Boelter correlation (Cao *et al.*, 2024):

$$M_c = \frac{1}{M_r} = 0.023 \frac{D}{d^2} (Re)^{0.8} (Sc)^{0.33} = 0.023 \frac{D}{d^2} \left(\frac{d^2 \rho H}{\mu} \right)^{0.8} \left(\frac{\mu}{\rho D} \right)^{0.33}, \tag{4.1}$$

where M_r represents mass transfer resistance (inverse of the mass transfer rate), while R_e and Sc denote the Reynolds and Schmidt numbers, respectively. The parameters D, ρ, μ correspond to diffusivity, density, and viscosity of waste cooking oil, while d is the reactor vessel diameter, and H is the applied ultrasound frequency.

Based on our previous studies (Cao *et al.*, 2024), we have identified that the optimal conditions for biodiesel production using ultrasound frequency are $H = 50$ kHz, $T = 50°C$, a methanol-to-triglyceride molar ratio is 5:1, and a reactor diameter $d = 1$ meter. This whole study is conducted under these optimized conditions. The

Parameter	Definition	Value
D	diffusivity of WCO	$1.00 \times 10^{-7} - 1.5 \times 10^{-7}$ m^2 s^{-1}
ρ	density of WCO	880 kg m^{-3}
μ	viscosity of WCO	26.1 kg m^{-1}s^{-1}
d	vessel diameter	1 m
H	ultrasound frequency	30–60 kHz

Table 4.1: *Liquid properties of waste cooking oil and input ranges of ultrasound frequency and vessel size used in the reaction at 50°C.*

transesterification reaction occurs in the presence of a KOH catalyst and follows a three-step reversible mechanism (Freedman *et al.*, 1986):

- Step 1: Triglyceride (TG) reacts with methanol (AL) to form diglyceride (DG) and biodiesel (BD).
- Step 2: Diglyceride (DG) reacts with methanol (AL) to produce monoglyceride (MG) and biodiesel (BD).
- Step 3: Monoglyceride (MG) reacts with methanol (AL) to yield biodiesel (BD) and glycerol (GL).

The overall reaction mechanism is:

$$\begin{aligned} \boldsymbol{TG + CH_3OH} &\underset{r_{1b}}{\overset{r_{1f}}{\rightleftharpoons}} \boldsymbol{DG + BD}, \\ \boldsymbol{DG + CH_3OH} &\underset{r_{2b}}{\overset{r_{2f}}{\rightleftharpoons}} \boldsymbol{MG + BD}, \\ \boldsymbol{MG + CH_3OH} &\underset{r_{3b}}{\overset{r_{3f}}{\rightleftharpoons}} \boldsymbol{GL + BD}. \end{aligned} \tag{4.2}$$

The rate constants r_{1f}, r_{2f}, r_{3f} (forward reaction) and r_{1b}, r_{2b}, r_{3b} (backward reaction) follow the Arrhenius equation:

$$r_i = A_i e^{\frac{-E_{A_i}}{RT}} \tag{4.3}$$

where A_i is the frequency factor, E_{A_i} is the activation energy, T is the reaction temperature, and R is the universal gas constant (Benavides and Diwekar, 2012). Table 4.1 lists the parameter values used in forming the mass transfer coefficient, while

Table 4.2 presents the reaction rates of the transesterification reaction.

1. Integer-Order Differential System:

The governing ordinary differential equations (ODEs) for the reaction mechanism, considering mass transfer effects, are formulated as follows:

$$\begin{cases} \frac{dT}{dt} & = -r_{1f}TA + r_{1b}DB, \\ \frac{dA}{dt} & = -r_{1f}TA + r_{1b}DB - r_{2f}DA + r_{2b}MB - r_{3f}MA + r_{3b}GB, \\ \frac{dD}{dt} & = r_{1f}TA - r_{1b}DB - r_{2f}DA + r_{2b}MB, \\ \frac{dM}{dt} & = r_{2f}DA - r_{2b}MB - r_{3f}MA + r_{3b}GB, \\ \frac{dB}{dt} & = r_{1f}TA - r_{1b}DB + r_{2f}DA - r_{2b}MB + r_{3f}MA - r_{3b}GB + \frac{B}{M_r}\left(1 - \frac{B}{B_{\max}}\right), \\ \frac{dG}{dt} & = r_{3f}MA - r_{3b}GB, \end{cases} \tag{4.4}$$

where B, T, D, M, A, and G are the concentration of biodiesel, triglyceride, diglyceride, monoglyceride, methanol, and glycerol respectively with initial condition $T(0) = T_0$, $A(0) = A_0$, $D(0) = 0$, $M(0) = 0$, $B(0) = 0$, and $G(0) = 0$.

Now, we extend the integer-order model to a fractional-order framework by replacing the time derivative with two distinct non-singular kernels: the exponentially decay type kernel and the Mittag-Leffler kernel. However, this substitution disrupts dimensional consistency, as directly replacing an integer-order derivative with a fractional derivative (CF or ABC) in a dimensionally balanced equation is mathematically still questionable. To resolve this issue, we introduce the memory rate parameter R with dimensions as same as (1/minute) on the left side of the fractional model. This memory rate parameter ensures dimensional coherence, preserving mathematical consistency and stability in the modified system.

2. Caputo–Fabrizio Fractional Model:

Using the CF fractional operator, the model is reformulated as:

$$\begin{cases} R^{(1-\phi)}\,{}^{CF}D_t^{\phi}T(t) & = -r_{1f}TA + r_{1b}DB, \\ R^{(1-\phi)}\,{}^{CF}D_t^{\phi}A(t) & = -r_{1f}TA + r_{1b}DB - r_{2f}DA + r_{2b}MB - r_{3f}MA + r_{3b}GB, \\ R^{(1-\phi)}\,{}^{CF}D_t^{\phi}D(t) & = r_{1f}TA - r_{1b}DB - r_{2f}DA + r_{2b}MB, \\ R^{(1-\phi)}\,{}^{CF}D_t^{\phi}M(t) & = r_{2f}DA - r_{2b}MB - r_{3f}MA + r_{3b}GB, \\ R^{(1-\phi)}\,{}^{CF}D_t^{\phi}B(t) & = r_{1f}TA - r_{1b}DB + r_{2f}DA - r_{2b}MB + r_{3f}MA - r_{3b}GB + \frac{B}{M_r}\left(1 - \frac{B}{B_{\max}}\right), \\ R^{(1-\phi)}\,{}^{CF}D_t^{\phi}G(t) & = r_{3f}MA - r_{3b}GB, \end{cases} \tag{4.5}$$

with the same initial condition as above and $\phi \in (0, 1]$ is the order of the CF fractional system.

3. ABC Fractional Model:

For the ABC fractional operator, considering the memory rate parameter R (previously defined), the governing equations are:

$$\begin{cases} R^{(1-\theta)}\ {}^{ABC}D_t^{\theta}T(t) & = -r_{1f}TA + r_{1b}DB, \\ R^{(1-\theta)}\ {}^{ABC}D_t^{\theta}A(t) & = -r_{1f}TA + r_{1b}DB - r_{2f}DA + r_{2b}MB - r_{3f}MA + r_{3b}GB, \\ R^{(1-\theta)}\ {}^{ABC}D_t^{\theta}D(t) & = r_{1f}TA - r_{1b}DB - r_{2f}DA + r_{2b}MB, \\ R^{(1-\theta)}\ {}^{ABC}D_t^{\theta}M(t) & = r_{2f}DA - r_{2b}MB - r_{3f}MA + r_{3b}GB, \\ R^{(1-\theta)}\ {}^{ABC}D_t^{\theta}B(t) & = r_{1f}TA - r_{1b}DB + r_{2f}DA - r_{2b}MB + r_{3f}MA - r_{3b}GB + \frac{B}{M_r}\left(1 - \frac{B}{B_{\max}}\right), \\ R^{(1-\theta)}\ {}^{ABC}D_t^{\theta}G(t) & = r_{3f}MA - r_{3b}GB, \end{cases} \tag{4.6}$$

with the same initial condition as above, i.e., $T(0) = T_0$, $A(0) = A_0$, $D(0) = 0$, $M(0) = 0$, $B(0) = 0$, and $G(0) = 0$ and here $\theta \in (0, 1]$ represents the order of the ABC fractional derivative.

Parameter	Definition	Value (mol^{-1} L min^{-1})
r_{1f}	forward reaction constant	0.102
r_{1b}	backward reaction constant	0.021
r_{2f}	forward reaction constant	0.053
r_{2b}	backward reaction constant	0.010
r_{3f}	forward reaction constant	0.015
r_{3b}	backward reaction constant	0.164

Table 4.2: *Values of various reaction rate constants used in the transesterification reaction, adopted from (Takase, 2022). These constants are essential for modeling the biodiesel production process and influence the reaction kinetics.*

4.3 Existence and Uniqueness of the Transesterification Reaction System

In this section, we establish the existence and uniqueness of solutions for the fractional Model (4.6) based on the ABC derivative. The existence of solutions ensures the mathematical consistency of the ABC fractional model, confirming that solutions can be obtained under well-defined conditions. Uniqueness guarantees deterministic and unambiguous outcomes, which are essential for reliable real-world predictions. These properties validate the robustness of the model, ensuring its reliable application in biodiesel production, where precision and reproducibility are essential for optimizing reaction efficiency, improving yield, and enhancing process sustainability in industrial and environmental settings. To illustrate the existence

and uniqueness of our proposed model, we employ the well-known Banach fixed-point theorem and the Arzelà-Ascoli theorem.

4.3.1 Existence of System

Applying the ABC integral operator to both sides of the System (4.6), we obtain:

$$\begin{cases} T(t)-T(0) = & R^{(\theta-1)}\,{}^{ABC}I^{\theta}_{0,t}(-r_{1f}TA+r_{1b}DB), \\ A(t)-A(0) = & R^{(\theta-1)}\,{}^{ABC}I^{\theta}_{0,t}(-r_{1f}TA+r_{1b}DB-r_{2f}DA+r_{2b}MB-r_{3f}MA+r_{3b}GB), \\ D(t)-D(0) = & R^{(\theta-1)}\,{}^{ABC}I^{\theta}_{0,t}(r_{1f}TA-r_{1b}DB-r_{2f}DA+r_{2b}MB), \\ M(t)-M(0) = & R^{(\theta-1)}\,{}^{ABC}I^{\theta}_{0,t}(r_{2f}DA-r_{2b}MB-r_{3f}MA+r_{3b}GB), \\ B(t)-B(0) = & R^{(\theta-1)}\,{}^{ABC}I^{\theta}_{0,t}(r_{1f}TA-r_{1b}DB+r_{2f}DA-r_{2b}MB+r_{3f}MA-r_{3b}GB \\ & +\frac{B}{M_r}\left(1-\frac{B}{B_{\max}}\right)), \\ G(t)-G(0) = & R^{(\theta-1)}\,{}^{ABC}I^{\theta}_{0,t}(r_{3f}MA-r_{3b}GB). \end{cases} \tag{4.7}$$

This implies that:

$$\begin{cases} T(t)-T(0) = \frac{R^{(\theta-1)}(1-\theta)}{\vartheta(\theta)}\mathcal{G}_1(T(t),t)+\frac{R^{(\theta-1)}\theta}{\vartheta(\theta)\Gamma(\theta)}\times\int_0^t(t-s)^{\theta-1}\mathcal{G}_1(T(s),s)ds, \\ A(t)-A(0) = \frac{R^{(\theta-1)}(1-\theta)}{\vartheta(\theta)}\mathcal{G}_2(A(t),t)+\frac{R^{(\theta-1)}\theta}{\vartheta(\theta)\Gamma(\theta)}\times\int_0^t(t-s)^{\theta-1}\mathcal{G}_2(A(s),s)ds, \\ D(t)-D(0) = \frac{R^{(\theta-1)}(1-\theta)}{\vartheta(\theta)}\mathcal{G}_3(D(t),t)+\frac{R^{(\theta-1)}\theta}{\vartheta(\theta)\Gamma(\theta)}\times\int_0^t(t-s)^{\theta-1}\mathcal{G}_3(D(s),s)ds, \\ M(t)-M(0) = \frac{R^{(\theta-1)}(1-\theta)}{\vartheta(\theta)}\mathcal{G}_4(M(t),t)+\frac{R^{(\theta-1)}\theta}{\vartheta(\theta)\Gamma(\theta)}\times\int_0^t(t-s)^{\theta-1}\mathcal{G}_4(M(s),s)ds, \\ B(t)-B(0) = \frac{R^{(\theta-1)}(1-\theta)}{\vartheta(\theta)}\mathcal{G}_5(B(t),t)+\frac{R^{(\theta-1)}\theta}{\vartheta(\theta)\Gamma(\theta)}\times\int_0^t(t-s)^{\theta-1}\mathcal{G}_5(B(s),s)ds, \\ G(t)-G(0) = \frac{R^{(\theta-1)}(1-\theta)}{\vartheta(\theta)}\mathcal{G}_6(G(t),t)+\frac{R^{(\theta-1)}\theta}{\vartheta(\theta)\Gamma(\theta)}\times\int_0^t(t-s)^{\theta-1}\mathcal{G}_6(G(s),s)ds. \end{cases} \tag{4.8}$$

Where the kernels $\mathcal{G}_i, i=1,2,...,6$ are defined as,

$$\begin{cases} \mathcal{G}_1(T(t),t) = -r_{1f}TA+r_{1b}DB, \\ \mathcal{G}_1(T(t),t) = -r_{1f}TA+r_{1b}DB-r_{2f}DA+r_{2b}MB-r_{3f}MA+r_{3b}GB, \\ \mathcal{G}_1(T(t),t) = r_{1f}TA-r_{1b}DB-r_{2f}DA+r_{2b}MB, \\ \mathcal{G}_1(T(t),t) = r_{2f}DA-r_{2b}MB-r_{3f}MA+r_{3b}GB, \\ \mathcal{G}_1(T(t),t) = r_{1f}TA-r_{1b}DB+r_{2f}DA-r_{2b}MB+r_{3f}MA-r_{3b}GB+\frac{B}{M_r}\left(1-\frac{B}{B_{\max}}\right), \\ \mathcal{G}_1(T(t),t) = r_{3f}MA-r_{3b}GB. \end{cases}$$

Let $\mathcal{L}$ be the linear operator acting on the entire System (4.8), defined as:

$$\begin{cases} \mathcal{L}(T(t)) = \frac{R^{(\theta-1)}(1-\theta)}{\vartheta(\theta)}\mathcal{G}_1(T(t),t)+\frac{R^{(\theta-1)}\theta}{\vartheta(\theta)\Gamma(\theta)}\times\int_0^t(t-s)^{\theta-1}\mathcal{G}_1(T(s),s)ds, \\ \mathcal{L}(A(t)) = \frac{R^{(\theta-1)}(1-\theta)}{\vartheta(\theta)}\mathcal{G}_2(A(t),t)+\frac{R^{(\theta-1)}\theta}{\vartheta(\theta)\Gamma(\theta)}\times\int_0^t(t-s)^{\theta-1}\mathcal{G}_2(A(s),s)ds, \\ \mathcal{L}(D(t)) = \frac{R^{(\theta-1)}(1-\theta)}{\vartheta(\theta)}\mathcal{G}_3(D(t),t)+\frac{R^{(\theta-1)}\theta}{\vartheta(\theta)\Gamma(\theta)}\times\int_0^t(t-s)^{\theta-1}\mathcal{G}_3(D(s),s)ds, \\ \mathcal{L}(M(t)) = \frac{R^{(\theta-1)}(1-\theta)}{\vartheta(\theta)}\mathcal{G}_4(M(t),t)+\frac{R^{(\theta-1)}\theta}{\vartheta(\theta)\Gamma(\theta)}\times\int_0^t(t-s)^{\theta-1}\mathcal{G}_4(M(s),s)ds, \\ \mathcal{L}(B(t)) = \frac{R^{(\theta-1)}(1-\theta)}{\vartheta(\theta)}\mathcal{G}_5(B(t),t)+\frac{R^{(\theta-1)}\theta}{\vartheta(\theta)\Gamma(\theta)}\times\int_0^t(t-s)^{\theta-1}\mathcal{G}_5(B(s),s)ds, \\ \mathcal{L}(G(t)) = \frac{R^{(\theta-1)}(1-\theta)}{\vartheta(\theta)}\mathcal{G}_6(G(t),t)+\frac{R^{(\theta-1)}\theta}{\vartheta(\theta)\Gamma(\theta)}\times\int_0^t(t-s)^{\theta-1}\mathcal{G}_6(G(s),s)ds. \end{cases} \tag{4.9}$$

Now we have to prove that $\mathcal{L}(H)$, where $H = [T(t), A(t), D(t), M(t), B(t), G(t)]^T$ is compact to ensure the existence and boundedness of the solutions of the System (4.6). Consider the first equation of the System (4.9), we can write,

$$\begin{aligned}
\|\mathcal{L}(T(t))\| &= \Big\|\frac{R^{(\theta-1)}(1-\theta)}{\vartheta(\theta)}\mathcal{G}_1(T(t),t) + \frac{R^{(\theta-1)}\theta}{\vartheta(\theta)\Gamma(\theta)} \times \int_0^t (t-s)^{\theta-1}\mathcal{G}_1(T(s),s)ds\Big\|, \\
&\leq \frac{R^{(\theta-1)}(1-\theta)}{\vartheta(\theta)}\|\mathcal{G}_1(T(t),t)\| + \frac{R^{(\theta-1)}\theta}{\vartheta(\theta)\Gamma(\theta)} \times \| \int_0^t (t-s)^{\theta-1}\mathcal{G}_1(T(s),s)ds\|, \\
&= \frac{R^{(\theta-1)}(1-\theta)}{\vartheta(\theta)}\|\mathcal{G}_1(T(t),t)\| + \frac{R^{(\theta-1)}T^{\theta}}{\vartheta(\theta)\Gamma(\theta)} \times \| \int_0^t \mathcal{G}_1(T(s),s)ds\|, \\
&\leq \Big[\frac{R^{(\theta-1)}(1-\theta)}{\vartheta(\theta)} + K_1\frac{R^{(\theta-1)}T^{\theta}}{\vartheta(\theta)\Gamma(\theta)}\Big]\|\mathcal{G}_1(T(t),t)\|.
\end{aligned} \tag{4.10}$$

We can assume that there exist some positive real numbers $\nu_1, \nu_2, \nu_3, \nu_4, \nu_4$, and ν_6 such that $\|T(t)\| \leq \nu_1$, $\|A(t)\| \leq \nu_2$, $\|D(t)\| \leq \nu_3$, $\|M(t)\| \leq \nu_4$, $\|B(t)\| \leq \nu_5$, and $\|G(t)\| \leq \nu_6$. Let

$$\mathcal{B}_1 = \max_{\substack{t\in[0,T]\\ T\in[0,\nu_1]}} \mathcal{G}_1(T(t),t),$$

and utilizing this in the Equation (4.10), we get

$$\|\mathcal{L}(T(t))\| \leq \mathcal{B}_1\Big[\frac{R^{(\theta-1)}(1-\theta)}{\vartheta(\theta)} + K_1\frac{R^{(\theta-1)}T^{\theta}}{\vartheta(\theta)\Gamma(\theta)}\Big]. \tag{4.11}$$

Proceeding similarly, we can obtain that

$$\begin{cases}
\|\mathcal{L}(A(t))\| \leq \mathcal{B}_2\Big[\frac{R^{(\theta-1)}(1-\theta)}{\vartheta(\theta)} + K_2\frac{R^{(\theta-1)}T^{\theta}}{\vartheta(\theta)\Gamma(\theta)}\Big], \\
\|\mathcal{L}(D(t))\| \leq \mathcal{B}_3\Big[\frac{R^{(\theta-1)}(1-\theta)}{\vartheta(\theta)} + K_3\frac{R^{(\theta-1)}T^{\theta}}{\vartheta(\theta)\Gamma(\theta)}\Big], \\
\|\mathcal{L}(M(t))\| \leq \mathcal{B}_4\Big[\frac{R^{(\theta-1)}(1-\theta)}{\vartheta(\theta)} + K_4\frac{R^{(\theta-1)}T^{\theta}}{\vartheta(\theta)\Gamma(\theta)}\Big], \\
\|\mathcal{L}(B(t))\| \leq \mathcal{B}_5\Big[\frac{R^{(\theta-1)}(1-\theta)}{\vartheta(\theta)} + K_5\frac{R^{(\theta-1)}T^{\theta}}{\vartheta(\theta)\Gamma(\theta)}\Big], \\
\|\mathcal{L}(G(t))\| \leq \mathcal{B}_6\Big[\frac{R^{(\theta-1)}(1-\theta)}{\vartheta(\theta)} + K_6\frac{R^{(\theta-1)}T^{\theta}}{\vartheta(\theta)\Gamma(\theta)}\Big].
\end{cases}$$

Where

$$\begin{cases}
\mathcal{B}_2 = \max\limits_{\substack{t\in[0,T]\\ A\in[0,\nu_2]}} \mathcal{G}_2(A(t),t), & \mathcal{B}_3 = \max\limits_{\substack{t\in[0,T]\\ D\in[0,\nu_3]}} \mathcal{G}_3(D(t),t), \\
\mathcal{B}_4 = \max\limits_{\substack{t\in[0,T]\\ M\in[0,\nu_4]}} \mathcal{G}_4(M(t),t), & \mathcal{B}_5 = \max\limits_{\substack{t\in[0,T]\\ B\in[0,\nu_5]}} \mathcal{G}_5(B(t),t), \\
\mathcal{B}_6 = \max\limits_{\substack{t\in[0,T]\\ G\in[0,\nu_6]}} \mathcal{G}_6(G(t),t). &
\end{cases}$$

Therefore $\mathcal{L}(H)$ is bounded. Let us consider $t_2 > t_1$ and for a given $\epsilon > 0$, there exist a $\delta > 0$ such that $\|t_2 - t_2\| < \delta$. Now we can write for that first equation as,

$$\begin{aligned}\|\mathcal{G}_1(T(t_2), t_2) - \mathcal{G}_1(T(t_1), t_1)\| &= \|(-r_{1f}T(t_2)A(t) + r_{1b}D(t)B(t)) \\ &\quad - (-r_{1f}T(t_1)A(t) + r_{1b}D(t)B(t))\|, \\ &\leq r_{1f}\nu_2\|T(t_2) - T(t_1)\|.\end{aligned} \tag{4.12}$$

Assuming that if the function $T(t)$ is Lipschitz continuous i.e. there exists for some real number $\chi_1 > 0$ and for all t_2, t_1, the inequality $\|T(t_2) - T(t_1)\| \leq \chi_1\|t_2 - t_1\|$ holds. We rewrite the Equation (4.12) as,

$$\|\mathcal{G}_1(T(t_2), t_2) - \mathcal{G}_1(T(t_1).t_1)\| \leq \mathcal{R}_1\|t_2 - t_1\|. \tag{4.13}$$

Where $\mathcal{R}_1 = r_{1f}\nu_2\chi_1$. Similarly, if the other population of the system $A(t)$, $D(t)$, $G(t)$, $B(t)$, and $G(t)$ are Lipschitz continuous, then there exist some positive real numbers $\mathcal{R}_i, i = 2, 3, ..., 6$, for which we can write as following:

$$\begin{cases} \|\mathcal{G}_2(A(t_2), t_2) - \mathcal{G}_2(A(t_1).t_1)\| & \leq \mathcal{R}_2\|t_2 - t_1\|, \\ \|\mathcal{G}_3(D(t_2), t_2) - \mathcal{G}_3(D(t_1).t_1)\| & \leq \mathcal{R}_3\|t_2 - t_1\|, \\ \|\mathcal{G}_4(M(t_2), t_2) - \mathcal{G}_4(M(t_1).t_1)\| & \leq \mathcal{R}_4\|t_2 - t_1\|, \\ \|\mathcal{G}_5(B(t_2), t_2) - \mathcal{G}_5(B(t_1).t_1)\| & \leq \mathcal{R}_5\|t_2 - t_1\|, \\ \|\mathcal{G}_6(G(t_2), t_2) - \mathcal{G}_6(G(t_1).t_1)\| & \leq \mathcal{R}_6\|t_2 - t_1\|. \end{cases} \tag{4.14}$$

Furthermore, Using the the Equation (4.10) with the inequality (4.13), we have

$$\begin{aligned}\|\mathcal{L}(T(t_2)) - \mathcal{L}(T(t_1))\| &\leq \left\| \left[\frac{R^{(\theta-1)}(1-\theta)}{\vartheta(\theta)} + K_1 \frac{R^{(\theta-1)}T^{\theta}}{\vartheta(\theta)\Gamma(\theta)} \right] (\mathcal{G}_1(T(t_2), t_2) - \mathcal{G}_1(T(t_1), t_1)) \right\|, \\ &\leq \left[\frac{R^{(\theta-1)}(1-\theta)}{\vartheta(\theta)} + K_1 \frac{R^{(\theta-1)}T^{\theta}}{\vartheta(\theta)\Gamma(\theta)} \right] \mathcal{R}_1\|t_2 - t_1\|.\end{aligned} \tag{4.15}$$

Choosing, $\delta = \dfrac{\epsilon}{\left[\frac{R^{(\theta-1)}(1-\theta)}{\vartheta(\theta)} + K_1 \frac{R^{(\theta-1)}T^{\theta}}{\vartheta(\theta)\Gamma(\theta)} \right] \mathcal{R}_1}$ and we can see that $\|\mathcal{L}(T(t_2)) - \mathcal{L}(T(t_1))\| < \epsilon$ whenever $\|t_2 - t_1\| < \delta$. Proceeding similarly, we can show that $\|\mathcal{L}(H(t_2)) - \mathcal{L}(H(t_1))\| < \epsilon$, where $H = [A(t), D(t), M(t), B(t), G(t)]^T$. Hence according to the Arzela-Ascoli theorem (Lebl, 2018), we can say that the operator $\mathcal{L}(H)$ is compact. Therefore the solutions of the fractional System (4.6), corresponding to the method exist. Now we prove the uniqueness of this solution in the subsequent section.

4.3.2 Uniqueness of System

Let $T(t)$ and $T'(t)$ be the two solutions of the fractional System (4.6). Then for the first population, we can write as,

$$\begin{aligned}\|\mathcal{G}_1(T(t),t)-\mathcal{G}_1(T'(t),t)\| &= \|-r_{1f}A(t)(T(t)-T'(t))\|,\\ &\leq \Delta_1\|T(t)-T'(t)\|,\end{aligned} \tag{4.16}$$

where $\Delta_1 = r_{1f}\nu_1$. Similarly, we obtain for the other population as follows:

$$\begin{cases}\|\mathcal{G}_2(A(t),t)-\mathcal{G}_2(A'(t),t)\| \leq \Delta_2\|A(t)-A'(t)\|,\\ \|\mathcal{G}_3(D(t),t)-\mathcal{G}_3(D'(t),t)\| \leq \Delta_3\|D(t)-D'(t)\|,\\ \|\mathcal{G}_4(M(t),t)-\mathcal{G}_4(M'(t),t)\| \leq \Delta_4\|M(t)-M'(t)\|,\\ \|\mathcal{G}_5(B(t),t)-\mathcal{G}_5(B'(t),t)\| \leq \Delta_5\|B(t)-B'(t)\|,\\ \|\mathcal{G}_6(G(t),t)-\mathcal{G}_6(G'(t),t)\| \leq \Delta_6\|G(t)-G'(t)\|.\end{cases}$$

Now we prove the uniqueness of the solution of the System (4.6). For this, let us consider the linear operator $\mathcal{L}$ again, which is defined in the previous section, and using the relation in Equation (4.16), we obtain,

$$\begin{aligned}\|\mathcal{L}(T(t))-\mathcal{L}(T'(t))\| &= \Big\|\frac{R^{(\theta-1)}(1-\theta)}{\vartheta(\theta)}(\mathcal{G}_1(T(t),t)-\mathcal{G}_1(T'(t),t))+\frac{R^{(\theta-1)}\theta}{\vartheta(\theta)\Gamma(\theta)}\times\\ &\qquad\int_0^t(t-s)^{\theta-1}(\mathcal{G}_1(T(s),s)-\mathcal{G}_1(T'(s),s))ds\Big\|,\\ &\leq \frac{R^{(\theta-1)}(1-\theta)}{\vartheta(\theta)}\|\mathcal{G}_1(T(t),t)-\mathcal{G}_1(T'(t),t)\|+\frac{R^{(\theta-1)}T^\theta}{\vartheta(\theta)\Gamma(\theta)}\times\\ &\qquad\Big\|\int_0^t\mathcal{G}_1(T(s),s)-\mathcal{G}_1(T'(s),s)ds\Big\|,\\ &\leq \Big[\frac{R^{(\theta-1)}(1-\theta)}{\vartheta(\theta)}\Delta_1+K_1\frac{R^{(\theta-1)}T^\theta}{\vartheta(\theta)\Gamma(\theta)}\Delta_1\Big]\|T(t)-T'(t)\|.\end{aligned}$$

Proceeding similarly for other equations, we can obtain

$$\begin{cases}\|\mathcal{L}(A(t))-\mathcal{L}(A'(t))\| \leq \Big[\frac{R^{(\theta-1)}(1-\theta)}{\vartheta(\theta)}\Delta_2+K_2\frac{R^{(\theta-1)}T^\theta}{\vartheta(\theta)\Gamma(\theta)}\Delta_2\Big]\|A(t)-A'(t)\|,\\ \|\mathcal{L}(D(t))-\mathcal{L}(D'(t))\| \leq \Big[\frac{R^{(\theta-1)}(1-\theta)}{\vartheta(\theta)}\Delta_3+K_3\frac{R^{(\theta-1)}T^\theta}{\vartheta(\theta)\Gamma(\theta)}\Delta_3\Big]\|D(t)-D'(t)\|,\\ \|\mathcal{L}(M(t))-\mathcal{L}(M'(t))\| \leq \Big[\frac{R^{(\theta-1)}(1-\theta)}{\vartheta(\theta)}\Delta_4+K_4\frac{R^{(\theta-1)}T^\theta}{\vartheta(\theta)\Gamma(\theta)}\Delta_4\Big]\|M(t)-M'(t)\|,\\ \|\mathcal{L}(B(t))-\mathcal{L}(B'(t))\| \leq \Big[\frac{R^{(\theta-1)}(1-\theta)}{\vartheta(\theta)}\Delta_5+K_5\frac{R^{(\theta-1)}T^\theta}{\vartheta(\theta)\Gamma(\theta)}\Delta_5\Big]\|B(t)-B'(t)\|,\\ \|\mathcal{L}(G(t))-\mathcal{L}(G'(t))\| \leq \Big[\frac{R^{(\theta-1)}(1-\theta)}{\vartheta(\theta)}\Delta_6+K_6\frac{R^{(\theta-1)}T^\theta}{\vartheta(\theta)\Gamma(\theta)}\Delta_6\Big]\|G(t)-G'(t)\|.\end{cases}$$

The linear operator $\mathcal{L}$ will be a contraction mapping if the following conditions are hold:

$$\begin{cases} \frac{R^{(\theta-1)}(1-\theta)}{\vartheta(\theta)}\Delta_1 + K_1\frac{R^{(\theta-1)}T^{\theta}}{\vartheta(\theta)\Gamma(\theta)}\Delta_1 \\ \frac{R^{(\theta-1)}(1-\theta)}{\vartheta(\theta)}\Delta_2 + K_2\frac{R^{(\theta-1)}T^{\theta}}{\vartheta(\theta)\Gamma(\theta)}\Delta_2 \\ \frac{R^{(\theta-1)}(1-\theta)}{\vartheta(\theta)}\Delta_3 + K_3\frac{R^{(\theta-1)}T^{\theta}}{\vartheta(\theta)\Gamma(\theta)}\Delta_3 \\ \frac{R^{(\theta-1)}(1-\theta)}{\vartheta(\theta)}\Delta_4 + K_4\frac{R^{(\theta-1)}T^{\theta}}{\vartheta(\theta)\Gamma(\theta)}\Delta_4 \\ \frac{R^{(\theta-1)}(1-\theta)}{\vartheta(\theta)}\Delta_5 + K_5\frac{R^{(\theta-1)}T^{\theta}}{\vartheta(\theta)\Gamma(\theta)}\Delta_5 \\ \frac{R^{(\theta-1)}(1-\theta)}{\vartheta(\theta)}\Delta_6 + K_6\frac{R^{(\theta-1)}T^{\theta}}{\vartheta(\theta)\Gamma(\theta)}\Delta_6 \end{cases} < 1. \tag{4.17}$$

Therefore, the fixed point theory (Zhou, 2023) ensures the uniqueness of the solution of System (4.6) if all the conditions in Equation (4.17) are satisfied.

4.4 Fractional Optimal-Control Problem (FOCP)

In this section, we examine the formulation and solution of an optimal control problem by using ABC operator for the Model (4.6). Generally, the formulation of a fractional optimal control problem (see Figure 4.2) involves first determining the optimal control, $z(t)$, that minimizes the cost function.

$$J(z) = \int_{t_0}^{t_f} G(t, y, z)dt,$$

subject to the constraints

$$R^{(1-\theta)\,ABC}D_t^{\theta}y = F(t, y, z);$$

with initial condition: $y(0) = y_0.$

where $0 < \theta \leq 1$, the state and control variables y and z respectively, G(t, y, z) and F(t, y, z) are differentiable functions. In this model, we considered the state variable as $y = (T, A, D, M, B, G) \in R^6$, and we aim to find the optimal control $z^*(t) \in R$ to minimize the mass-transfer resistance between methanol and WCO. Let us consider the following cost functional

$$J[z] = \int_{t_0}^{t_f} \left[W_1 z^2 - W_2 B^2\right] dt,$$

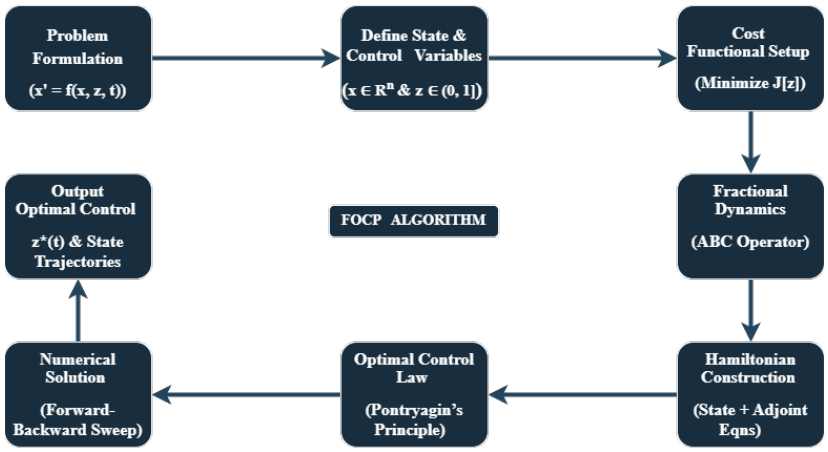

Figure 4.2: *Flowchart of the Fractional Optimal Control Problem (FOCP) Algorithm, illustrating the sequential steps from problem formulation to the derivation of optimal control and state trajectories using the Atangana-Baleanu (ABC) fractional operator and Pontryagin's principle.*

where W_1 represents the weight constant with $W_1 > 0$, while W_2 stands for the penalty multiplier. Let the control input variable $z(t)$ represent the ultrasonic frequency applied at time t, where $0 \leq z(t) \leq 1$. A value of $z(t) = 1$ corresponds to the maximum utilization of ultrasound frequency, while $z(t) = 0$ signifies no ultrasound application. Hence, the System (4.6) becomes:

$$\begin{cases} F_1 = R^{(1-\theta)ABC}D_t^{\theta}T(t) = & -r_{1f}TA + r_{1b}DB, \\ F_2 = R^{(1-\theta)ABC}D_t^{\theta}A(t) = & -r_{1f}TA + r_{1b}DB - r_{2f}DA + r_{2b}MB - r_{3f}MA + r_{3b}GB, \\ F_3 = R^{(1-\theta)ABC}D_t^{\theta}D(t) = & r_{1f}TA - r_{1b}DB - r_{2f}DA + r_{2b}MB, \\ F_4 = R^{(1-\theta)ABC}D_t^{\theta}M(t) = & r_{2f}DA - r_{2b}MB - r_{3f}MA + r_{3b}GB, \\ F_5 = R^{(1-\theta)ABC}D_t^{\theta}B(t) = & r_{1f}TA - r_{1b}DB + r_{2f}DA - r_{2b}MB + r_{3f}MA - r_{3b}GB \\ & + \frac{B}{zM_r}\left(1 - \frac{B}{B_{\max}}\right), \\ F_6 = R^{(1-\theta)ABC}D_t^{\theta}G(t) = & r_{3f}MA - r_{3b}GB, \end{cases} \tag{4.18}$$

with initial conditions: $T(0) = T_0$, $A(0) = A_0$, $D(0) = 0$, $M(0) = 0$, $B(0) = 0$, and $G(0) = 0$. Our objective is to find the optimal control $z^*(t)$ that minimizes the functional $J(z)$, i.e.,

$$J(z^*) = \min\{J(z) : z \in Z\}.$$

The set of feasible controls, Z, consists of all measurable functions satisfying:

$$Z = \left\{z \mid z \text{ is measurable and satisfies } 0 \leq z \leq 1, \quad \forall t \in [t_0, t_f]\right\}.$$

To determine $z^*(t)$, we utilize Pontryagin's Minimum Principle (Pontryagin, 2018). The Hamiltonian is expressed as:

$$\begin{aligned}\mathcal{H} =& W_1 z^2 - W_2 B^2 + \sum_{n=1}^{6} \Phi_i F_i, \\ =& W_1 z^2 - W_2 B^2 + \Phi_T(-r_{1f}TA + r_{1b}DB) + \Phi_A(-r_{1f}TA + r_{1b}DB - r_{2f}DA + r_{2b}MB \\ & - r_{3f}MA + r_{3b}GB) + \Phi_D(r_{1f}TA - r_{1b}DB - r_{2f}DA + r_{2b}MB) + \Phi_M(r_{2f}DA - r_{2b}MB \\ & - r_{3f}MA + r_{3b}GB) + \Phi_G(r_{3f}MA - r_{3b}GB) + \Phi_B(r_{1f}TA - r_{1b}DB + r_{2f}DA - r_{2b}MB \\ & + r_{3f}MA - r_{3b}GB) + \frac{\Phi_B B}{zM_r}\left(1 - \frac{B}{B_{\max}}\right),\end{aligned} \tag{4.19}$$

where Φ_T, Φ_A,. . . ., Φ_G are adjoint variables and F_1, F_2,..., F_6 are functions defined in Equation (4.18) with the properties

$$\begin{cases} R^{(1-\theta)ABC}D_t^\theta \Phi_T = -\frac{\partial \mathcal{H}}{\partial T} = & r_{1f}A(\Phi_A + \Phi_T - \Phi_D - \Phi_B), \\ R^{(1-\theta)ABC}D_t^\theta \Phi_A = -\frac{\partial \mathcal{H}}{\partial A} = & r_{1f}T(\Phi_A + \Phi_T - \Phi_D - \Phi_B) + r_{2f}D(\Phi_A + \Phi_D - \Phi_M - \Phi_B) \\ & +r_{3f}M(\Phi_A + \Phi_M - \Phi_B - \Phi_G), \\ R^{(1-\theta)ABC}D_t^\theta \Phi_D = -\frac{\partial \mathcal{H}}{\partial D} = & r_{1b}B(-\Phi_A - \Phi_T + \Phi_D + \Phi_B) + r_{2f}A(\Phi_A + \Phi_D - \Phi_M - \Phi_B), \\ R^{(1-\theta)ABC}D_t^\theta \Phi_M = -\frac{\partial \mathcal{H}}{\partial M} = & r_{2b}B(-\Phi_A - \Phi_D + \Phi_M + \Phi_B) + r_{3f}A(\Phi_A + \Phi_M - \Phi_B - \Phi_G), \\ R^{(1-\theta)ABC}D_t^\theta \Phi_B = -\frac{\partial \mathcal{H}}{\partial B} = & 2W_2 B + r_{1b}D(-\Phi_A - \Phi_T + \Phi_D + \Phi_B) + r_{2b}M(-\Phi_A - \Phi_D \\ & +\Phi_M + \Phi_B) + r_{3b}G(-\Phi_A - \Phi_M + \Phi_B + \Phi_G) - \frac{1}{zM_r}\left(1 - \frac{2B}{B_{max}}\right), \\ R^{(1-\theta)ABC}D_t^\theta \Phi_G = -\frac{\partial \mathcal{H}}{\partial G} = & r_{3b}B(-\Phi_A - \Phi_M + \Phi_B + \Phi_G). \end{cases} \tag{4.20}$$

The transversality conditions are

$$\Phi_T(t_f) = \Phi_A(t_f) = \Phi_D(t_f) = \Phi_M(t_f) = \Phi_B(t_f) = \Phi_G(t_f) = 0.$$

Theorem 4.4.1. *The control parameter z^* that minimizes $J(z)$ over Z are given by*

$$z^*(t) = max\left(0, min\left(1, \left\{\frac{\Phi_B B(B_{max} - B)}{2W_1 M_r B_{max}}\right\}^{\frac{1}{3}}\right)\right),$$

where Φ_T, Φ_A, Φ_D, Φ_M, Φ_B, Φ_G are the adjoint variables satisfying Equation (4.20) and the following transversality conditions:

$$\Phi_T(0) = \Phi_A(0) = \Phi_D(0) = \Phi_M(0) = \Phi_B(0) = \Phi_G(0) = 0,$$

and

$$z^*(t) = \begin{cases} 0, & \left\{\frac{\Phi_B B(B_{max}-B)}{2W_1 M_r B_{max}}\right\}^{\frac{1}{3}} \leq 0; \\ \left\{\frac{\Phi_B B(B_{max}-B)}{2W_1 M_r B_{max}}\right\}^{\frac{1}{3}}, & 0 < \left\{\frac{\Phi_B B(B_{max}-B)}{2W_1 M_r B_{max}}\right\}^{\frac{1}{3}} < 1; \\ 1, & \left\{\frac{\Phi_B B(B_{max}-B)}{2W_1 M_r B_{max}}\right\}^{\frac{1}{3}} \geq 1. \end{cases}$$

Proof. Differentiating the Hamiltonian (4.19) with respect to z we get:

$$\frac{\partial H}{\partial z^*} = 0 = 2W_1 z^* - \frac{\Phi_B B(B_{max} - B)}{2W_1 M_r^\theta B_{max} z^{*2}},$$

$$\implies z^* = \left\{\frac{\Phi_B B(B_{max} - B)}{2W_1 M_r^\theta B_{max}}\right\}^{\frac{1}{3}}.$$

Applying the Pontryagin Minimum Principle, we get

$$\begin{cases} {}^{(1-\theta)ABC}R D_t^\theta \Phi_T = -\frac{\partial \mathcal{H}}{\partial T}, & {}^{(1-\theta)ABC}R D_t^\theta \Phi_A = -\frac{\partial \mathcal{H}}{\partial A}, & {}^{(1-\theta)ABC}R D_t^\theta \Phi_D = -\frac{\partial \mathcal{H}}{\partial D}, \\ {}^{(1-\theta)ABC}R D_t^\theta \Phi_M = -\frac{\partial \mathcal{H}}{\partial M}, & {}^{(1-\theta)ABC}R D_t^\theta \Phi_B = -\frac{\partial \mathcal{H}}{\partial B}, & {}^{(1-\theta)ABC}R D_t^\theta \Phi_G = -\frac{\partial \mathcal{H}}{\partial G}, \end{cases}$$

with transversality condition

$$\Phi_T(t_f) = \Phi_A(t_f) = \Phi_D(t_f) = \Phi_M(t_f) = \Phi_B(t_f) = \Phi_G(t_f) = 0.$$

□

4.5 Numerical Validation

This section presents the numerical illustration of our biodiesel model results. We employ MATLAB 2021a and Python for the numerical simulations. First, we outline the complete numerical scheme corresponding to different fractional derivative operators, specifically the ABC derivative and the CF derivative. The numerical solution uses these numerical schemes to analyze the model's behavior effectively.

4.5.1 Numerical Solution Scheme for Reaction System

ABC Fractional Operator:

The fractional System (4.6) corresponding to Atangana Baleanu in the Caputo sense

can be written as,

$$R^{1-\theta\ ABC}D_t^{\theta}(f(t)) = \Psi(t, f(t)), \tag{4.21}$$

where $f(t) = [T(t), A(t), D(t), M(t), B(t), G(t)]^T$ and $\Psi(t, f(t))$ denotes the right hand side of the fractional System (4.6). Applying **Definition 4**, in Equation (4.21), we get

$$f(t) - f(0) = \frac{R^{(\theta-1)}(1-\theta)}{\vartheta(\theta)}\Psi(f(t), t) + \frac{R^{(\theta-1)}\theta}{\vartheta(\theta)\Gamma(\theta)} \times \int_0^t (t-s)^{\theta-1}\Psi(f(s), s)ds.$$

Using iteration, the equation is reformulated as:

$$f(t_{n+1}) = f(0) + \frac{R^{(\theta-1)}(1-\theta)}{\vartheta(\theta)}\Psi(f(t_n), t_n) + \frac{R^{(\theta-1)}\theta}{\vartheta(\theta)\Gamma(\theta)} \times \sum_{k=0}^{n}\int_{t_k}^{t_{k+1}} (t_{n+1}-s)^{\theta-1}\Psi(f(s), s)ds. \tag{4.22}$$

Utilizing the two-step Lagrange interpolation polynomial, the function $\Psi(f(s), s)$ approximated in the interval $[t_k, t_{k+1}]$ as follows:

$$\Psi(f(s), s) \approx \frac{\Psi(f(t_k), t_k)}{h}(s - t_{k-1}) - \frac{\Psi(f(t_{k-1}), t_{k-1})}{h}(s - t_k). \tag{4.23}$$

Where h is the time step size. Now,

$$\begin{aligned}
&\int_{t_k}^{t_{k+1}} (t_{n+1}-s)^{\theta-1}\Psi(f(s), s)ds,\\
=&\int_{t_k}^{t_{k+1}} \Big[(t_{n+1}-s)^{\theta-1}(s-t_{k-1})\frac{\Psi(f(t_k), t_k)}{h} - (t_{n+1}-s)^{\theta-1}(s-t_k)\frac{\Psi(f(t_{k-1}), t_{k-1})}{h}\Big]ds,\\
=&\frac{h^{\theta}}{\theta(\theta+1)}\big[(n-k+1)^{\theta}(n-k+\theta+2) - (n-k)^{\theta}(n-k+2\theta+2)\big]\Psi(f(t_k), t_k) -\\
&\frac{h^{\theta}}{\theta(\theta+1)}\big[(n-k+1)^{\theta+1} - (n-k)^{\theta}(n-k+\theta+1)\big]\Psi(f(t_{k-1}), t_{k-1}).
\end{aligned}$$

Using this result in Equation (4.22), we have the numerical solution of the fractional System (4.6) corresponding to Atangana Baleanu in the Caputo sense, as follows:

$$\begin{aligned}
f(t_{n+1}) =& f(0) + \frac{R^{(\theta-1)}(1-\theta)}{\vartheta(\theta)}\Psi(f(t_n), t_n) + \frac{R^{(\theta-1)}h^{\theta}}{\vartheta(\theta)\Gamma(\theta)(\theta+1)} \times \sum_{k=0}^{n}\Big[\big[(n-k+1)^{\theta}\\
&(n-k+\theta+2) - (n-k)^{\theta}(n-k+2\theta+2)\big]\Psi(f(t_k), t_k) - \big[(n-k+1)^{\theta+1}\\
&- (n-k)^{\theta}(n-k+\theta+1)\big]\Psi(f(t_{k-1}), t_{k-1})\Big].
\end{aligned} \tag{4.24}$$

Caputo Fabrizio Fractional Operator:

The fractional System (4.5) corresponding to the CF differential operator can be written as,

$$R^{1-\phi\ CF}D_t^{\phi}(g(t)) = \Psi'(g(t),t), \tag{4.25}$$

where $g(t) = [T(t), A(t), D(t), M(t), B(t), G(t)]^T$ and $\Psi'(t, g(t))$ denotes the right hand side of the fractional System (4.5). Applying the fundamental theorem in the Equation (4.25), we obtain

$$g(t) - g(0) = \frac{R^{(\phi-1)}(1-\phi)}{M(\phi)}\Psi'(g(t),t) + \frac{R^{(\phi-1)}\phi}{M(\phi)} \times \int_0^t \Psi'(g(s'),s')ds'.$$

Now this equation can be written as follows:

$$\begin{cases} g(t_{n+1}) - g(0) = \frac{R^{(\phi-1)}(1-\phi)}{M(\phi)}\Psi'(g(t_n),t_n) + \frac{R^{(\phi-1)}\phi}{M(\phi)} \times \int_0^{t_{n+1}} \Psi'(g(s'),s')ds', \\ g(t_n) - g(0) = \frac{R^{(\phi-1)}(1-\phi)}{M(\phi)}\Psi'(g(t_{n-1}),t_{n-1}) + \frac{R^{(\phi-1)}\phi}{M(\phi)} \times \int_0^{t_n} \Psi'(g(s'),s')ds'. \end{cases}$$

Replacing the second equation in the first equation, we obtain that

$$\begin{aligned} g(t_{n+1}) - g(t_n) =& \frac{R^{(\phi-1)}(1-\phi)}{M(\phi)}(\Psi'(g(t_n),t_n) - \Psi'(g(t_{n-1}),t_{n-1})) \\ &+ \frac{R^{(\phi-1)}\phi}{M(\phi)} \times \int_{t_n}^{t_{n+1}} \Psi'(g(s'),s')ds'. \end{aligned} \tag{4.26}$$

Utilizing the result as in Equation (4.23), we have

$$\int_{t_n}^{t_{n+1}} \Psi'(g(s'),s')ds' = \frac{3h}{2}\Psi'(g(t_n),t_n) - \frac{h}{2}\Psi'(g(t_{n-1}),t_{n-1}). \tag{4.27}$$

Where h is the time step size. Therefore using these two Equation (4.26) and Equation (4.27), we get the numerical solution for the CF fractional System (4.25), as follows:

$$g(t_{n+1}) = g(t_n) + \tfrac{R^{(\phi-1)}}{M(\phi)}\left[(1-\phi+\tfrac{3h\phi}{2})(\Psi'(g(t_n),t_n) - (1-\phi+\tfrac{h\phi}{2})\Psi'(g(t_{n-1}),t_{n-1})\right]. \tag{4.28}$$

4.5.2 Sensitivity Analysis of Reaction Parameters

To assess the impact of model parameters on the biodiesel production system, we perform a sensitivity analysis using the Pearson correlation coefficient method. Sensitivity analysis plays a crucial role in determining how variations in input parameters influence the system's output, thereby identifying key parameters that significantly affect the biodiesel yield and efficiency. Uncertainty analysis is essential

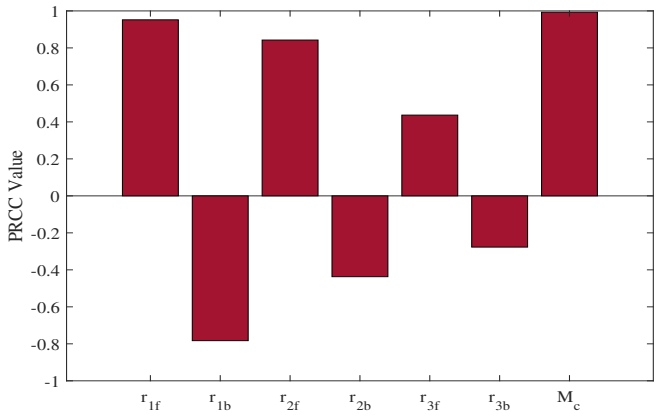

Figure 4.3: *Bar diagram depicting the sensitivity of model parameters on biodiesel yield using integer order system, assessed through Partial Rank Correlation Coefficients (PRCC) using Pearson's correlation coefficient.*

for assessing the reliability and sensitivity of system parameters in biodiesel production. The Pearson Correlation Coefficient (PCC) is a key statistical measure that quantifies the strength and direction of the linear relationship between input parameters and model outputs. Unlike rank-based methods, PCC evaluates direct proportionality, helping identify dominant parameters that significantly influence system behavior. By performing uncertainty analysis, we can quantify parameter sensitivity, improve model robustness, and enhance predictive accuracy, ensuring that variations in system inputs do not lead to misleading conclusions in process optimization and decision-making.

We calculate Pearson correlation coefficients between each reaction parameter (input variables) and biodiesel yield (output variable). The correlation values range from -1 to 1 and are represented in the bar diagram (Figure 4.3). Figure 4.3 illustrates that reaction parameters r_{1f}, r_{2f}, and M_c positively influence biodiesel production, whereas reaction parameters r_{1b} have a negative impact on biodiesel yield. This analysis helps identify the most significant factors that affect the efficiency of biodiesel production. Figure 4.4 presents the scatter plot corresponding to the PRCC

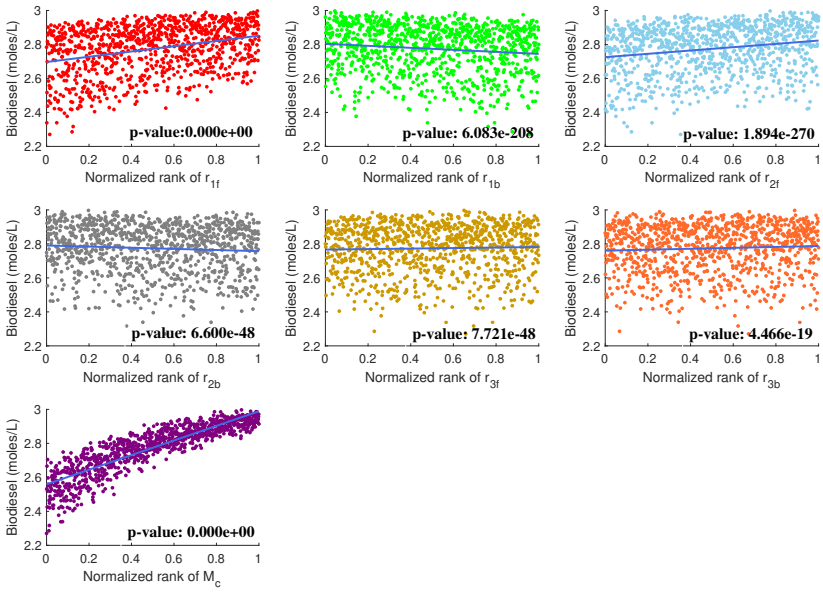

Figure 4.4: *Scatter plot is presented for biodiesel production, illustrating the relationship between all reaction rates, including the mass transfer coefficient M_c. The statistical significance level is set at 0.05, meaning there is a 5 % probability of rejecting a true null hypothesis. Each parameter is sampled 1,000 times using the Latin Hypercube Sampling (LHS) approach with a uniform probability distribution, ensuring comprehensive exploration of parameter space while maintaining statistical robustness.*

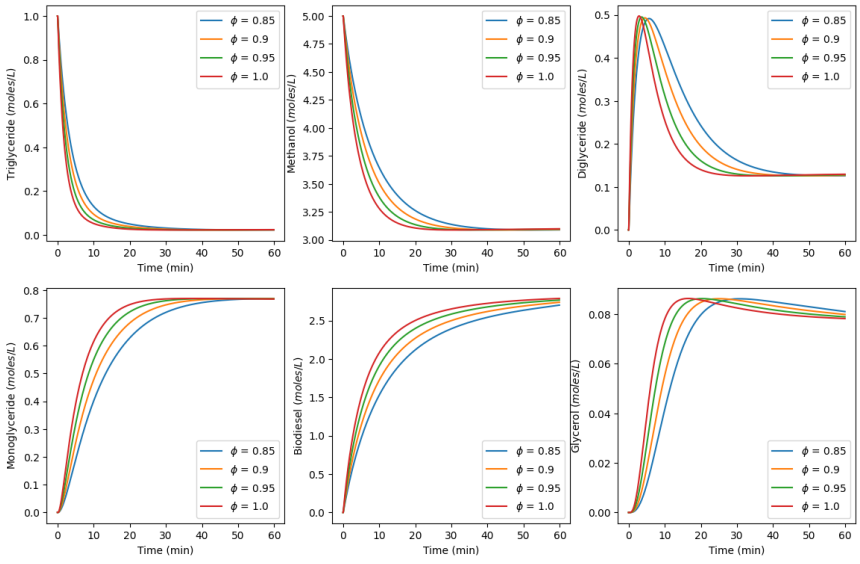

Figure 4.5: *Concentration variation of all reactants over time in base-catalyzed transesterification using the CF method with fractional order ϕ = 0.85, 0.9, 0.95, and 1. Memory rate parameter, R = 0.3, and other parameter values are specified in Table 4.1 and Table 4.2. Here, the ultrasound frequency, H = 50 kHz, temperature, T = 50°C, and methanol-to-oil ratio is 5:1.*

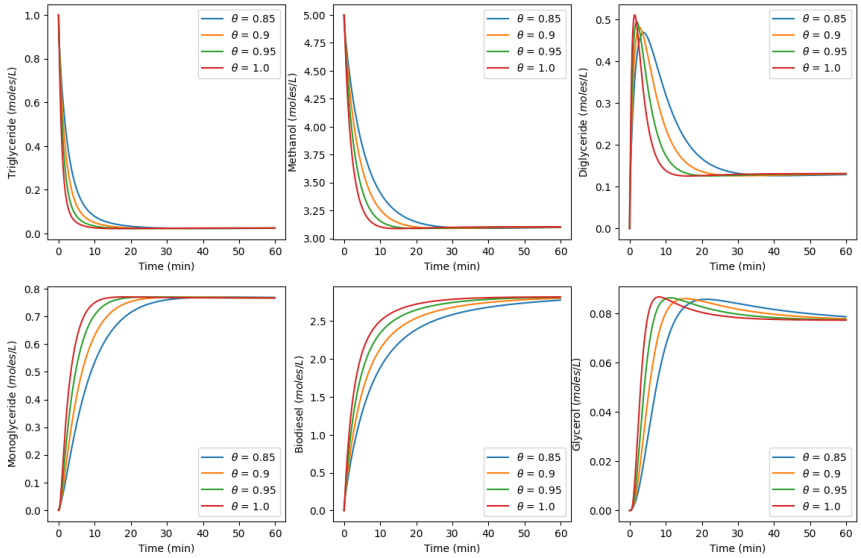

Figure 4.6: *Variation of concentration of all the reactants over time in base-catalyzed transesterification using the ABC method with fractional order θ = 0.85, 0.9, 0.95 and 1. Other parameter values are specified in Table 4.1 and Table 4.2. Here, memory rate parameter, R = 0.3, the ultrasound frequency, H = 50 kHz, temperature, T = 50°C, and methanol-to-oil ratio is 5:1.*

analysis (partial rank correlation coefficient), illustrating the relationship between reaction parameters and biodiesel production. In the plot, the X-axis represents the normalized values of each reaction parameter, while the Y-axis denotes the biodiesel yield. This visualization helps in understanding the strength and direction of the correlation between individual parameters and biodiesel production efficiency.

4.5.3 Numerical Illustration

In the biodiesel production process, we employ the molar ratio of WCO to methanol, along with ultrasound, to investigate their respective effects. Figure 4.5 represents the concentration trajectories of triglyceride, methanol, diglyceride, monoglyceride, biodiesel, and glycerol utilizing 50 kHz ultrasound frequency and $5:1$ methanol-to-WCO molar ratio using CF method of System (4.5) for fractional order ϕ = 0.85, 0.9, 0.95 and 1 with reaction rate parameter R = 0.3. The trajectories highlight the influence of fractional-order derivatives on the reaction kinetics, where lower fractional orders $(\phi < 1)$ introduce memory effects that slow down the depletion of reactants and the formation of products compared to the integer-order case $(\phi = 1)$. This behavior is biologically significant as it suggests that transesterification exhibits a non-instantaneous response to reactant interactions.

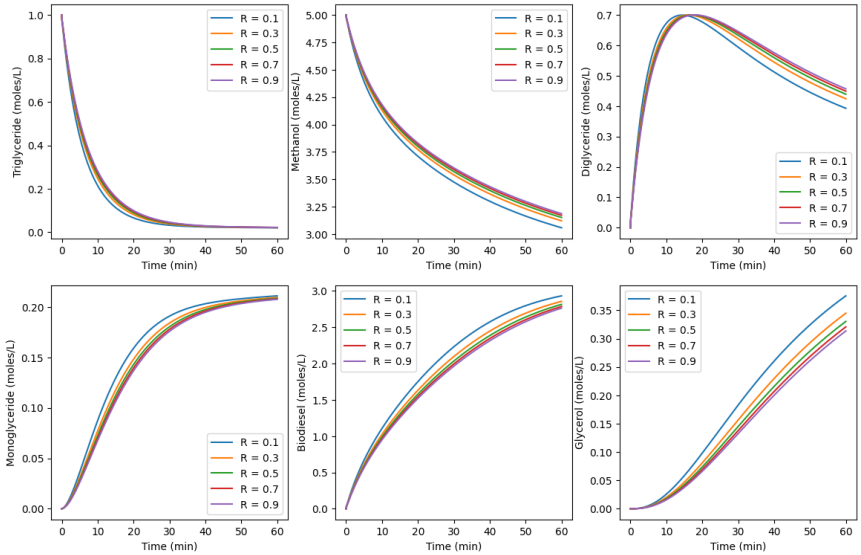

Figure 4.7: *Time-dependent variation of concentration profiles for all reactants involved in the transesterification reaction using the CF fractional-order method with fractional order $\phi = 0.95$. The simulations are performed for five different values of the memory rate parameter R = 0.1, 0.3, 0.5, 0.7, and 0.9 to analyze its influence on reaction kinetics. All parameter values are taken as specified in Table 4.1 and Table 4.2.*

Figure 4.6 shows the concentration trajectories of all six reactants for the same ultrasound frequency and molar ratio with $\theta = 0.85, 0.9, 0.95$, and 1 with the same R-value as previous of ABC method. The observed variations in reactant concentration trends highlight the effectiveness of the non-singular kernel in capturing memory effects, which are absent in the integer-order model $(\theta = 1)$. Figure 4.7 and Figure 4.8 illustrate the impact of varying the memory rate parameter R on the chemical system using the CF and ABC fractional operators, with the fractional order fixed at 0.95 and memory rate values set at R = 0.1, 0.3, 0.5, 0.7, 0.9. Biologically, this variation in R reflects the extent to which past states of the reaction influence the present biodiesel formation rate, which is crucial in complex biochemical and catalytic processes. A higher memory rate enhances the system's ability to retain past kinetic information, leading to a more sustained biodiesel yield, whereas lower values of R indicate a reaction dynamic that is more dependent on instantaneous conditions rather than historical effects. The comparison between the CF and ABC methods in Figure 4.9, with $\phi = \theta = 0.95$ and R = 0.3, reveals that biodiesel conversion from triglycerides (TG) is higher in the ABC method, as observed in subplots (2,3,5). This difference arises due to the distinct kernel structures of the two fractional operators, where the ABC method, utilizing a Mittag-Leffler function, accounts for a broader

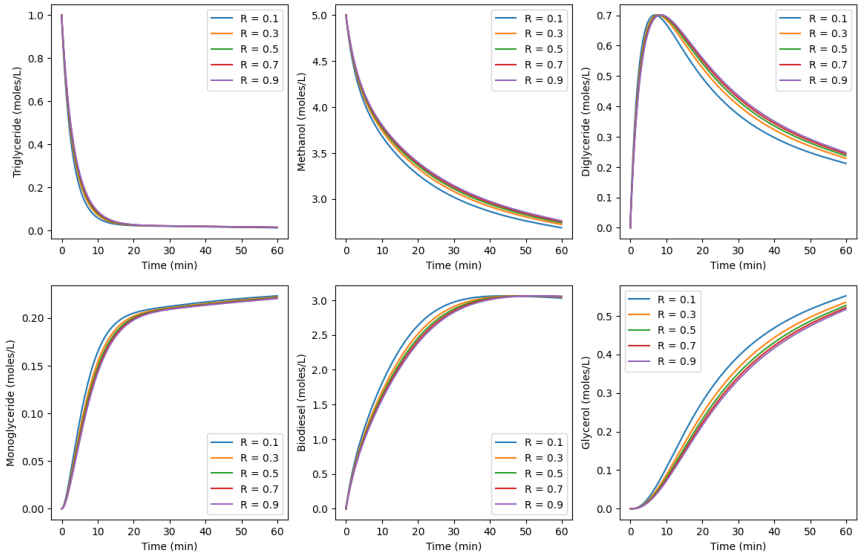

Figure 4.8: *Variation of concentration profiles for all reactants involved in the transesterification reaction over time, modeled using the ABC fractional-order method with a fractional order of $\theta = 0.95$. R remains consistent with the values specified earlier. Model parameters are taken from Table 4.1 and Table 4.2. These figures illustrate the dynamic behavior of reactants and products, highlighting the influence of fractional-order derivatives on reaction kinetics and memory effects in biodiesel production.*

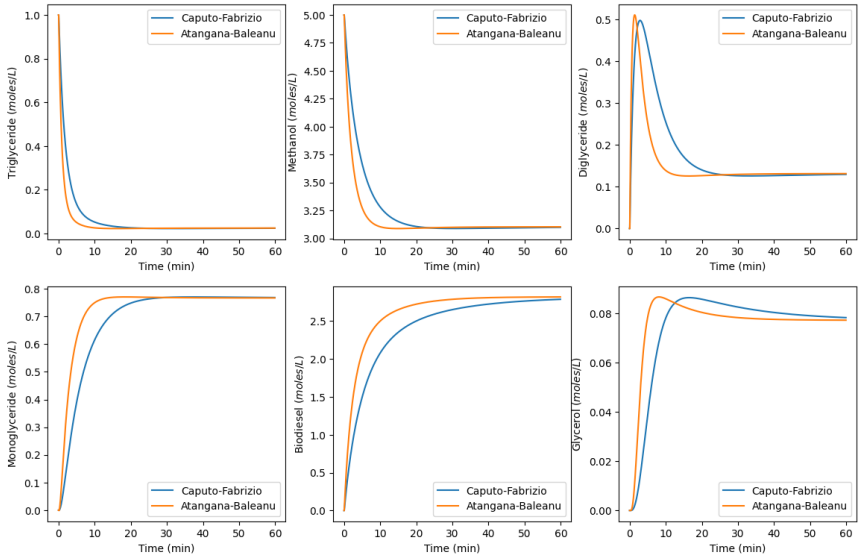

Figure 4.9: *Comparison of the concentration profile of reactants in the transesterification reaction modeled with the CF and ABC fractional operators. With fractional orders $\phi = \theta = 0.95$ and R = 0.3, the figure highlights differences in reactant consumption and product formation, demonstrating how each fractional model captures the reaction dynamics.*

and more persistent memory effect compared to the CF method's exponential kernel. The enhanced memory retention in the ABC model allows for a more sustained

reaction rate, leading to greater biodiesel yield over time.

Figure 4.10 and Figure 4.11 represent the comparison through the surface plot for

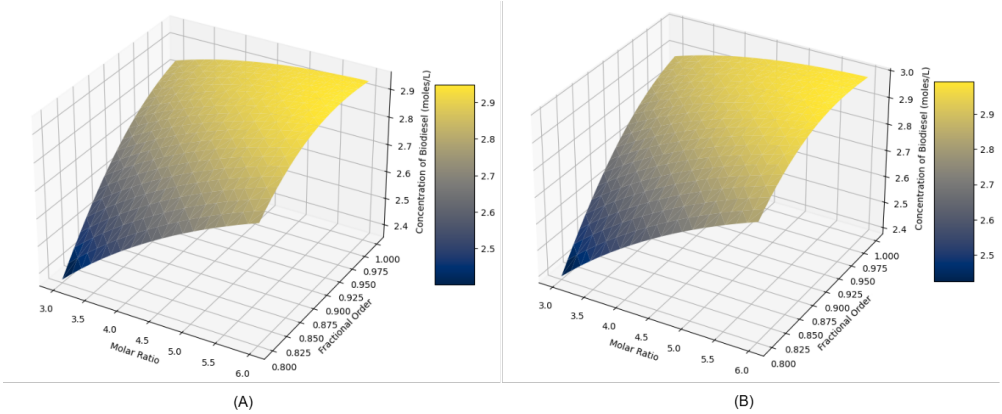

Figure 4.10: *Surface plot for the concentration of biodiesel after 60 minutes with the variation of molar ratio of methanol and WCO from 3:1 to 6:1 and fractional order ϕ or θ from 0.8 to 1 using (A) CF and (B) ABC fractional operator. Here H = 50 kHz, R = 0.3, and other parameter values taken from Table 4.1 and Table 4.2.*

CF and ABC-induced systems with memory rate parameter value R = 0.3. In particular, 4.10(A) shows the surface plot of the biodiesel production with respect to the variation of fractional order 'ϕ' and the molar ratio between methanol and WCO of the CF model 4.5. Figure 4.10(B) represents the surface plots for biodiesel production with the variation of fractional order 'θ' and molar ratio using ABC method. Any coordinates on this surface represent the final molar conversion of biodiesel after 60 minutes for a particular molar ratio and fractional order. Similarly, Figure 4.11(A) represents the surface plot for biodiesel production with the variation of applied ultrasound frequency 'H' and fractional order 'ϕ' in CF method and Figure 4.11(B) represents the surface plots for biodiesel production with the variation of fractional order 'θ' and ultrasound frequency for ABC method. In these cases, the range of fractional order ϕ or θ, molar ratio of methanol and WCO, and ultrasound frequency are from 0.8 to 1, 3:1 to 6:1, and 30 kHz to 60 kHz, respectively.

4.5.4 Experimental Validity

To validate our simulated data over time, we compared it with experimental data from Takase (Takase, 2022) using both the ABC and CF methods. For this validation, 12 fractional order values θ or ϕ ranging from 0.7 to 1 were considered over a

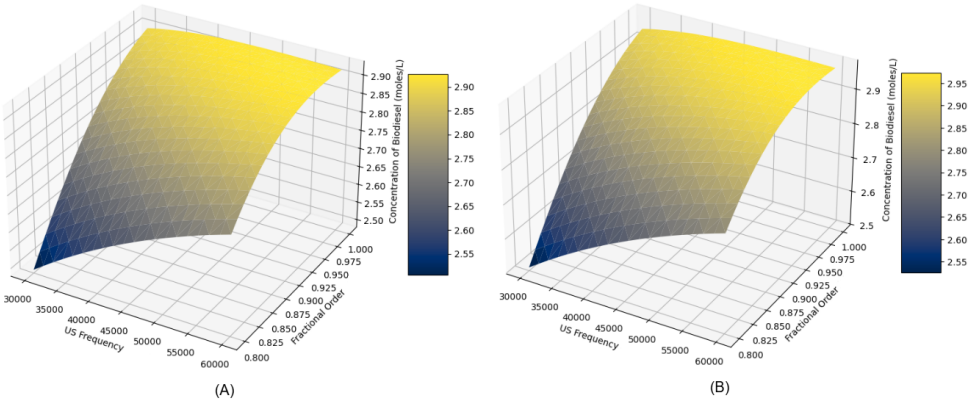

Figure 4.11: *Surface plot for the concentration of biodiesel after 60 minutes with the variation of ultrasound frequency from 30 kHz to 60 kHz and fractional order ϕ or θ from 0.8 to 1 using (A) CF and (B) ABC fractional operator. Here the molar ratio of methanol and WCO is 5 : 1, R = 0.3, and other parameter values taken from Table 4.1 and Table 4.2.*

120-minute period, utilizing 2400 iterations to ensure accuracy. From this range of fractional orders, two values for ABC and two values of CF are chosen.

- **For ABC Method:** The bar diagram 4.12 compares biodiesel production between experimental data and the ABC fractional-order model at $\theta = 0.89$ and $\theta = 0.918$ over reaction times from 0 to 120 minutes. Initially (5–20 min), both ABC models and experimental data follow a similar increasing trend, though ABC ($\theta = 0.89$) slightly underestimates yield while ABC ($\theta = 0.918$) aligns more closely. At 10–15 minutes, both ABC models approximate experimental values

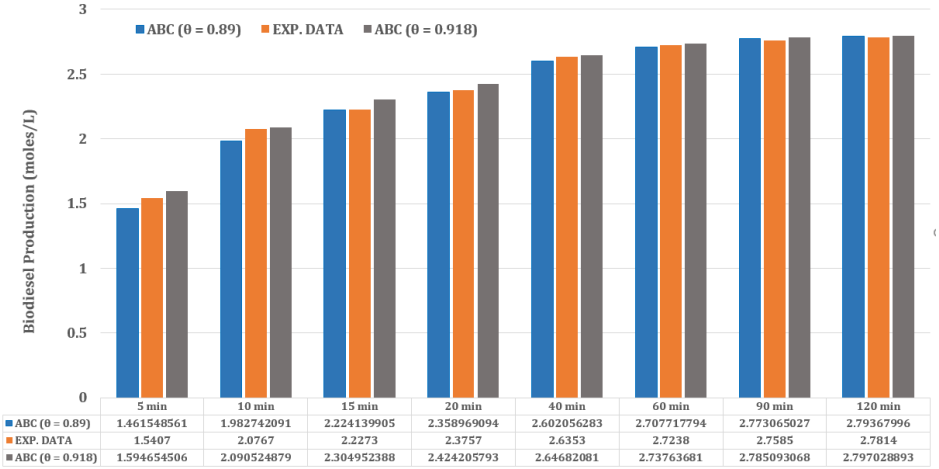

	5 min	10 min	15 min	20 min	40 min	60 min	90 min	120 min
ABC (θ = 0.89)	1.461548561	1.982742091	2.224139905	2.358969094	2.602056283	2.707717794	2.773065027	2.79367996
EXP. DATA	1.5407	2.0767	2.2273	2.3757	2.6353	2.7238	2.7585	2.7814
ABC (θ = 0.918)	1.594654506	2.090524879	2.304952388	2.424205793	2.64682081	2.73763681	2.785093068	2.797028893

Figure 4.12: *Comparison of experimental data against simulated data for biodiesel production using ABC fractional operator with fractional order $\theta = 0.89$ and $\theta = 0.918$. Data at eight different times has also been given in tabular form.*

well, though $\theta = 0.918$ slightly overestimates. At 20 minutes, both models predict a slightly higher yield than experimental data. In the mid-reaction phase (40–60 min), all datasets align closely, with minimal deviations at 40 min and near-identical values at 60 min, confirming the ABC model's accuracy in capturing biodiesel production rates. In the final phase (90–120 min), biodiesel production saturates, with all datasets converging at nearly the same values, demonstrating the ABC model's effectiveness in predicting steady-state production. The results indicate that while $\theta = 0.918$ provides a closer match at lower reaction times, both models perform well beyond 40 minutes, highlighting the fractional-order derivative's ability to capture memory effects and improve long-term predictions. The smooth convergence to experimental values suggests that the ABC fractional-order model effectively retains historical reaction dynamics, making it a promising approach for biodiesel production modeling. Among the tested values, $\theta = 0.918$ offers the best overall fit, emphasizing the importance of optimizing fractional order for improved accuracy, with further experimental validation required to refine the model under different reaction conditions.

- **For CF Method:** The bar diagram 4.13 compares biodiesel production using experimental data with the CF fractional-order model at two different values of fractional order: CF ($\phi = 0.97$) – Blue bars, CF ($\phi = 1$) – Gray bars, and Experimental Data – Orange bars. In the early phase (5–20 min), the CF ($\phi = 0.97$) model slightly underestimates biodiesel yield at 5 min compared to experimental data, while CF ($\phi = 1$) is closer. At 10 min and 15 min, both CF models approach experimental values but still remain slightly lower. At 20 min, the CF ($\phi = 1$) model more accurately follows experimental data than CF ($\phi = 0.97$), which slightly underpredicts the yield. In the mid-reaction phase (40–60 min), both CF models align well with experimental values, with minimal deviation at 40 min. At 60 min, experimental and simulated results converge, indicating the CF method effectively captures reaction dynamics. In the final phase (90–120 min), all three datasets converge, confirming that both CF models accurately predict steady-state biodiesel production. Overall, the CF fractional operator provides a better fit for integer order $\phi = 1$ across reaction times compared to fractional order $\phi = 0.97$, especially in the initial phase. The results suggest that the CF fractional-order model effectively retains reaction memory for the range 0.97 to 1, but precise tuning of ϕ is essential for improved

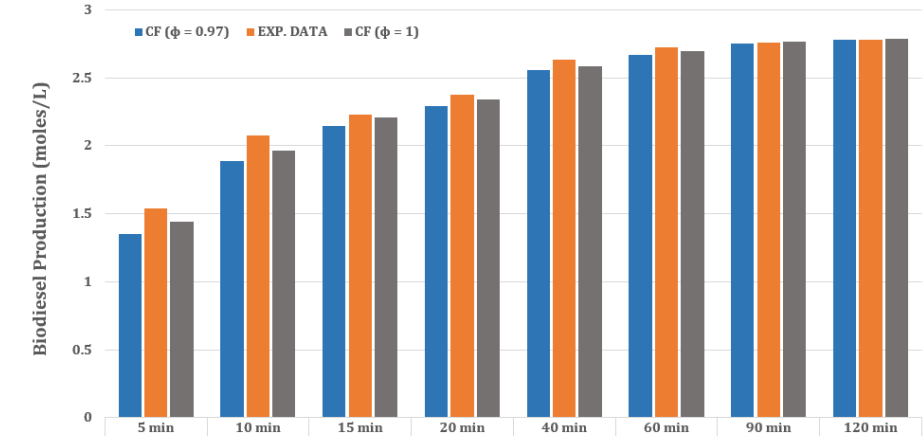

	5 min	10 min	15 min	20 min	40 min	60 min	90 min	120 min
CF (ϕ = 0.97)	1.348990157	1.887541987	2.147681099	2.294381283	2.553867775	2.669601176	2.751190679	2.782666012
EXP. DATA	1.5407	2.0767	2.2273	2.3757	2.6353	2.7238	2.7585	2.7814
CF (ϕ = 1)	1.439649041	1.966335114	2.208601687	2.343529909	2.587065218	2.694548894	2.764143982	2.787963737

Figure 4.13: *Comparison of experimental data against simulated data for biodiesel production using CF fractional operator with fractional order* $\phi = 0.97$ *and* $\phi = 1$*. Data in eight different times also been given in tabular form.*

accuracy.

Optimal Control: To overcome the initial mass transfer resistance between methanol and WCO, ultrasound frequency is applied at the start of the reaction. Once the reaction gains momentum, ultrasound frequency is no longer required. To enhance cost-effectiveness, we can switch off the frequency at that stage. Figure 4.14(a) shows the comparison of biodiesel production after employing an optimal control technique on the ultrasound frequency for the ABC fractional method with using the best fitted fractional order $\theta = 0.918$, and Figure 4.14(b) is the corresponding control profile. From the Figure, it is evident that after 30 minutes, we can switch off the ultrasound frequency. Figure 4.14(a) demonstrates that by applying control on ultrasound frequency, the production of biodiesel can be enhanced by 4-6% and also the process will be more cost-effective.

4.6 Discussion and Conclusion

In this chapter, we have studied the transesterification reaction mechanism for biodiesel production from waste cooking oil (WCO) with a fractional order derivative. We investigate the memory effect in the transesterification reaction of biodiesel using two distinct non-singular kernels: the exponential decay kernel and the Mittag-Leffler kernel. The whole study is conducted within a 1-meter of vessel diameter, at constant $50°C$ temperature, and 5:1 methanol to WCO molar ratio. Additionally, a 50

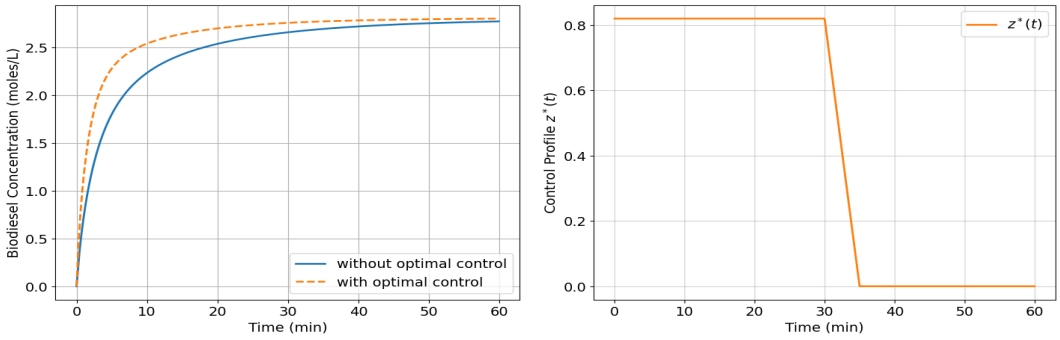

(a) (b)

Figure 4.14: *(a) Comparison of the concentration profile of biodiesel after using the optimal control technique for the ABC fractional method, utilizing the best fitted fractional order $\theta = 0.918$, and (b) is the corresponding optimal control profile. Here $H = 50$ kHz, methanol:WCO = 5:1, and all the other parameter values taken from Table 4.1 and Table 4.2.*

kHz ultrasound frequency is applied to the system to enhance mixing and reduce the initial mass transfer resistance between oil and methanol.

In subsection 4.3.1 and subsection 4.3.2, we analyzed the existence and uniqueness of the System (4.6) for the ABC fractional operator using the well-established Banach fixed-point theorem and the Arzelà-Ascoli theorem. Section 4.4 explores the formulation and solution of an optimal control problem for the Model (4.6) using the ABC operator. By applying the Pontryagin Minimum Principle and Hamiltonian approach, we derived the optimal control profile $z^*(t)$. A comprehensive numerical scheme for both the CF and ABC operators is developed in subsection 4.5.1. Using these numerical schemes, the solution of the System (4.5) and System (4.6) are graphically represented in subsection 4.5.2.

In Figure 4.5 and Figure 4.6, the effect of memory on the reactants through the non-singular kernel is shown using both CF and ABC fractional operators for a fixed memory rate parameter's value, R = 0.3 with the variation of fractional order ϕ and θ. In Figure 4.7 and Figure 4.8, the effect of memory rate parameter R is shown for both the fractional method for order $\phi = \theta = 0.95$. In Figure 4.9 comparison is made for fractional order 0.95 between two non-singular kernel methods. In Figure 4.10 and Figure 4.11, surface plots for final biodiesel production with respect to fractional order, the molar ratio of methanol and WCO, and ultrasound frequency are plotted for both the fractional method. In subsection 4.5.4, detailed experimental validity

is given for both CF and ABC systems and determines the order of the fractional derivatives. Additionally, the optimal control profile for maximum biodiesel production utilizing the best-fitted fractional order for the ABC fractional method and the corresponding improvements of production is plotted in Figure 4.14.

In conclusion, the study confirms that the ABC fractional-order Model ($\theta = 0.918$) provides the best fit with experimental data, particularly in the early phase, due to its superior ability to retain memory effects. While the CF model aligns well at integer order ($\phi = 1$), it lacks accuracy at fractional orders (i.e. for $0 < \phi < 1$). Both models converge with experimental data in later stages, demonstrating their reliability in biodiesel kinetics modeling. Overall, the ABC model proves to be a more effective tool for capturing the history-dependent nature of transesterification reactions, making it a promising approach for optimizing biodiesel production. Finally, by controlling ultrasound frequency over time, biodiesel production can be increased by 4-6%.

5

Effect of Ultrasound Technique for Production of Biodiesel using Enzyme as Catalyst: A Mathematical Study

Earlier, we have used base-catalyzed transesterification process for biodiesel production, formulating different mathematical model and its in-depth analysis with the application of ultrasound in such systems. Biodiesel production through mechanical stirring with enzyme (lipase) catalysts has been extensively explored in earlier studies (Al Basir *et al.*, 2015; Al Basir and Roy, 2014, 2017), where we observed that the process is neither cost-effective nor time-efficient. Although lipase-catalyzed transesterification offers clear advantages in terms of tolerance to high FFA feedstocks and reduced byproduct formation, its application under conventional stirring is limited by high enzyme costs and prolonged reaction times, thereby reducing its economic feasibility. From previous chapters, it is evident that ultrasound technique is more effective than mechanical stirring in reducing mass transfer resistance during transesterification reaction. However, its role in enzymatic biodiesel production is yet to be explored through mathematical modeling. In this chapter [1], we aim to investigate whether the application of ultrasound can shorten the biodiesel conversion time and improve the overall cost-effectiveness of the process. To investigate this, we formulate a mathematical model based on the enzymatic reaction mechanism to capture the influence of ultrasound, and by applying optimal control theory, we derive an optimal ultrasound frequency profile for cost-effective biodiesel production, guided by the Pontryagin Minimum Principle.

[1]The major part of this chapter is published as a book chapter in International Conference on Mathematical Analysis and Application in Modeling, Springer Nature Singapore Pte Ltd. 2023, *doi.org*/10.1007/978 − 981 − 97 − 9194 − 1_18

5.1 The Mathematical Model

To formulate a simple mathematical model for the enzyme-catalyzed transesterification reaction, we make the following assumptions: (A) Jatropha oil primarily consists of triglycerides (TG) and free fatty acids (F), both of which undergo enzymatic transesterification reaction to produce biodiesel. (B) The enzymatic transesterification of Jatropha oil with alcohol (AL) can be represented as a two-step process.

- **Step 1:** One molecule of TG interacts with the enzyme E, leading to the formation of the enzyme–substrate complex C_1 ($E \cdot TG$) at a rate r_1. This complex subsequently dissociates, producing free fatty acids (F) and glycerol (GL) at a rate r_2, with possible reversal at rate r_{-2}.
- **Step 2:** The free fatty acid (F) combines with alcohol (AL) to form the second complex C_2 ($F \cdot AL$) at a rate r_3. This complex is converted to biodiesel (BD), regenerating the free enzyme (E), at a rate r_4. The reverse reactions occur at rates r_{-1} (for C_1) and r_{-3}, r_{-4} (for C_2 and BD respectively) (Al Basir *et al.*, 2015; Al Basir and Roy, 2014).

These steps can be represented schematically as follows:

$$\begin{aligned} \boldsymbol{E + TG} &\underset{\boldsymbol{r_{-1}}}{\overset{\boldsymbol{r_1}}{\rightleftharpoons}} \boldsymbol{[E \cdot TG]} \underset{\boldsymbol{r_{-2}}}{\overset{\boldsymbol{r_2}}{\rightleftharpoons}} \boldsymbol{F + GL}, \\ \boldsymbol{F + AL} &\underset{\boldsymbol{r_{-3}}}{\overset{\boldsymbol{r_3}}{\rightleftharpoons}} \boldsymbol{[F \cdot AL]} \underset{\boldsymbol{r_{-4}}}{\overset{\boldsymbol{r_4}}{\rightleftharpoons}} \boldsymbol{E + BD}, \end{aligned} \tag{5.1}$$

where r_1, r_2, r_3, and r_4 represent the forward rate constants, and $r_{-1}, r_{-2}, r_{-3}, r_{-4}$ correspond to the reverse rate constants. The values of these parameters are summarized in Table 5.2.

Under these mechanistic assumptions, the corresponding system of differential equations describing the dynamics of substrates, complexes, and products can be formulated as follows:

$$\begin{cases} \frac{dY_E}{dt} = -r_1 Y_T Y_E + r_{-1} Y_{C_1} + r_4 Y_{C_2} - r_{-4} Y_E Y_B, \\ \frac{dY_T}{dt} = -r_1 Y_T Y_E + r_{-1} Y_{C_1}, \\ \frac{dY_F}{dt} = r_2 Y_{C_1} - r_{-2} Y_F Y_G - r_3 Y_F Y_A + r_{-3} Y_{C_2}, \\ \frac{dY_B}{dt} = r_4 Y_{C_2} - r_{-4} Y_E Y_B + M_c Y_B \left(1 - \frac{Y_B}{B_{\max}}\right), \\ \frac{dY_A}{dt} = -r_3 Y_F Y_A + r_{-3} Y_{C_2}, \\ \frac{dY_{C_1}}{dt} = r_1 Y_T Y_E - r_{-1} Y_{C_1} - r_2 Y_{C_1} + r_{-2} Y_F Y_G, \\ \frac{dY_{C_2}}{dt} = r_3 Y_F Y_A - r_{-3} Y_{C_2} - r_4 Y_{C_2} + r_{-4} Y_E Y_B, \\ \frac{dY_G}{dt} = r_2 Y_{C_1} - r_{-2} Y_F Y_G, \end{cases} \tag{5.2}$$

with the initial condition, $Y_E(0) = Y_{E_0}$, $Y_{C_1}(0) = 0$, $Y_F(0) = 0$, $Y_A(0) = Y_{A_0}$, $Y_T(0) = Y_{T_0}$, $Y_{C_2}(0) = 0$, $Y_B(0) = 0$, and $Y_G(0) = 0$ letting the concentration of TG, E, F, C_1, C_2, AL, BD and GL as Y_T, Y_E, Y_F, Y_{C_1}, Y_{C_2}, Y_A, Y_B and Y_G respectively. We have formulated our model using a logistic framework by incorporating the term $M_c Y_B \left(1 - \frac{Y_B}{B_{\max}}\right)$ where, Y_B denotes the biodiesel concentration at any time t, and $B_{\max}$ represents the maximum achievable biodiesel concentration in the transesterification reaction. This expression has been utilized in a logistical sense, since the total mass transfer rate increases as mass transfer resistance decreases, and after reaching a specific ultrasound frequency and vessel diameter, the mass transfer resistance becomes negligible. M_c is the total mass transfer coefficient defined in (Cao *et al.*, 2024) as

$$M_c = \frac{k_c}{d} = 0.023 \frac{D}{d^2} (Re)^{0.8} (Sc)^{0.33} = 0.023 \frac{D}{d^2} \left(\frac{d^2 \rho H}{\mu}\right)^{0.8} \left(\frac{\mu}{\rho D}\right)^{0.33}, \tag{5.3}$$

where $Re = \frac{d^2 \rho H}{\mu}$ is Reynolds number and $Sc = \frac{\mu}{\rho D}$ is Schmidt number. μ, D, and ρ are viscosity, density, and the molecular diffusivity of jatropha oil, respectively. H stands for the ultrasound frequency used in the transesterification reaction, and d stands for the vessel's diameter. Numerical values of these parameters are given in Table 5.1.

5.2 The optimal control problem

Our main objective is to theoretically determine the optimal ultrasound frequency range that maximizes biodiesel yield, shortens reaction time, and minimizes production cost. Let ξ is the control variable that signifies the ultrasound frequency input, ranging within the interval of 0 to 1. The value $\xi = 1$ indicates full utilization

Parameter	Definition	Value
μ	viscosity	24.8646 kg·m^{-1}·s^{-1} (Pramanik, 2003)
ρ	density	896.5 kg·m^{-3} (Pramanik, 2003)
D	diffusivity	$(5.49 \times 10^{-6} - 1.17 \times 10^{-5})$ m^2·s^{-1} (Posom and Sirisomboon, 2014)
d	vessel diameter	$0.5 - 2$ m
H	ultrasound frequency	$40 - 60$ kHz

Table 5.1: *Some fundamental characteristics of Jatropha curcas oil.*

of ultrasound frequency, whereas $\xi = 0$ denotes no frequency.

The control-based system corresponding to System (5.2) is mathematically represented as:

$$\begin{cases} f_1 = \frac{dY_E}{dt} = -r_1 Y_T Y_E + r_{-1} Y_{C_1} + r_4 Y_{C_2} - r_{-4} Y_E Y_B, \\ f_2 = \frac{dY_T}{dt} = -r_1 Y_T Y_E + r_{-1} Y_{C_1}, \\ f_3 = \frac{dY_F}{dt} = r_2 Y_{C_1} - r_{-2} Y_F Y_G - r_3 Y_F Y_A + r_{-3} Y_{C_2}, \\ f_4 = \frac{dY_B}{dt} = r_4 Y_{C_2} - r_{-4} Y_E Y_B + \xi M_c Y_B \left(1 - \frac{Y_B}{B_{\max}}\right), \\ f_5 = \frac{dY_A}{dt} = -r_3 Y_F Y_A + r_{-3} Y_{C_2}, \\ f_6 = \frac{dY_{C_1}}{dt} = r_1 Y_T Y_E - r_{-1} Y_{C_1} - r_2 Y_{C_1} + r_{-2} Y_F Y_G, \\ f_7 = \frac{dY_{C_2}}{dt} = r_3 Y_F Y_A - r_{-3} Y_{C_2} - r_4 Y_{C_2} + r_{-4} Y_E Y_B, \\ f_8 = \frac{dY_G}{dt} = r_2 Y_{C_1} - r_{-2} Y_F Y_G, \end{cases} \tag{5.4}$$

with initial condition, $Y_E(0) = Y_{E_0}, Y_{C_1}(0) = 0, Y_F(0) = 0, Y_A(0) = Y_{A_0}, Y_T(0) = Y_{T_0}, Y_{C_2}(0) = 0, Y_B(0) = 0, Y_G(0) = 0$.

Our goal is to optimize biodiesel production while minimizing production costs. Therefore, the following cost function has been formulated:

$$J[\xi] = \int_{t_0}^{t_f} \left[W\xi^2 - PY_B^2\right] dt, \tag{5.5}$$

where $W > 0$ represents the weight constant assigned to the benefit of production costs, while P serves as the penalty multiplier. Now, we want to find out the optimal control ξ^* such that

$$J(\xi^*) = min\{J(\xi) : \xi \in Z\},$$

Z is the set of admissible control defined by

$$Z = \{\xi : \xi \text{ is measurable}, 0 \leq \xi \leq 1, t \in [t_i, t_f]\}.$$

The Hamiltonian can be written as:

$$H = W\xi^2 - PY_B^2 + \sum_{n=1}^{8} \Psi_i f_i, \tag{5.6}$$

where Ψ_1, Ψ_2,. . . ., Ψ_8 are adjoint variables.

Theorem 5.2.1. *If the given optimal control $\xi^*(t)$ and the solution $(Y_E, Y_T, Y_F, Y_B, Y_A, Y_{C_1}, Y_{C_2}, Y_G)$ of the System (5.4) minimize $J(\xi)$ over Z, then $\exists$ adjoint variables $\Psi_1, \Psi_2...., \Psi_8$ which satisfying:*

$$\begin{cases} \frac{d\Psi_1}{dt} = r_1 Y_T \left(\Psi_1 - \Psi_6\right) + r_{-4} Y_B \left(\Psi_4 - \Psi_7\right), \\ \frac{d\Psi_2}{dt} = r_1 Y_E \left(\Psi_1 + \Psi_2 - \Psi_6\right), \\ \frac{d\Psi_3}{dt} = r_3 Y_A \left(\Psi_5 - \Psi_7\right) + r_{-2} Y_G \left(\Psi_3 - \Psi_6\right), \\ \frac{d\Psi_4}{dt} = 2PY_B + \Psi_4 \left\{ r_{-4} Y_E + \frac{M_c Y_B \xi}{B_{\max}} - M_c \xi \left(1 - \frac{Y_B}{B_{\max}}\right) \right\} - \Psi_7 r_{-4} Y_E, \\ \frac{d\Psi_5}{dt} = r_3 Y_F \left(\Psi_5 - \Psi_7\right), \\ \frac{d\Psi_6}{dt} = r_{-1} \left(\Psi_6 - \Psi_2\right) + r_2 \left(\Psi_6 - \Psi_3\right), \\ \frac{d\Psi_7}{dt} = -r_4 \Psi_4 - r_{-3} + r_{-3} \Psi_7, \\ \frac{d\Psi_8}{dt} = r_{-2} \left(\Psi_8 - \Psi_6\right), \end{cases} \tag{5.7}$$

along with the transversality condition $\Psi_i\left(t_f\right) = 0$, $i = 1, ..., 8$, and

$$\xi^* = \max\left(0, \min\left(\frac{-M_c\left[\Psi_4 Y_B\left(1 - \frac{Y_B}{B_{\max}}\right)\right]}{2W}, 1\right)\right). \tag{5.8}$$

Proof. The Hamiltonian (5.6) is:

$$H = W\xi^2 + M_c\xi\left[\Psi_4 Y_B\left(1 - \frac{Y_B}{B_{\max}}\right)\right] + \text{ terms without } \xi. \tag{5.9}$$

As per the Minimum Principle of Pontryagin, the optimal control ξ^* satisfies

$$\frac{\partial H}{\partial \xi^*} = 0.$$

Now, from System (5.7) and Equation (5.9), we have

$$\frac{\partial H}{\partial \xi^*} = 2W\xi^* + M_c Y_B \left(1 - \frac{Y_B}{B_{\max}}\right)(\Psi_4) = 0.$$

Solving we get,

$$\xi^* = \frac{-M_c \left[\Psi_4 Y_B \left(1 - \frac{Y_B}{B_{\max}}\right)\right]}{2W}.$$

Hence the optimal control $\xi^*(t)$ will be

$$\xi^* = \max\left(0, \min\left(\frac{-M_c \left[\Psi_4 Y_B \left(1 - \frac{Y_B}{B_{\max}}\right)\right]}{2W}, 1\right)\right).$$

By Pontryagin's Minimum Principle, adjoint variables satisfy,

$$\frac{d\Psi_i}{dt} = -\frac{\partial H}{\partial Y_i},$$

with $Y_i \equiv (Y_E, Y_T, Y_F, Y_B, Y_A, Y_{C_1}, Y_{C_2}, Y_G)$ i.e. $Y_1 = Y_E$, $Y_2 = Y_T$, etc. and thus adjoint System (5.7) can be obtained from Equation (5.6) with transversality conditions $\Psi_i\left(t_f\right) = 0, (i = 1, 2, ..., 8)$. □

5.3 Numerical Validation

The system dynamics are numerically solved in this section using the ode45 solver for better prediction about the system. This study seeks to investigate the dynamical behavior of the transesterification reaction for biodiesel synthesis using a lipase enzyme as the catalyst. To overcome the mass transfer resistance between the reactants, ultrasound frequency is utilized, and a comparison of biodiesel yields with and without control is conducted using the Pontryagin Minimum Principle and Hamiltonian. To investigate potential mass-transfer effects on biodiesel production, simulations of the System (5.2) are performed using various ultrasound frequencies (40-60 kHz). In Figure 5.1, the biodiesel concentration is plotted at a fixed molar ratio (5:1) and 0.5 m of vessel diameter, indicating a clear positive correlation between

Parameter	Value
r_1	7.5128 mol·L^{-1}·h^{-1}
r_{-1}	0.1147 h^{-1}
r_2	0.1032 h^{-1}
r_{-2}	0.0988 mol·L^{-1}·h^{-1}
r_3	1.9370 mol·L^{-1}·h^{-1}
r_{-3}	0.0323 h^{-1}
r_4	1.9230 h^{-1}
r_{-4}	0.0011 mol·L^{-1}·h^{-1}
$B_{\max}$	3 mol·L^{-1}

Table 5.2: *Rate constants at 40 °C and other parameters used for the numerical validation.*

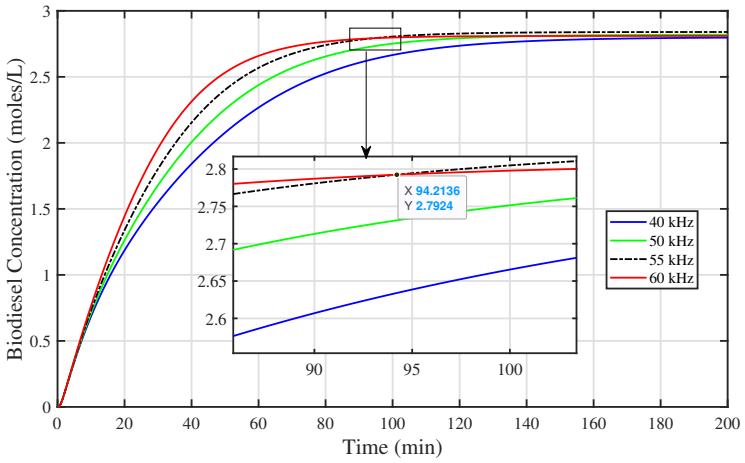

Figure 5.1: *Variation of biodiesel yield for different ultrasound frequencies is shown in this figure, with parameters as given in Table 5.1 and Table 5.2. Here, d = 0.5 m, 1:5 oil to methanol molar ratio.*

ultrasound frequency and both biodiesel production and mass transfer. The reaction rate exhibits a significant increase with ultrasound frequency up to 55 kHz. However, with a further increase in ultrasound frequency, the concentration of biodiesel decreases over time (after 94 min). At higher ultrasound frequencies, methanol molecules transform rapidly from the liquid phase into the vapor phase. As a result, the reaction medium becomes unstable, and the effective methanol concentration available for the reaction decreases. Moreover, excessive ultrasound frequencies increase the reaction temperature, which promotes foam formation and consequently disrupts efficient mass transfer during biodiesel synthesis. The impact of vessel diameter on reaction kinetics is evident in Figure 5.2. It shows that reducing the vessel

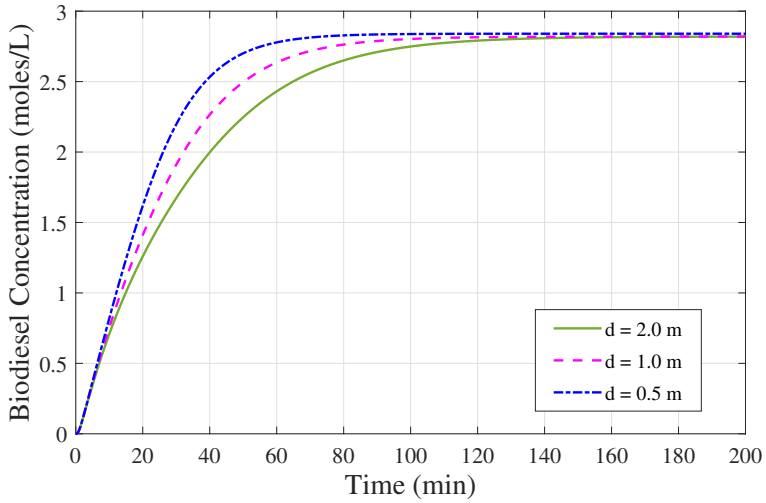

Figure 5.2: *Impact of varying vessel diameters on the production of biodiesel. Here H = 55 kHz, Oil : Methanol = 1 : 5.*

diameter, with the ultrasound frequency set at 55 kHz and the oil-to-methanol molar ratio at 1:5, enhances biodiesel production. When the vessel diameter increases, the turbulence between Jatropha oil and methanol decreases because the mixing energy is distributed over a larger cross-sectional area, which makes the fluid interactions weaker. On the other hand, a smaller vessel diameter confines the mixing energy in a smaller volume, which makes turbulence stronger. Consequently, a smaller vessel diameter lowers mass transfer resistance and enhances biodiesel production. Hence, the diameter of the vessel is a key factor in biodiesel production. Figure 5.3

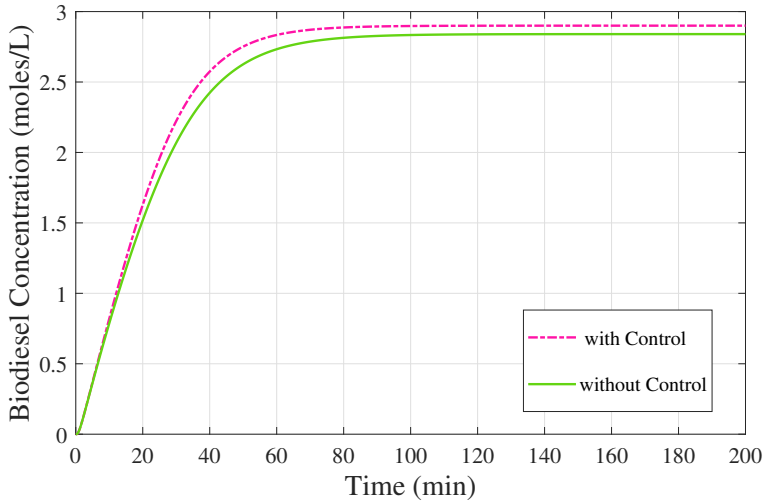

Figure 5.3: *Concentration trajectories of biodiesel with and without optimal control at H = 55 kHz, 1:5 oil:methanol molar ratio, and d = 0.5 m.*

outlines a comparative study on the concentration of biodiesel with and without a

control approach with ultrasound frequency. The figure demonstrates that the yield of biodiesel increases by about 5.66% in one hour with this control operation, with the best conditions for the reaction setup being ultrasound frequency, $H = 55$ kHz, vessel diameter, $d = 0.5$ m, and a 5:1 alcohol-to-oil molar ratio. Even though a higher frequency rate initially produces greater mixing intensity, applying control only to the ultrasound frequency improves the production of biodiesel, saves time and energy. In this chapter, a mathematical model is proposed to study the influence of ultrasound on the enzymatic transesterification process for producing biodiesel from Jatropha oil. The process faces a slow reaction rate because of heavy mass-transfer resistance, hindering cost-effective biodiesel production through lipase-catalyzed reactions. To address this, we have implemented a control theoretic approach to regulate mixing intensity and observed a significant impact on the reaction system, which contributes to higher biodiesel production. Numerical simulations determine the influence of ultrasound frequency on biodiesel production in terms of mass transfer coefficient.

It can be concluded that a higher control of the ultrasound frequency at the start of the reaction is necessary until the continuous phase is produced, after which a lesser amount of control is sufficient for proper mixing of alcohol and Jatropha oil during the transesterification reaction. Moreover, optimization of enzymatic production indicates that maximum biodiesel can be achieved in less than 2 hours of reaction time by employing the optimal ultrasound frequency with the Pontryagin Minimum Principle. Finally, this study demonstrates that a biodiesel yield of 94% can be achieved in less than 2 hours by appropriately regulating the ultrasound frequency, where the optimal operating conditions are identified as ultrasound frequency, $H = 55$ kHz, a vessel diameter, $d = 0.5$ m, and an alcohol-to-Jatropha oil molar ratio is 5:1. This finding highlights the crucial role of process parameter optimization in enhancing transesterification efficiency and provides a reliable guideline for the experimental researcher for the ultrasound-assisted biodiesel production.

6

Mathematical Modelling of Pest Control on *Jatropha curcas* using Sterile Insect Technology

Biodiesel has emerged as a promising renewable fuel, and extensive research has been directed toward optimizing the transesterification process for its efficient production. However, the ecological challenges that influence feedstock availability have received comparatively less attention. *Jatropha curcas*, a prominent biodiesel crop, often suffers significant yield losses due to pest infestations, particularly by *Pempelia morosalis*, a major pest of Jatropha plants. This vulnerability hampers its potential for large-scale cultivation. To address this issue, the final chapter[1] of this thesis introduces three mathematical models that incorporate the Sterile Insect Technique (SIT) to control pest populations and ensure the long-term sustainability of Jatropha biomass. Our proposed mathematical framework rigorously evaluates two principal release modalities, continuous and impulsive (periodic) introductions, to determine cost-effective strategies that achieve maximal pest eradication while minimizing resource expenditure. This ecological modeling approach addresses a critical gap by aligning pest management with the broader goal of securing biodiesel feedstock.

[1]Maximum portion of this chapter has been communicated in a peer-reviewed international journal.

6.1 Model without Sterile Male

6.1.1 Formulation of the mathematical model

In this subsection, we first describe the basic framework and formulation of a mathematical model that comprises four compartments of the pest population and one compartment indicating the *Jatropha curcas* plant biomass (denoted as J). The significance of the system parameters and the detailed description of the dynamical interactions between the system populations are noted below.

- Two main developmental stages of pest populations are considered: the immature stage (P_I), which includes larvae, pupae, and eggs, and the adult stage. The adult stage is further divided into three compartments: wild males (P_M), wild females available for mating (P_F), and fertilized females (P_R).
- Due to the finite size of plantations, however, it may be large, we assume logistic growth for the biomass of *Jatropha curcas* plant (Al Basir *et al.*, 2018; Venturino *et al.*, 2016), with net growth rate r_J and carrying capacity K_J. This growth is hindered by the feeding activity of immature pests, where the feeding loss is modeled by the term $\beta_J J P_I$, with β_J being the consumption rate of plant biomass per immature pest.
- The immature pest population increases due to egg production by fertilized females at a rate r_1. However, this population is reduced by natural mortality at a rate d_1.
- Some larvae transform from immature pests to mature pests by consuming Jatropha biomass. If larvae consume biomass at a rate of β_J, then they will transform into mature ones at a conversion rate of β'_J for biomass consumption, where it is important to note that $\beta_J \geq \beta'_J$.
- Upon maturing, a proportion d of the immature pests become female adults, while the remaining $(1 - d)$ become wild males. The wild females seek mates, and successful mating occurs between P_F and P_M at a rate γ, resulting in the production of fertilized females.
- The fertilized females later return to the mating pool at a rate r_2, or die naturally at a rate d_3. Meanwhile, both female and male adult pests suffer natural mortality, modeled by rates d_2 and d_4, respectively.

All the system parameters are considered to be positive and based on the assumptions made above, the proposed mathematical model is described as below:

$$\begin{cases} \frac{dJ}{dt} & = r_J J\left(1-\frac{J}{K_J}\right) - \beta_J J P_I, \\ \frac{dP_I}{dt} & = r_1 P_R - d_1 P_I - \beta'_J J P_I, \\ \frac{dP_F}{dt} & = d\beta'_J J P_I - \gamma P_F P_M + r_2 P_R - d_2 P_F, \\ \frac{dP_R}{dt} & = \gamma P_F P_M - r_2 P_R - d_3 P_R, \\ \frac{dP_M}{dt} & = (1-d)\beta'_J J P_I - d_4 P_M, \end{cases} \tag{6.1}$$

with initial conditions: $J(0) \geq 0$, $P_I(0) \geq 0$, $P_F(0) \geq 0$, $P_R(0) \geq 0$, $P_M(0) \geq 0$.

6.1.2 Theoretical study of the system

In this section, we provide a detailed description of the theoretical analysis of system (6.1) in various aspects. We begin by verifying the non-negativity of the system solutions, followed by the boundedness and other crucial properties.

6.1.2.1 Non-Negative invariance of the system solutions

Theorem 6.1.1. *The solutions of system (6.1) with the given non-negative initial conditions are non-negative; i.e., $J(t) \geq 0$, $P_I(t) \geq 0$, $P_F(t) \geq 0$, $P_R(t) \geq 0$, and $P_M(t) \geq 0$ for all possible $t > 0$.*

Proof. Let us define the biologically feasible region:

$$\Omega = \{(J, P_I, P_F, P_R, P_M) \in \mathbb{R}^5 \geq 0\}.$$

We will show that the solutions of the system remain positive for all $t > 0$ provided they start with non-negative initial conditions. Let us check the behavior of the system when each variable individually becomes zero while the others remain non-negative:
When the Jatropha biomass J is zero, it remains non-negative, and in this case, no negative flow is observed i.e.

$$\Omega\{0, P_I, P_F, P_R, P_M\} = 0.$$

When the immature pest population P_I is zero, it can only increase due to reproduction by fertilized females i.e.

$$\Omega\{J, 0, P_F, P_R, P_M\} = r_1 P_R \geq 0 \quad \text{(since } r_1 \geq 0 \text{ and } P_R \geq 0\text{)}.$$

When the mating female population P_F is considered to be zero, it is observed that the increment is regulated by the maturation of the immature pests and partly contributed by the fertilized females i.e.

$$\Omega\{J, P_I, 0, P_R, P_M\} = d\beta'_J J P_I + r_2 P_R \geq 0 \quad \text{(since } d, \beta'_J, r_2 \geq 0 \text{ and } J, P_I, P_R \geq 0\text{)}.$$

When the fertilized female population P_R is zero, it can be generated through mating between wild males and mating females which is analytically represented as

$$\Omega\{J, P_I, P_F, 0, P_M\} = \gamma P_F P_M \geq 0 \quad \text{(since } \gamma \geq 0, \text{ and } P_F \geq 0, P_M \geq 0\text{)}.$$

When the fertilized female population P_R is zero, it can be generated through mating between wild males and mating females i.e.

$$\Omega\{J, P_I, P_F, P_R, 0\} = (1-d)\beta'_J J P_I \geq 0 \quad \text{(since } d, \beta'_J \geq 0, \text{ and } J, P_I \geq 0\text{)}.$$

Thus, in every situation, the derivative of each variable at the boundary of the positive orthant either vanishes or points into the positive orthant. Therefore, we conclude that the system is positive invariant in Ω, meaning that if the initial conditions are non-negative, then the solutions remain non-negative for all future time. Hence, the system preserves positivity in Ω. □

6.1.2.2 Boundedness of the solutions

Theorem 6.1.2. *All non-negative solutions of the system (6.1) enter into the region* $\Omega \subseteq R^5_+$ *and are ultimately bounded where* Ω *is defined by* $\Omega = \{(J, P_I, P_F, P_R, P_M) \in \mathbb{R}^5_+ : 0 \leq J + P_I + P_F + P_R + P_M \leq \frac{r_J K_J}{4\lambda}\}$.

Proof. Let us define the total population and biomass as:

$$W(t) = J(t) + P_I(t) + P_F(t) + P_R(t) + P_M(t).$$

Differentiating $W(t)$ with respect to time, we get:

$$\frac{dW}{dt} = \frac{dJ}{dt} + \frac{dP_I}{dt} + \frac{dP_F}{dt} + \frac{dP_R}{dt} + \frac{dP_M}{dt}.$$

Substituting from System (6.1), and by simplifying, we get:

$$\frac{dW}{dt} = r_J J - \frac{r_J J^2}{K_J} - d_1 P_I - d_2 P_F - (d_3 - r_1) P_R - d_4 P_M.$$

Since all compartments $P_I, P_F, P_R, P_M \geq 0$, we observe that:

$$\frac{dW}{dt} \leq r_J J - \frac{r_J J^2}{K_J}. \tag{6.2}$$

Now, to facilitate the analysis, we add a damping term λW to both of the sides of inequality (6.2), where we have assumed that $\lambda = \min\{d_1, d_2, d_3 - r_1, d_4\}$. Thus, we obtain that

$$\frac{dW}{dt} + \lambda W \leq r_J J - \frac{r_J J^2}{K_J} \implies \frac{dW}{dt} + \lambda W \leq \frac{r_J K_J}{4}.$$

From this, using the standard comparison theorem for differential inequalities, we obtain:

$$W(t) \leq \frac{r_J K_J}{4\lambda} + C_1 e^{-\lambda t},$$

where C_1 is a constant depending on the initial condition. When $t \to \infty$, the exponential term decays to zero, and it follows that

$$W(t) \leq W_0 \quad \text{with} \quad W_0 = \frac{r_J K_J}{4\lambda}.$$

Hence, the system is bounded and all the solutions of system (6.1) eventually enter a compact absorbing set. □

6.1.3 Existence of equilibria

The system (6.1) has three equilibrium points, namely,

1. the trivial equilibrium point $E_0^* = (0, 0, 0, 0, 0)$,
2. the pest-free equilibrium point $E_1^* = (K_J, 0, 0, 0, 0)$,
3. the interior equilibrium point $E_2^* = (J^*, P_I^*, P_F^*, P_R^*, P_M^*)$,

where

$$P_I^* = r_J(\frac{K_J - J^*}{\beta_J K_J}),\ P_F^* = \frac{d_4(r_2 + d_3)(d_1 + \beta'_J J^*)}{\gamma r_1 \beta'_J (1-d) J^*},$$
$$P_R^* = r_J(\frac{K_J - J^*}{r_1 \beta_J K_J})(d_1 + \beta'_J J^*),\ P_M^* = \frac{(1-d)\beta'_J r_J J^*}{d_4 \beta_J K_J}(K_J - J^*).$$

Utilizing these, we get a polynomial of J^* of degree three such that

$$J^{*3}\{\gamma r_J \beta_J'^2 (1-d)(d_3 - dr_1)\} + J^{*2}\{\gamma r_J K_J \beta_J'^2 (1-d)(dr_1 - d_3) + \gamma d_1 d_3 r_J \beta'_J (1-d)\}$$
$$- J^*\{\gamma d_1 d_3 r_J K_J \beta'_J (1-d) + (r_2 + d_3) d_2 d_4 \beta_J \beta'_J K_J\} - d_1 d_2 d_4 \beta_J K_J (r_2 + d_3) = 0. \tag{6.3}$$

The number of changes of sign in the coefficients of the polynomial (6.3) for positive J^* is exactly one if $d_3 > dr_1$. Therefore, by Descartes' Rule of Signs, we conclude that the polynomial has at least one positive real root. This ensures the existence of a biologically feasible solution for J^*. Consequently, as a result of the previous discussion, we now state the following theorem.

Theorem 6.1.3. *System (6.1) always admits a coexistence equilibrium point, provided that the condition $d_3 > dr_1$ holds.*

6.1.3.1 Stability analysis

We now investigate the local stability properties of the system around three equilibria: the trivial equilibrium E_0, the pest-free equilibrium E_1, and the endemic equilibrium E_2^*. The nature of these equilibria can be determined by evaluating the sign of the eigenvalues associated with the linearized system around each equilibrium. However, we present the results directly without explicitly displaying the corresponding Jacobian matrices.

Theorem 6.1.4. *System (6.1) exhibits the following stability behaviors:*

(i) The trivial equilibrium point $E_0 = (0, 0, 0, 0, 0)$ is always unstable.

(ii) The pest-free equilibrium point $E_1 = (K_J, 0, 0, 0, 0)$ is locally asymptotically stable.

Proof. The variational matrix of the System (6.1) is given by:

$$V = \begin{bmatrix} r_J - \frac{2r_J J}{K_J} - \beta_J P_I & -\beta_J J & 0 & 0 & 0 \\ -\beta'_J P_I & -d_1 - \beta'_J J & 0 & r_1 & 0 \\ d\beta'_J P_I & d\beta'_J J & -\gamma P_M - d_2 & r_2 & -\gamma P_F \\ 0 & 0 & \gamma P_M & -(r_2 + d_3) & \gamma P_F \\ (1-d)\beta'_J P_I & (1-d)\beta'_J J & 0 & 0 & -d_4 \end{bmatrix}. \tag{6.4}$$

(i) At the trivial equilibrium point E_0, matrix (6.4) reduces to:

$$V_0 = \begin{bmatrix} r_J & 0 & 0 & 0 & 0 \\ 0 & -d_1 & 0 & r_1 & 0 \\ 0 & 0 & -d_2 & r_2 & 0 \\ 0 & 0 & 0 & -(r_2 + d_3) & 0 \\ 0 & 0 & 0 & 0 & -d_4 \end{bmatrix}. \tag{6.5}$$

Here, only one eigenvalue is positive and the others are negative. Therefore, the trivial equilibrium E_0 is unstable always.

(ii) At the pest-free equilibrium point E_1, the Jacobian matrix of the System (6.1) is given by from (6.4):

$$V_1 = \begin{bmatrix} -r_J & -\beta_J K_J & 0 & 0 & 0 \\ 0 & -d_1 - \beta'_J K_J & 0 & r_1 & 0 \\ 0 & d\beta'_J K_J & -d_2 & r_2 & 0 \\ 0 & 0 & 0 & -(r_2 + d_3) & 0 \\ 0 & (1-d)\beta'_J K_J & 0 & 0 & -d_4 \end{bmatrix}. \tag{6.6}$$

All the eigenvalues for the above Jacobian Matrix are negative in nature, and hence the system (6.1) is stable around the pest-free equilibrium point E_1.

□

We now turn to the endemic equilibrium point $E_2^* = (J^*, P_I^*, P_F^*, P_R^*, P_M^*)$, where both the plant and pest populations coexist. At the endemic equilibrium point E_2^*, the variational matrix of the System (6.1) is given by:

$$V_2 = \begin{bmatrix} -\frac{r_J J^*}{K_J} & -\beta_J J^* & 0 & 0 & 0 \\ -\beta'_J P_I^* & -\frac{r_1 P_R^*}{P_I^*} & 0 & r_1 & 0 \\ d\beta'_J P_I^* & d\beta'_J J^* & -\gamma P_M^* - d_2 & r_2 & -\gamma P_F^* \\ 0 & 0 & \gamma P_M^* & -(r_2 + d_3) & \gamma P_F^* \\ \frac{d_4 P_M^*}{J^*} & \frac{d_4 P_M^*}{P_I^*} & 0 & 0 & -d_4 \end{bmatrix}.$$

The characteristic equation of the linearized system at E_2^* is given by:

$$x^5 + A_1 x^4 + A_2 x^3 + A_3 x^2 + A_4 x + A_5 = 0, \tag{6.7}$$

where the coefficients A_1, A_2, A_3, A_4, A_5 are positive expressions depending on model parameters and equilibrium values. To determine the stability of E_2^*, we apply the Routh–Hurwitz criterion, which provides necessary and sufficient conditions for all the roots of the polynomial equation (6.7) to have negative real parts.

Theorem 6.1.5. *The endemic equilibrium point $E_2^* = (J^*, P_I^*, P_F^*, P_R^*, P_M^*)$ of System (6.1) is locally asymptotically stable if the following Routh–Hurwitz conditions hold:*
(i) $A_1 > 0, A_5 > 0$, *(ii)* $A_1 A_2 - A_3 > 0$, *(iii)* $A_3 (A_1 A_2 - A_3) - A_1^2 A_4 + A_1 A_5 > 0$, *and (iv)* $A_1 \{A_2 (A_3 A_4 - A_2 A_5) - A_4 (A_1 A_2 - A_3)\} - A_3 (A_3 A_4 - A_2 A_5) + A_5 (A_1 A_4 - A_5) > 0$.

If all the above conditions are satisfied, then the system will return to the endemic equilibrium E_2^* following small perturbations, confirming its local asymptotic stability.

6.2 System with Continuous Release of Sterile Males

6.2.1 Formulation of the modified model

A control strategy is introduced by continuously releasing sterile male pests into the environment. These sterile males, denoted by $P_S(t)$, do not contribute to reproduction but compete with wild males for mating opportunities. The sterile males are introduced at a constant rate π and die naturally at a rate d_5. So, the population evolves according to the balance between input and mortality. To incorporate mating competition, the mating process is now divided between wild and sterile males. A female mates with a wild male with probability proportional to $\frac{P_M}{P_M+P_S}$, and with a sterile male at $\frac{P_S}{P_M+P_S}$. The actual rates of mating are governed by parameters γ_1 and γ_2 for wild and sterile males, respectively. Since sterile matings are non-reproductive, only matings with wild males lead to the production of fertilized females. Consequently, the rate of fertilization is given by $\gamma_1 P_F(\frac{P_M}{P_M+P_S})$, and the loss of females to sterile matings is captured by $\gamma_2 P_F(\frac{P_S}{P_M+P_S})$. Incorporating this effect into the dynamics of system (6.1), the modified and improvised system can be written as:

$$\begin{cases} \frac{dJ}{dt} &= r_J J\left(1-\frac{J}{K_J}\right) - \beta_J J P_I, \\ \frac{dP_I}{dt} &= r_1 P_R - d_1 P_I - \beta'_J J P_I, \\ \frac{dP_F}{dt} &= d\beta'_J J P_I - \gamma_1 P_F\left(\frac{P_M}{P_M+P_S}\right) - \gamma_2 P_F\left(\frac{P_S}{P_M+P_S}\right) + r_2 P_R - d_2 P_F, \\ \frac{dP_R}{dt} &= \gamma_1 P_F\left(\frac{P_M}{P_M+P_S}\right) - r_2 P_R - d_3 P_R, \\ \frac{dP_M}{dt} &= (1-d)\beta'_J J P_I - d_4 P_M, \\ \frac{dP_S}{dt} &= \pi - d_5 P_S, \end{cases} \tag{6.8}$$

with initial conditions: $J(0) \geq 0, \quad P_I(0) \geq 0, \quad P_F(0) \geq 0, \quad P_R(0) \geq 0, \quad P_M(0) \geq 0, \quad P_S(0) \geq 0.$

6.2.2 Theoretical study of the system

6.2.2.1 Boundedness of the system solutions

Theorem 6.2.1. *For the sterile pest introduced system i.e., for system (6.8), all the solutions start from $\mathbb{R}^6_+$ are bounded by $\frac{1}{\lambda'}(\pi + \frac{r_J K_J}{4}) + ce^{-\lambda' t}$ with c is a constant and as t tends to infinity, $Y(t) \leq Y_0$ where $Y_0 = \frac{1}{\lambda'}(\pi + \frac{r_J K_J}{4})$.*

Proof. The proof is straightforward and similar to the proof of boundedness of solutions of system (6.1) described in Theorem 6.1.2. □

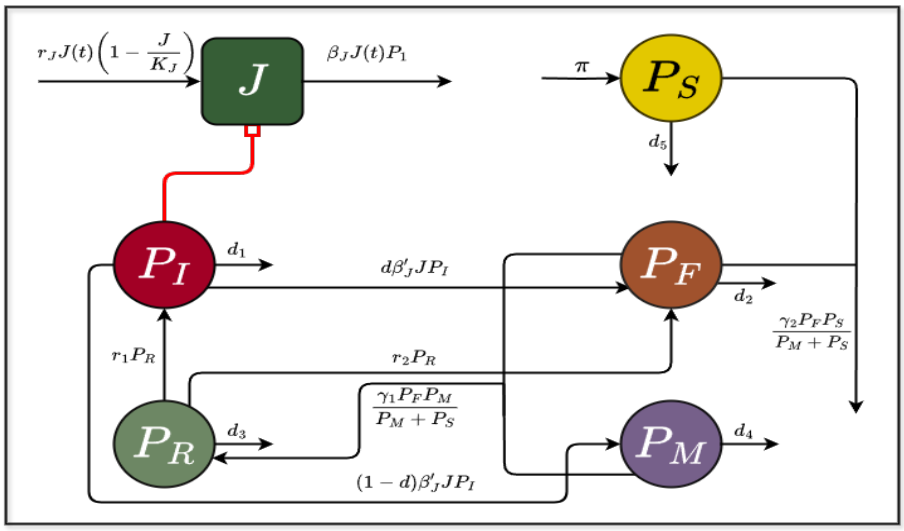

Figure 6.1: *Schematic diagram for the interaction of Jatropha curcas biomass and Pempelia morosalis pest population when sterile male is introduced in the system.*

6.2.2.2 Steady states of the system

The system with continuous release of sterile male i.e. system (6.8) has three equilibrium points which are noted below.
(i) Axial equilibrium described as $E'_1(0, 0, 0, 0, 0, \frac{\pi}{d_5})$,
(ii) Natural pest-free equilibrium i.e. $E'_2(K_J, 0, 0, 0, 0, \frac{\pi}{d_5})$ and
(iii) Endemic equilibrium i.e. $E^*_3(J^*, P^*_I, P^*_F, P^*_R, P^*_M, P^*_S)$.

6.2.2.3 Global stability of the endemic equilibrium

We now approach to evaluate the required conditions for the global asymptotic stability of system (6.8) at the endemic steady state E^*_3. To perform this, firstly, suppose the Lyapunov function is defined as follows:

$$L = \frac{1}{2}[(J - J^*)^2 + (P_I - P^*_I)^2 + (P_F - P^*_F)^2 + (P_R - P^*_R)^2 + (P_M - P^*_M)^2 + (P_S - P^*_S)^2].$$

This implies

$$\begin{aligned}
\frac{dL}{dt} &= (J-J^*)\frac{dJ}{dt} + (P_I - P_I^*)\frac{dP_I}{dt} + (P_F - P_F^*)\frac{dP_F}{dt} + (P_R - P_R^*)\frac{dP_R}{dt} + (P_M - P_M^*)\frac{dP_M}{dt} + (P_S - P_S^*)\frac{dP_S}{dt},\\
&= (J-J^*)[r_J J(1-\frac{J}{K_J}) - \beta_J J P_I] + (P_I - P_I^*)[r_1 P_R - d_1 P_I - \beta_J' J P_I] + (P_F - P_F^*)[d\beta_J' J P_I - \frac{\gamma_1 P_F P_M}{P_M + P_S}\\
&- \frac{\gamma_2 P_F P_S}{P_M + P_S} + r_2 P_R - d_2 P_F] + (P_R - P_R^*)[\frac{\gamma_1 P_F P_M}{P_M + P_S} - r_2 P_R - d_3 P_R] + (P_M - P_M^*)[(1-d)\beta_J' J P_I - d_4 P_M]\\
&+ (P_S - P_S^*)(\pi - d_5 P_S),\\
&= r_J(J-J^*)^2 - \frac{r_J(J-J^*)^3}{K_J} - \beta_J(J-J^*)(JP_I - J^*P_I^*) + r_1(P_I - P_I^*)(P_R - P_R^*) - d_1(P_I - P_I^*)^2\\
&- \beta_J'(P_I - P_I^*)(JP_I - J^*P_I^*) + d\beta_J'(P_F - P_F^*)(JP_I - J^*P_I^*) - \frac{\gamma_1(P_F - P_F^*)(P_F P_M - P_F^* P_M^*)}{(P_M - P_M^*) + (P_S - P_S^*)}\\
&- \frac{\gamma_2(P_F - P_F^*)(P_F P_S - P_F^* P_S^*)}{(P_M - P_M^*) + (P_S - P_S^*)} + r_2(P_F - P_F^*)(P_R - P_R^*) - d_2(P_F - P_F^*)^2 + \frac{\gamma_1(P_R - P_R^*)(P_F P_M - P_F^* P_M^*)}{(P_M - P_M^*) + (P_S - P_S^*)}\\
&- (r_2 + d_3)(P_R - P_R^*)^2 + (1-d)\beta_J'(P_M - P_M^*)(JP_I - J^*P_I^*) - d_4(P_M - P_M^*)^2 + \pi(P_S - P_S^*) - d_5(P_S - P_S^*)^2.
\end{aligned}$$

From this, it follows

$$\begin{aligned}
&\frac{dL}{dt}\\
&\leq r_J(J-J^*)^2 - \frac{r_J(J-J^*)^3}{K_J} - \beta_J(J-J^*)(JP_I - J^*P_I + J^*P_I - J^*P_I^*) + r_1(P_I - P_I^*)(P_R - P_R^*)\\
&- \beta_J'(P_I - P_I^*)(JP_I - J^*P_I + J^*P_I - J^*P_I^*) + d\beta_J'(P_F - P_F^*)(JP_I - J^*P_I^*)\\
&- \frac{\gamma_1(P_F - P_F^*)(P_F P_M - P_F^* P_M + P_F^* P_M - P_F^* P_M^*)}{(P_M - P_M^*) + (P_S - P_S^*)} - \frac{\gamma_2(P_F - P_F^*)(P_F P_S - P_F^* P_S + P_F^* P_S - P_F^* P_S^*)}{(P_M - P_M^*) + (P_S - P_S^*)}\\
&+ r_2(P_F - P_F^*)(P_R - P_R^*) + \frac{\gamma_1(P_R - P_R^*)(P_F P_M - P_F^* P_M^*)}{(P_M - P_M^*) + (P_S - P_S^*)} + (1-d)\beta_J'(P_M - P_M^*)(JP_I - J^*P_I^*) + \pi(P_S - P_S^*),\\
&\leq r_J(J-J^*)^2 - \frac{r_J(J-J^*)^3}{K_J} - \beta_J(J-J^*)\{P_I(J-J^*) + J^*(P_I - P_I^*)\} + r_1(P_I - P_I^*)(P_R - P_R^*) - \beta_J'(P_I - P_I^*)\\
&\{P_I(J-J^*) + J^*(P_I - P_I^*)\} + d\beta_J'(P_F - P_F^*)(JP_I - J^*P_I^*) - \frac{\gamma_1(P_F - P_F^*)\{P_M(P_F - P_F^*) + P_F^*(P_M - P_M^*)\}}{(P_M - P_M^*) + (P_S - P_S^*)}\\
&- \frac{\gamma_2(P_F - P_F^*)\{P_S(P_F - P_F^*) + P_F^*(P_S - P_S^*)\}}{(P_M - P_M^*) + (P_S - P_S^*)} + r_2(P_F - P_F^*)(P_R - P_R^*) + \frac{\gamma_1(P_R - P_R^*)(P_F P_M - P_F^* P_M^*)}{(P_M - P_M^*) + (P_S - P_S^*)}\\
&+ (1-d)\beta_J'(P_M - P_M^*)(JP_I - J^*P_I^*) + \pi(P_S - P_S^*),\\
&\leq r_J(J_{\max} - J^*)^2 - \frac{r_J(J_{\max} - J^*)^3}{K_J} - \beta_J J^*(J_{\max} - J^*)(P_{I\max} - P_I^*) + r_1(P_{I\max} - P_I^*)(P_{R\max} - P_R^*)\\
&- \beta_J' P_I(J_{\max} - J^*)(P_{I\max} - P_I^*) + d\beta_J'(P_{F\max} - P_F^*)(J_{\max}P_{I\max} - J^*P_I^*) - \frac{\gamma_1 P_M(P_{F\max} - P_F^*)^2}{(\alpha P_{M\min} - P_M^*) + (\alpha P_{S\min} - P_S^*)}\\
&- \frac{\gamma_1 P_F^*(P_{F\max} - P_F^*)(P_{M\max} - P_M^*)}{(\alpha P_{M\min} - P_M^*) + (\alpha P_{S\min} - P_S^*)} - \frac{\gamma_2 P_S(P_{F\max} - P_F^*)^2}{(\alpha P_{M\min} - P_M^*) + (\alpha P_{S\min} - P_S^*)} - \frac{\gamma_2 P_F^*(P_{F\max} - P_F^*)(P_{S\max} - P_S^*)}{(\alpha P_{M\min} - P_M^*) + (\alpha P_{S\min} - P_S^*)}\\
&+ r_2(P_{F\max} - P_F^*)(P_{R\max} - P_R^*) + \frac{\gamma_1(P_{R\max} - P_R^*)(P_{F\max}P_{M\max} - P_F^* P_M^*)}{(\alpha P_{M\min} - P_M^*) + (\alpha P_{S\min} - P_S^*)}\\
&+ (1-d)\beta_J'(P_{M\max} - P_M^*)(J_{\max}P_{I\max} - J^*P_I^*) + \pi(P_{S\max} - P_S^*), \quad [\text{where} \quad 0 < \alpha < 1]\\
&\leq r_J(J_{\max} - J^*)^2 + r_1(P_{I\max} - P_I^*)(P_{R\max} - P_R^*) + d\beta_J'(P_{F\max} - P_F^*)(J_{\max}P_{I\max} - J^*P_I^*)\\
&+ \gamma_1[\frac{(P_{R\max} - P_R^*)(P_{F\max}P_{M\max} - P_F^* P_M^*) - P_M(P_{F\max} - P_F^*)^2 - P_F^*(P_{F\max} - P_F^*)(P_{M\max} - P_M^*)}{(\alpha P_{M\min} - P_M^*) + (\alpha P_{S\min} - P_S^*)}\\
&+ r_2(P_{F\max} - P_F^*)(P_{R\max} - P_R^*) + (1-d)\beta_J'(P_{M\max} - P_M^*)(J_{\max}P_{I\max} - J^*P_I^*) + \pi(P_{S\max} - P_S^*)\\
&- \gamma_2[\frac{P_S(P_{F\max} - P_F^*)^2 + P_F^*(P_{F\max} - P_F^*)(P_{S\max} - P_S^*)}{(\alpha P_{M\min} - P_M^*) + (\alpha P_{S\min} - P_S^*)}.
\end{aligned}$$

We assume the following:

$$\begin{cases} J_{max} - J^* = m_1, & P_{I\max} - P_I^* = m_2, & P_{F\max} - P_F^* = m_3, \\ P_{R\max} - P_R^* = m_4, & P_{M\max} - P_M^* = m_5, & P_{S\max} - P_S^* = m_6, \\ J_{\max} P_{I\max} - J^* P_I^* = n_1, \\ P_{F\max} P_{M\max} - P_F^* P_M^* = n_2, \\ (\alpha P_{M\min} - P_M^*) + (\alpha P_{S\min} - P_S^*) = p. \end{cases}$$

As a result, it is obtained that

$$\begin{aligned} \frac{dL}{dt} &\leq r_J m_1^2 + r_1 m_2 m_4 + d\beta_J' m_3 n_1 + \gamma_1 \{ \frac{m_4 n_2 - m_3 P_M - P_F^* m_3 m_4}{p} \} + r_2 m_3 m_4 + \\ &\quad (1-d)\beta_J' m_5 n_1 + \pi m_6 - \gamma_2 \{ \frac{P_{S\min} m_3 + P_F^* m_3 m_6}{p} \}, \\ &\quad \leq T(\frac{S}{T} - 1), \end{aligned}$$

where

$$\begin{aligned} S &= r_J m_1^2 + r_1 m_2 m_4 + d\beta_J' m_3 n_1 + \gamma_1 \{ \frac{m_4 n_2 - m_3 P_M - P_F^* m_3 m_4}{p} \} + r_2 m_3 m_4 \\ &\quad + (1-d)\beta_J' m_5 n_1 + \pi m_6, \quad \textit{and} \quad T = \gamma_2 \{ \frac{P_{S\min} m_3 + P_F^* m_3 m_6}{p} \}. \end{aligned}$$

Thus, finally, we get

$$\frac{dL}{dt} \leq T(R_G - 1), \quad [\text{where} \quad R_G = \frac{S}{T}]. \tag{6.9}$$

Based on this previous analysis, we now have the following theorem.

Theorem 6.2.2. *System (6.8) will be globally asymptotically stable at the endemic equilibrium point* $E_3 = (J^*, P_I^*, P_F^*, P_R^*, P_M^*, P_S^*)$ *if the value of* R_G *is greater than* 1.

6.3 System with Periodic Release of Sterile Males

6.3.1 Framework of the system equipped with impulsive strategy

In this section, we have modified the previously developed model i.e. system (6.8) from the earlier structure where the strategy with continuous release of sterile males was adopted. Whenever modifying the previous system, the strategy is that the

sterile males will not be released continuously but rather in fixed-size batches at regular time intervals. We redesign system (6.8) by first considering that at every instant $t = nT$, where T is the release period and n is an integer, a fixed number π of sterile males is added to the population. Between these impulses, the sterile male population declines due to natural death at a rate d_5, following the equation $\frac{dP_S}{dt} = -d_5 P_S$. Jatropha biomass continues to grow logistically and is affected by immature pest feeding. Immature pests increase through reproduction, and mature into adults. A portion of the matured/adult pest becomes females and the other portion gets converted into males. Mating now involves both wild and sterile males, with the same competitive probabilities as before. Only matings with wild males yield new fertilized females. These fertilized females eventually transit back to the mating pool or die, and adult pests die naturally as well. The key difference in this model lies in the impulsive nature of sterile male release, which creates fluctuations in the sterile male population. Incorporation of this pulsatile intervention instead of continuous release leads to the impulsive mathematical model written as:

$$\begin{cases} \dfrac{dJ}{dt} = r_J J\left(1 - \dfrac{J}{K_J}\right) - \beta_J J P_I, & t \neq nT, \\ \dfrac{dP_I}{dt} = r_1 P_R - d_1 P_I - \beta'_J J P_I, & t \neq nT, \\ \dfrac{dP_F}{dt} = d\beta'_J J P_I - \gamma_1 P_F\left(\dfrac{P_M}{P_M + P_S}\right) - \gamma_2 P_F\left(\dfrac{P_S}{P_M + P_S}\right) + r_2 P_R - d_2 P_F, & t \neq nT, \\ \dfrac{dP_R}{dt} = \gamma_1 P_F\left(\dfrac{P_M}{P_M + P_S}\right) - r_2 P_R - d_3 P_R, & t \neq nT, \\ \dfrac{dP_M}{dt} = (1-d)\beta'_J J P_I - d_4 P_M, & t \neq nT, \\ \dfrac{dP_S}{dt} = -d_5 P_S, & t \neq nT, \\ P_S(t^+) = P_S(t^-) + \pi, & t = nT. \end{cases} \tag{6.10}$$

with initial conditions: $J(0) \geq 0$, $P_I(0) \geq 0$, $P_F(0) \geq 0$, $P_R(0) \geq 0$, $P_M(0) \geq 0$, $P_S(0) \geq 0$.

6.3.2 Boundedness of the model variables

Theorem 6.3.1. *For system (6.10), there exists a positive constant B such that $J(t) \leq B$, $P_I(t) \leq B$, $P_F(t) \leq B$, $P_R(t) \leq B$, $P_M(t) \leq B$ and $P_S(t) \leq B$ for all t large enough.*

Proof. Let

$$W'(t) = J + P_I + P_F + P_R + P_M + P_S.$$

Then,

$$\frac{dW'}{dt} = \dot{J} + \dot{P}_I + \dot{P}_F + \dot{P}_R + \dot{P}_M + \dot{P}_S.$$

Substituting the system dynamics, it is obtained that

$$\tfrac{dW'}{dt} = r_J\left(J - \tfrac{J^2}{K_J}\right) - \beta_J J P_I + r_1 P_R - d_1 P_I - \gamma_2 P_F\left(\tfrac{P_S}{P_M+P_S}\right) - d_2 P_F - d_3 P_R - d_4 P_M - d_5 P_S.$$

Bounding the nonlinear and decay terms, it follows that

$$\frac{dW'}{dt} \leq r_J J - \frac{r_J J^2}{K_J} - d_1 P_I - d_2 P_F - (d_3 - r_1) P_R - d_4 P_M - d_5 P_S.$$

Now, adding a damping term $\mu W'$ on both sides of this previous inequality, we obtain:

$$\frac{dW'}{dt} + \mu W' \leq r_J J - \frac{r_J J^2}{K_J}, \quad \text{where } \mu = \min\{d_1, d_2, d_3 - r_1, d_4, d_5\},$$
$$\implies \frac{dW'}{dt} + \mu W' \leq \frac{r_J K_J}{4}.$$

Therefore, $W'(t) \leq \dfrac{r_J K_J}{4\mu} + C_1 e^{-\mu t}$, (by the Grönwall-type inequality),

As $t \to \infty$, the exponential term vanishes, and we get the long-term bound:

$$W'(t) \leq W_0', \quad \text{where} \quad W_0' = \frac{r_J K_J}{4\mu}.$$

When, $t = nT$:

$$W'\left(nT^+\right) \leq W'(nT) + \pi.$$

By Comparison theorem, for $t \geq 0$, we have

$$W'(t) \leq W'(0)\, e^{-\mu t} + \frac{W_0'\left(1 - e^{-\mu\tau}\right)}{\mu} + \pi\frac{e^{-\mu(t-\varepsilon_1)}}{1 - e^{\mu T}}$$
$$+ \pi\frac{e^{\mu T}}{e^{\mu T} - 1} \to \frac{W_0'}{\mu} + \pi\frac{e^{\mu T}}{e^{\mu T} - 1} \quad \text{as} \quad t \to \infty.$$

Thus, $W'(t)$ is uniformly bounded and hence, there exist $B > 0$ such that $J(t) \leq B$, $P_I(t) \leq B$, $P_F(t) \leq B$, $P_R(t) \leq B$, $P_M(t) \leq B$ and $P_S(t) \leq B$ for all t large enough. □

6.3.3 Natural pest-free periodic solution

In this section, we discuss the natural pest eradication solution of system (6.10), i.e., for $P_I = 0$, $P_F = 0$, $P_R = 0$, and $P_M = 0$, $t \geq 0$ then the sixth equation of the System (6.10) will be
For $t \neq nT$,

$$\frac{\mathrm{d}P_S}{\mathrm{d}t} = -\mathrm{d}_5 P_S, \tag{6.11}$$

For $t = nT$

$$P_S\left(t^+\right) = P_S\left(t^-\right) + \pi. \tag{6.12}$$

Thus, for $t \in \left(nT, (n+1)T\right]$, the solution of first equation of the subsystem (6.11) is given as follows,

$$P_S(t) = \left\{P_S\left(0^+\right) - P_S^*\left(0^+\right)\right\} e^{-dt} + P_S^*(t), \tag{6.13}$$

where $P_S^*(t)$ is the positive periodic solution of System (6.10) which is given as

$$P_S^*(t) = \frac{\pi e^{-d(t-nT)}}{1 - e^{-dT}}, \tag{6.14}$$

with initial values

$$P_S^*\left(0^+\right) = \frac{\pi}{1 - e^{-dT}}. \tag{6.15}$$

If $P_I(t) = 0$, $P_F(t) = 0$, $P_R(t) = 0$ and $P_M(t) = 0$, then the first equation of System (6.10) is

$$\frac{dJ}{dt} = r_J J\left(1 - \frac{J}{K_J}\right), \tag{6.16}$$

which is a logistic equation, and its solution is

$$J(t) = \frac{K_J J(0)}{J(0) + (K_J - J(0))e^{r_J t}} \quad \text{for} \quad t \neq nT. \tag{6.17}$$

Clearly, (6.17) has two equilibria, such as $J = 0$ and $J = K_J$. Therefore, system (6.10) has two natural pest eradication solutions, $\left(0, 0, 0, 0, 0, P_S^*\right)$ and $\left(K_J, 0, 0, 0, 0, P_S^*\right)$. But $J = 0$ is not possible. For this reason, in the following subsection we study the stability for the system (6.10) at $E = \left(K_J, 0, 0, 0, 0, P_S^*\right)$.

6.3.4 Stability of the natural pest-free periodic solution

We establish the following theorem for the stability of the pest-free periodic orbit.

Theorem 6.3.2. *System (6.10) is locally stable around the natural pest-free periodic solution* $E = \left(K_J, 0, 0, 0, 0, P_S^*\right)$ *for the application of sterile male release at time interval* $t = nT$.

Proof. We need to prove the stability of the system for the application of sterile male release at the system at every T interval. We discuss the stability of the system through the small amplitude perturbation method at the periodic solution E.
Let

$$J(t) = K_J + \epsilon_1(t), \quad P_I(t) = \epsilon_2(t), \quad P_F(t) = \epsilon_3(t),$$
$$P_R(t) = \epsilon_4(t), \quad P_M(t) = \epsilon_5(t), \quad P_S(t) = P_S^*(t) + \epsilon_6(t),$$

where $\epsilon_1, \epsilon_2, \epsilon_3, \epsilon_4, \epsilon_5$ and ϵ_6 denote small amplitude perturbations. Thus, the corresponding system of (6.10) at E is given by

$$\begin{cases} \frac{d\epsilon_1}{dt} = r_J\left\{K_J + \epsilon_1(t)\right\}\left(1 - \frac{K_J + \epsilon_1(t)}{K_J}\right) - \beta\left\{K_J + \epsilon_1(t)\right\}\epsilon_2(t), & t \neq nT, \\ \frac{d\epsilon_2}{dt} = r_1\epsilon_4(t) - d_1\epsilon_2(t) - \beta'\left\{K_J + \epsilon_1(t)\right\}\epsilon_2(t), & t \neq nT, \\ \frac{d\epsilon_3}{dt} = d\beta'\left\{K_J + \epsilon_1(t)\right\}\epsilon_2(t) - \frac{\gamma_1\epsilon_3(t)\epsilon_5(t)}{\epsilon_5(t) + \epsilon_6(t) + P_S^*(t)} - \frac{\gamma_2\epsilon_3(t)\{\epsilon_6(t) + P_S^*\}}{\epsilon_5(t) + \epsilon_6(t) + P_S^*(t)} \\ \qquad +r_2\epsilon_4(t) - d_2\epsilon_3(t), & t \neq nT, \\ \frac{d\epsilon_4}{dt} = \frac{\gamma_1\epsilon_3(t)\epsilon_5(t)}{\epsilon_5(t) + \epsilon_6(t) + P_S^*(t)} - r_2\epsilon_4(t) - d_3\epsilon_4(t), & t \neq nT, \\ \frac{d\epsilon_5}{dt} = (1-d)\beta'\left\{K_J + \epsilon_1(t)\right\}\epsilon_2(t) - d_4\epsilon_5(t), & t \neq nT, \\ \frac{d\epsilon_6}{dt} = -d_5\{P_S^*(t) + \epsilon_6\}, & t \neq nT, \\ \Delta\left\{P_S^*(t) + \epsilon_6(t)\right\} = \pi, & t = nT. \end{cases} \tag{6.18}$$

Now, the linear system corresponding to the system (6.18) is given as

$$\begin{cases} \frac{d\epsilon_1}{dt} = -r_J\epsilon_1(t) - \beta_J K_J \epsilon_2(t), & t \neq nT, \\ \frac{d\epsilon_2}{dt} = r_1\epsilon_4(t) - d_1\epsilon_2(t) - \beta' K_J \epsilon_2(t), & t \neq nT, \\ \frac{d\epsilon_3}{dt} = d\beta' K_J \epsilon_2(t) + r_2\epsilon_4(t) - d_2\epsilon_3(t), & t \neq nT, \\ \frac{d\epsilon_4}{dt} = -r_2\epsilon_4(t) - d_4\epsilon_4(t) & t \neq nT, \\ \frac{d\epsilon_5}{dt} = (1-d)\beta' K_J \epsilon_2(t) - d_4\epsilon_5(t), & t \neq nT, \\ \frac{d\epsilon_6}{dt} = -d_5 P_S^*(t) - d_5\epsilon_6(t), & t \neq nT, \\ \Delta\epsilon_6(t) = s, & t = nT. \end{cases} \tag{6.19}$$

The fundamental matrix $M(t)$ of (6.19) is obtained as

$$\frac{dM(t)}{dt} = \begin{bmatrix} -r_J & -\beta_J K_J & 0 & 0 & 0 & 0 \\ 0 & -d_1 - \beta'_J K_J & 0 & r_1 & 0 & 0 \\ 0 & d\beta'_J K_J & -d_2 & r_2 & 0 & 0 \\ 0 & 0 & 0 & -r_2 - d_3 & 0 & 0 \\ 0 & (1-d)\beta'_J K_J & 0 & 0 & -d_4 & 0 \\ 0 & 0 & 0 & 0 & 0 & -d_5 \end{bmatrix}, \tag{6.20}$$

with initial condition $M(0) = I_6$. Now, the fundamental solution matrix is given by

$$M(t) = \frac{1}{m} \begin{bmatrix} e^{-r_J t} & e^{-\beta_J K_J t} & 0 & 0 & 0 & 0 \\ 0 & e^{-(d_1+\beta'_J K_J)t} & 0 & e^{r_1 t} & 0 & 0 \\ 0 & e^{d\beta'_J K_J t} & e^{-d_2 t} & e^{r_2 t} & 0 & 0 \\ 0 & 0 & 0 & e^{-(r_2+d_3)t} & 0 & 0 \\ 0 & e^{(1-d)\beta'_J K_J t} & 0 & 0 & e^{-d_4 t} & 0 \\ 0 & 0 & 0 & 0 & 0 & e^{-d_5 t} \end{bmatrix}. \tag{6.21}$$

According to Floquet theory (Klausmeier, 2008), the periodic solution $E\left(K_J, 0, 0, 0, 0, P_S^*\right)$ is asymptotically stable if the absolute values of the eigenvalues of $M(T)$ are less than one.

The eigenvalues of $M(T)$ are

$$\lambda_1 = \exp\{-r_J T\}, \quad \lambda_2 = \exp(-(d_1 + \beta'_J K_J)T), \quad \lambda_3 = \exp(-d_2 T),$$
$$\lambda_4 = \exp(-(r_2 + d_3)T), \quad \lambda_5 = \exp(-d_4 T), \quad \lambda_6 = \exp(-d_5 T).$$

It is evident that all the eigenvalues of the fundamental matrix $M(T)$ lies in the ranges given as: $0 < \lambda_1 < 1$, $0 < \lambda_2 < 1$, $0 < \lambda_3 < 1$, $0 < \lambda_4 < 1$, $0 < \lambda_5 < 1$ and $0 < \lambda_6 < 1$. Thus, when sterile male are released in the system with time interval T, the system remains locally stable around the pest-free periodic solution $E = \left(K_J, 0, 0, 0, 0, P_S^*\right)$. □

6.4 Numerical Simulation

Parameter	Definition	Value / Range
r_J	Intrinsic growth rate of Jatropha biomass	0.2 day^{-1}
K_J	Carrying capacity of Jatropha biomass	100 units
β_J	Consumption rate of biomass by immature pest	0.0002–0.0006 units^{-1}·day^{-1}
r_1	Birth rate of immature pest from fertilized female pest	5–15 day^{-1}
β'_J	Conversion rate of immature pest to mature pest	0.00005–0.0004 units^{-1}·day^{-1}
d	Coefficient of conversion from immature to mature pest	0.5
γ_1	Mating rate between female and wild male pest	0.001–0.01 units^{-1}·day^{-1}
γ_2	Mating rate between female and sterile male pest	0.001–0.01 units^{-1}·day^{-1}
r_2	Transition rate from fertilized female to female pest	0.05–0.5 day^{-1}
π	Release rate of sterile male to the system	1–50 units·day^{-1}
d_1	Natural death rate of immature pest	0.01–0.1 day^{-1}
d_2	Natural death rate of wild female pest	0.01 day^{-1}
d_3	Natural death rate of fertilized female pest	0.01 day^{-1}
d_4	Natural death rate of wild male pest	0.01 day^{-1}
d_5	Natural death rate of sterile male pest	0.01 day^{-1}

Table 6.1: *Model parameters, their definitions, and corresponding values/ranges used in the numerical simulations.*

In this section, we employ numerical techniques to explore and validate the dynamical behavior of the Jatropha–pest interaction models under various control

strategies based on the sterile insect technique (SIT). Our aim is to perform a comparative investigation between two distinct SIT implementations: (i) the continuous release of sterile male pests at a constant rate, and (ii) the periodic impulsive release of sterile males at fixed intervals. Through numerical simulations, we analyze how these two approaches influence pest suppression and biomass restoration under different parametric settings. The key objective is to identify which implementation strategy offers more efficient and sustainable pest control outcomes.

Figure 6.2 represents the scenario of uncontrolled pest outbreak where the value of

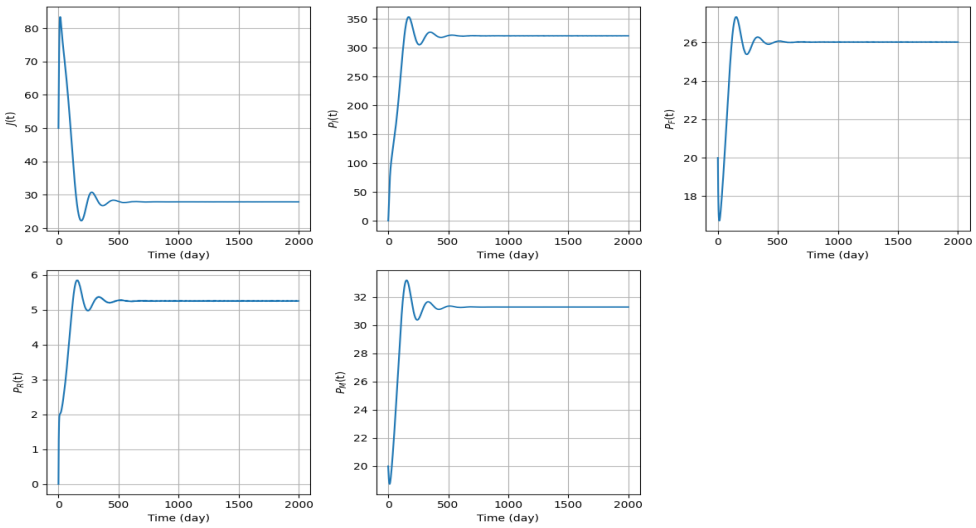

Figure 6.2: *Temporal dynamics of the Jatropha curcas biomass and pest population compartments for system (6.1) in the absence of sterile male pests. The plant biomass declines sharply due to pest feeding pressure, while all pest subpopulations, immature pests, wild females, fertilized females, and wild males, increase and stabilize over time, illustrating the harmful effect of uncontrolled pest proliferation on crop sustainability. For this simulation, it is chosen that* $\gamma = 0.0024$ *and the other values are given as:* $r_J = 0.2$, $K_J = 100$, $\beta_J = 0.00045$, $d_1 = 0.08$, $\beta'_J = 0.00007$, $d = 0.5$, $r_2 = 0.3$, $d_2 = 0.01$, $d_3 = 0.01$, $d_4 = 0.01$.

the mating rate is considered as $\gamma = 0.0024$. We can observe that the natural growth of the pest population leads to a sharp decline in the plant biomass (J) initially and then gradually stabilizes at a low level. This depletion occurs due to intense feeding pressure by immature pests, modeled by the term $\beta_J J P_I$ in the system dynamics. Simultaneously, it indicates the destructive impact of pest infestation on plantation productivity. The pest compartments become stabilized at high densities which signifies the establishment of a persistent pest population. The plant biomass reaches a low equilibrium value, reflecting long-term damage. These dynamics highlight

the essence for novel pest control strategies which should be coupled with or implemented over system (6.1).

Figure 6.3 depicts the temporal dynamics of the Jatropha–pest system without any control intervention. The characteristic behaviour of plant biomass $J(t)$ and pest compartments i.e. immature pests $P_I(t)$, fertilized females $P_F(t)$, reproductive females $P_R(t)$, and wild males $P_M(t)$, is shown over time. In this uncontrolled scenario, pest populations persist across all stages of development. The immature pests $P_I(t)$ exhibit high-amplitude oscillations, reflecting periodic surges in recruitment. This behavior arises as the mating rate between wild females and wild males is chosen considerably higher than the previous circumstance i.e. $\gamma = 0.0065$ is assigned to exhibit this simulation. These recurrent pest outbreaks continually suppress the growth of the Jatropha plant. The *Jatropha curcas* biomass initially rises but then falls into a damped oscillatory pattern, never reaching its carrying capacity. This is a direct consequence of the sustained herbivory pressure from the larvae of the immature pest population.

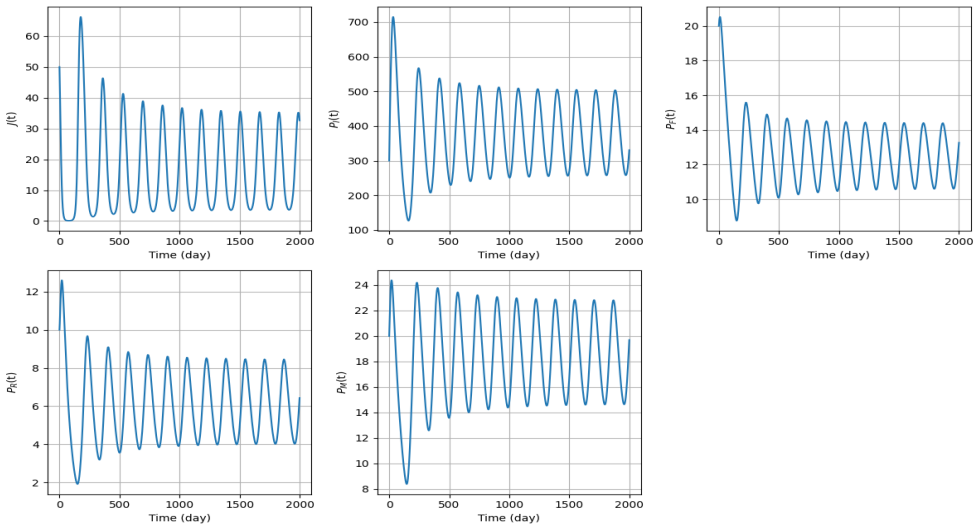

Figure 6.3: *Time evolution of the Jatropha–pest system i.e. system (6.1) in the absence of control. The panels show: (top-left) Jatropha biomass $J(t)$, (top-middle) immature pests $P_I(t)$, (top-right) fertilized females $P_F(t)$, (bottom-left) reproductive females $P_R(t)$, and (bottom-right) wild male pests $P_M(t)$. During the simulation of this Figure, we have assigned the particular value of $\gamma = 0.0065$ and the values of the other system parameters are noted as: $r_J = 0.2$, $K_J = 100$, $\beta_J = 0.00045$, $d_1 = 0.08$, $\beta'_J = 0.00007$, $d = 0.5$, $r_2 = 0.3$, $d_2 = 0.01$, $d_3 = 0.01$, $d_4 = 0.01$.*

To investigate the dynamical behavior of the Jatropha–pest interaction model denoted as system (6.1) with respect to variations in the fertilization rate parameter γ, crucial bifurcation analysis is conducted. The parameter γ represents the rate at

which reproductive females become fertilized via interactions with wild males. Understanding its influence is critical because it directly affects the reproduction rate of pests and thereby influences the population dynamics and plant biomass significantly. In this context, Figure 6.4 has been simulated and it presents the Hopf

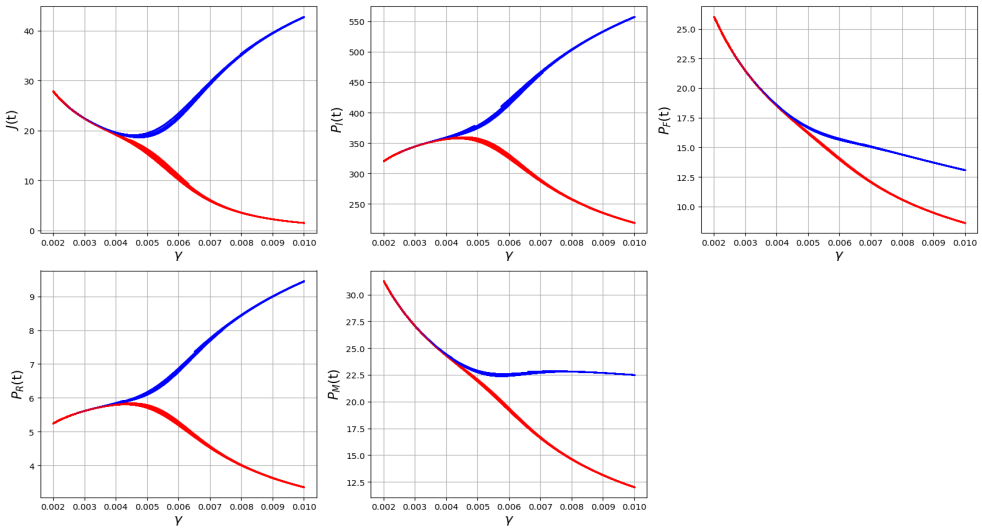

Figure 6.4: *Hopf bifurcation diagrams of the state populations of system (6.1) with respect to the fertilization rate γ. Each panel shows the bifurcation profile of different state variables. A supercritical Hopf bifurcation occurs at $\gamma_c \approx 0.0054$, beyond which the system exhibits stable limit cycles. Red and blue curves indicate the lower and upper bounds of oscillations, respectively.*

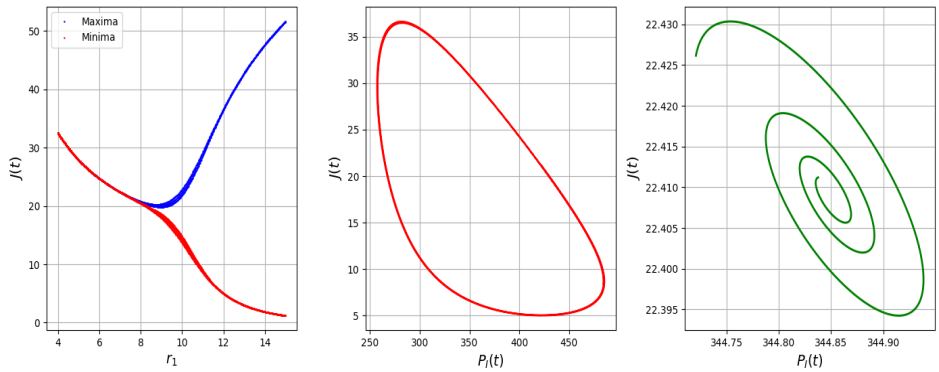

Figure 6.5: *(i) Subfigure in the left panel exhibits Hopf bifurcation diagrams with respect to the birth rate of immature pest from fertilized female r_1. Bifurcating solutions begin to generate when birth rate r_1 of immature pest exceeds 8 units/day. Other parameter values are $r_J = 0.2$, $K_J = 100$, $\beta_J = 0.00045$, $d_1 = 0.08$, $\beta'_J = 0.00007$, $d = 0.5$, $\gamma = 0.002$, $r_2 = 0.3$, $d_2 = 0.01$, $d_3 = 0.01$, $d_4 = 0.01$. (ii) Subfigure in the middle panel demonstrates limit cycle solution of the Jatropha biomass $J(t)$ with respect to immature pest when the birth rate is considered as $r_1 = 12$ units/day. (iii) Subfigure in the right panel presents limit cycle solution of $J(t)$ with respect to $P_i(t)$ where the value of r_1 is varied from the previous scenario and fixed as $r_1 = 7$ units/day.*

bifurcation diagram for the system over the range $\gamma \in [0.002, 0.01]$. For each variable, the red and blue curves denote the minimum and maximum values achieved by the state in the asymptotic time interval, capturing the emergence of limit cycles when the solutions of the system becomes oscillatory. Bifurcation occurs at a critical threshold $\gamma_c \approx 0.0054$. For values $\gamma < \gamma_c$, the system remains stabilized to an equilibrium point, indicating that the pest and plant populations reach steady levels after transients dissipate. However, when γ exceeds the critical value γ_c, the equilibrium loses stability, and the system undergoes a supercritical Hopf bifurcation. This leads to the emergence of sustained periodic oscillations (limit cycles) in the densities of all the state variables. For the plant biomass $J(t)$, it can be observed that

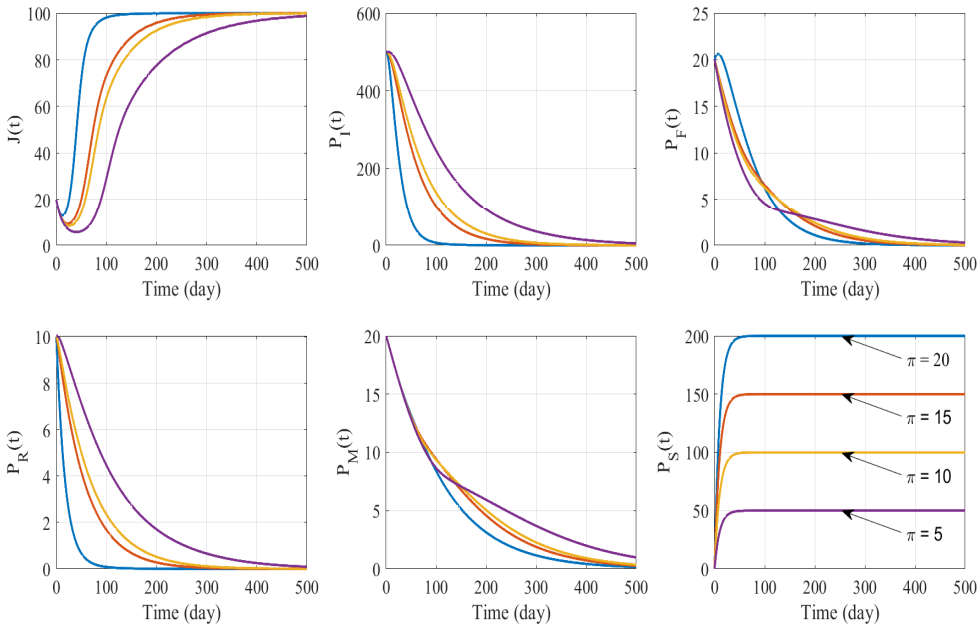

Figure 6.6: *Time evolution of system (6.8) under continuous sterile male release strategy for various values of π (the number of sterile males released per unit time). Simulations suggests that increasing π leads to faster pest eradication and biomass restoration.*

the amplitude of the oscillations exhibits an increasing pattern after the bifurcation takes place. This clearly suggests that higher fertilization efficiency leads to more pronounced fluctuations in biomass due to pest pressure. The bifurcation analysis, thus, identifies $\gamma_c \approx 0.0054$ as a threshold parameter value that separates stable coexistence from cyclic dominance in the Jatropha–pest ecosystem. This finding is crucial for pest management strategies, as it suggests that exceeding this threshold could trigger persistent pest outbreaks and biomass degradation unless effective controls are introduced. In addition, another interesting simulation is performed in

Figure 6.5 to investigate the dynamical change or shift in $J(t)$ whenever r_1 is varied. Observations present that the birth rate of immature pest population greatly impacts the Jatropha biomass. Here, the specific value of $r_1 = 8$ acts as a critical threshold. Values before $r_1 = 8$ indicate a stable scenario while oscillatory periodic solutions occur once r_1 crosses the critical value as validated strongly by the limit cycle solutions provided in the Subfigures of the rightmost and middle panel in Figure 6.5.

Figure 6.6 illustrates the temporal evolution of the Jatropha biomass and the pest population compartments under the implementation of a continuous sterile insect release strategy. In this control strategy, a constant number π of sterile male pests per day is introduced into the system. During these simulations, we have considered four different release rates: $\pi = 5$ units/day, $\pi = 10$ units/day, $\pi = 15$ units/day, and $\pi = 20$ units/day. The Jatropha biomass $J(t)$ shows a strong positive response

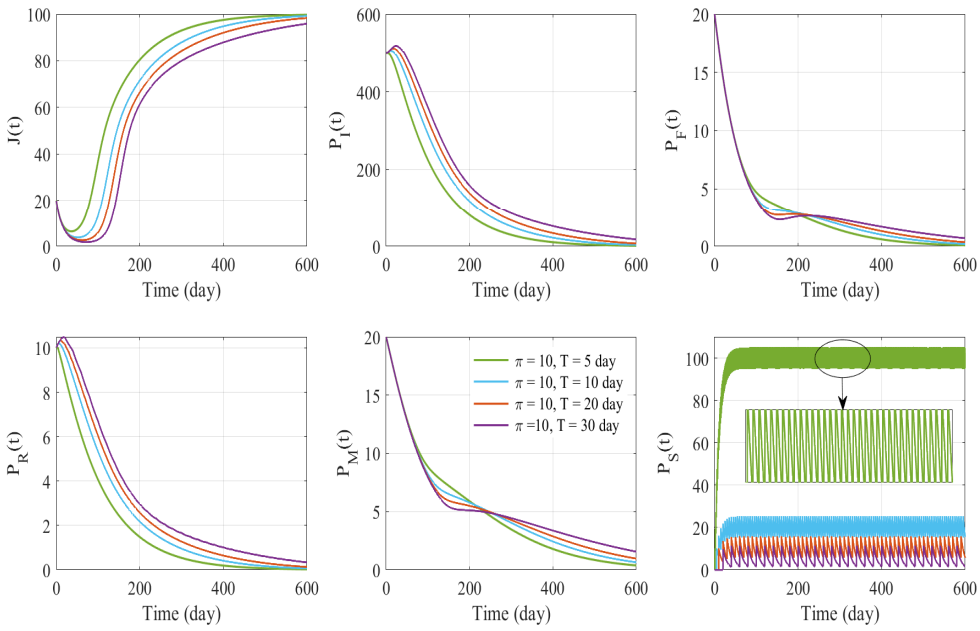

Figure 6.7: *Time evolution of Jatropha biomass $J(t)$ and pest populations under impulsive SIT control with sterile release rate $\pi = 10$. Four release intervals are considered: $T = 5, 10, 20,$ and 30 days. Frequent releases (smaller T) enhance pest suppression and lead to a faster increase in $J(t)$, while longer intervals reduce the efficiency of the control. Oscillatory behavior in $P_S(t)$ reflects the impulsive nature of sterile male introductions.*

to increasing π. For higher values of π, the damage done by the pest affecting the plant health is more effectively suppressed, leading to faster recovery and stabilization of plant biomass. When $\pi = 20$ units/day, the biomass reaches its maximum

capacity rapidly, whereas for lower π, the recovery is slower and less pronounced. The pest population compartments $P_I(t)$, $P_F(t)$, $P_R(t)$, and $P_M(t)$ all display a monotonic decline over time, with the decay rate strongly influenced by the release rate π. When the sterile male release rate is fixed at $\pi = 20$ units/day, the immature and reproductive pest populations approach extinction within approximately 100 days. In contrast, wild female pests are eradicated by around 300 days, and the wild male pest population becomes exterminated by nearly 450 days. However, for a lower release rate of $\pi = 5$, the control strategy exhibits a much weaker response. In this case, the reduction in pest populations is considerably slower and takes a much longer time to achieve a remarkably low density. The sterile male population $P_S(t)$, shown in the bottom-right panel of Figure 6.6, increases monotonically and stabilizes at a constant level for each release scenario, with the final equilibrium proportional to the release rate π. The results clearly demonstrate that continuous release of sterile males can effectively suppress the pest population and facilitate the rapid restoration of the Jatropha biomass.

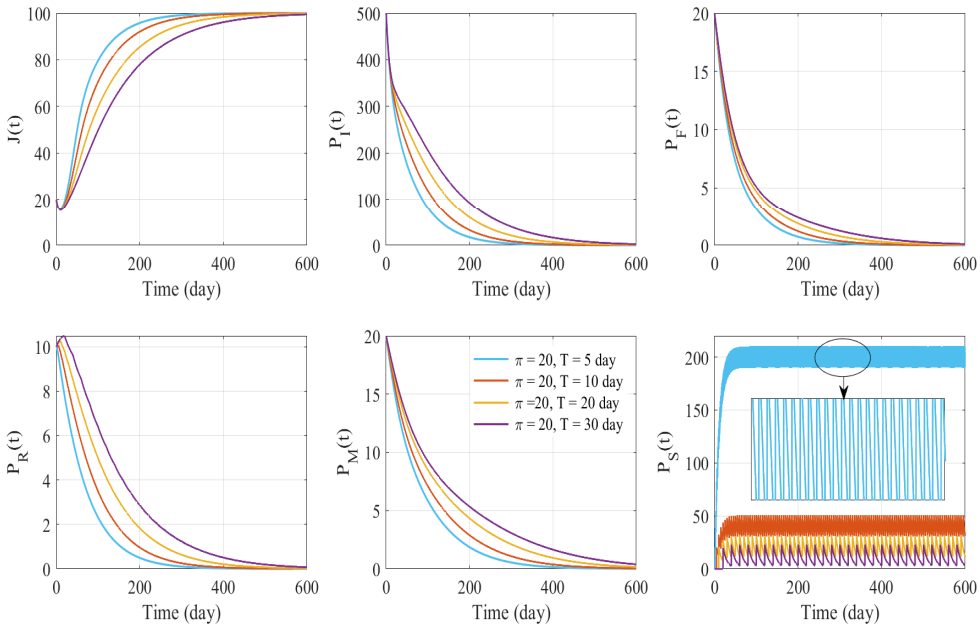

Figure 6.8: *Time series of Jatropha biomass and pest compartments under sterile release rate $\pi = 20$ and varying release intervals $T = 5$, 10, 20, and 30 days. The moderate release intensity leads to enhanced pest suppression compared to $\pi = 10$, with faster decline in pest populations and more rapid biomass recovery. Sterile males remain sufficiently competitive across all T, with reduced oscillatory amplitude in $P_S(t)$ compared to lower release rates.*

To scrutinize the effectiveness of the sterile insect technique (SIT) with impulsive releases, simulations are performed for system (6.10) for three different sterile release sizes, $\pi = 10$ units, 20 units, and 50 units, under varying release intervals $T = 5$, 10, 20, and 30 days. The results are illustrated in Figures 6.7, 6.8 and 6.9, respectively, where each figure shows the time evolution of Jatropha biomass and pest population compartments: immature pests, wild females, fertile females, wild males, and sterile males. For $\pi = 10$ units as demonstrated in Figure 6.7, the release intensity is observed to be low which conveys that effective pest control depends heavily on frequent releases. Whenever the release interval is $T = 5$ or 10 days, the Jatropha biomass gradually increases and eventually stabilizes at more than 400 days and the immature, female and reproductive female pest populations are eradicated in around 400 days. The wild male pest populations take more than 600 days to be eradicated in this particular scenario. However, for $T = 20$ or 30 days, the pest populations decline slowly, reflecting delayed pest suppression.

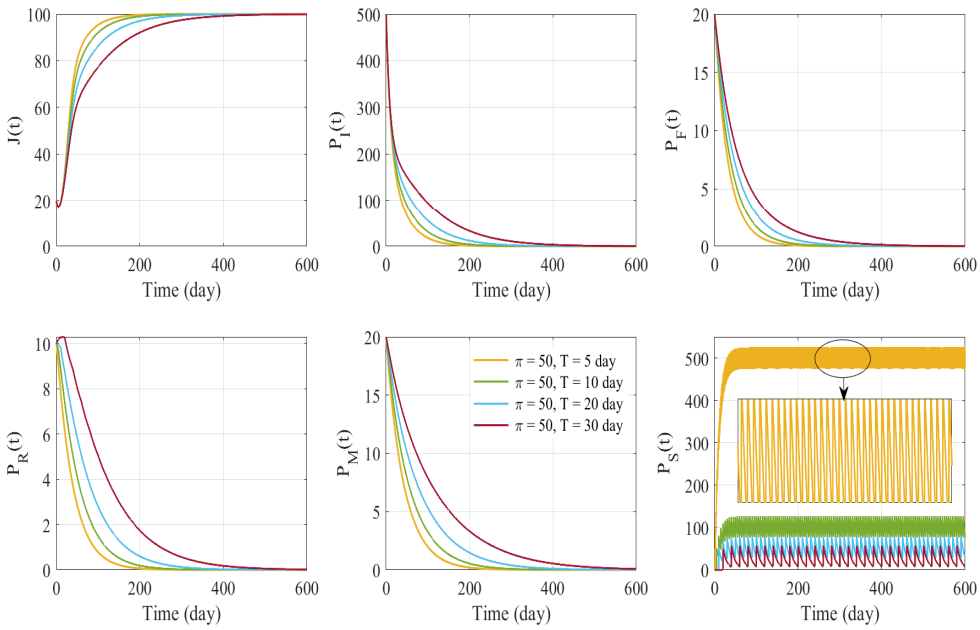

Figure 6.9: *Dynamics of the Jatropha–pest system with high sterile male release rate $\pi = 50$, for four release intervals $T = 5, 10, 20,$ and 30 days. Strong suppression of all pest compartments is observed, with Jatropha biomass reaching its maximum rapidly. The strategy is effective even for less frequent releases, indicating robustness of SIT at high π. The sterile male population $P_S(t)$ shows strong periodicity, particularly for small T, due to large impulsive inputs.*

For a moderate release intensity, $\pi = 20$ units in Figure 6.8, significantly improves pest control. The Jatropha biomass increases rapidly across all values of T,

and pest classes exhibit faster decline compared to $\pi = 10$ units release of sterile males impulsively. When the release interval is $T = 5$ or 10 days, the Jatropha biomass steadily increases and stabilizes by around 250 days. During this period, the immature pests, wild females, and reproductive females are effectively eradicated within approximately 250 days, whereas the wild male pests require over 400 days for complete elimination. Even with less frequent releases, such as $T = 20$ days, the suppression of pests is effective. Oscillations in $P_S(t)$ become less sharp and more stable as the amplitude of each impulsive release compensates for the longer interval.

For $\pi = 50$ units release of sterile male as shown in Figure 6.9, a high release rate ensures robust pest suppression regardless of release interval. The biomass $J(t)$ rises swiftly to its maximum across all T. The pest compartments diminish rapidly within the first 100 to 200 days. Even for $T = 30$ days, sterile males effectively compete for mates, preventing reproduction and reducing pest populations. The oscillations in $P_S(t)$ are pronounced for small T, due to dense and frequent releases, while longer intervals result in more spaced and controlled pulses.

The success of the SIT strategy depends on the balance between the release rate π of sterile male and the release interval T. When π is small, more frequent releases (small T) are needed to suppress pests effectively. As π increases, the model becomes less sensitive to T, indicating that larger pulses can compensate for less frequent intervention. In all cases, an increase in sterile male population leads to reduced mating success of fertile pests, resulting in an increase in Jatropha biomass. The oscillatory dynamics of $P_S(t)$ is a natural consequence of the impulsive release mechanism and do not indicate instability.

6.5 Discussion and Conclusions

In this chapter, we investigate the impact of pest infestation on *Jatropha curcas* plantations and explore its management using sterile insect technique (SIT). The study is structured into three main parts. In the first part, we develop a mathematical model that captures the life cycle of the pest population and its detrimental effects on *Jatropha curcas* biomass. To mitigate these effects, we introduce sterile male pests into the system as a biological control strategy. Two distinct release strategies are considered: continuous release and impulsive (periodic) release of sterile males. The second part of the study presents the mathematical formulation and analysis of the

continuous release model, while the third part focuses on the impulsive release scenario.

Analytically, we have established the positivity, boundedness, and existence of equilibrium points of the model, along with a detailed local stability analysis of each equilibrium. Numerically, we have demonstrated the harmful impact of immature pests on *Jatropha curcas* biomass, highlighting significant leaf depletion in the absence of control as presented in Figure 6.2. Additionally, we have observed the occurrence of a Hopf bifurcation with respect to the fertilization rate parameter γ, indicating a transition to oscillatory dynamics beyond a critical threshold γ_c (see Figure 6.4). This bifurcation signifies the potential for sustained pest outbreaks and ongoing biomass degradation, emphasizing the need for effective pest control strategies.

Analytical as well as the numerical outcomes convey that the application of the sterile insect technique (SIT) with continuous release strategy effectively eliminates oscillatory behavior in the pest–plant interaction system, leading to a stable long-term dynamics. A rigorous global stability analysis has been carried out for the model incorporating continuous release of sterile male pests, confirming the system's convergence toward a pest-suppressed equilibrium. To evaluate the effectiveness of SIT, four different daily release rates ($\pi = 5, 10, 15$ and 20) of sterile males have been simulated. The results clearly demonstrate a significant decline in all pest population compartments, including immature pests, wild males, wild females, and fertilized females. Concurrently, a noticeable recovery and increase in the biomass of *Jatropha curcas* is observed (see Figure 6.6).

The impulsive implementation of the sterile insect technique (SIT), involving periodic releases of sterile male pests at fixed time intervals, also proves to be an efficient control strategy in stabilizing the pest–plant system. Through appropriate mathematical formulation, the system has been analyzed under the theory of impulsive differential equations. Conditions ensuring pest eradication have been evaluated and stability of the system equipped with impulsive strategy is established. Numerical simulations have been performed for various release magnitudes and periods (see Figures 6.7, 6.8, and 6.9), illustrating that even with less frequent but strategically timed releases, the pest population can be significantly reduced. As a result, the biomass of *Jatropha curcas* experiences steady recovery and growth. The periodic SIT strategy offers practical advantages in terms of operational feasibility and resource optimization, while maintaining strong biological control efficacy.

Investigations and experiments with three different mathematical models highlight the critical role of pest dynamics in the degradation of Jatropha biomass and underscore the effectiveness of the sterile insect technique (SIT) as a viable control strategy. Simulations justify that implementation of SIT, whether through continuous or impulsive sterile male releases, successfully suppresses pest subpopulations and restores plant biomass. High-intensity releases solely hold the potential to compensate for wider intervals while on the other hand, the efficiency of impulsive pest control strategy gets improved with higher release rates and more frequent interventions.

Pest populations in Jatropha plantations often have seasonal population surges tied to leaf phenology i.e. the timing of leaf growth and shedding cycles (Shanker and Dhyani, 2006). Periodic releases can target peak reproductive periods, overwhelming wild populations when they are most vulnerable which enables synchronization with pest life cycles (Dyck *et al.*, 2021). Rearing sterile insects is resource-intensive. Periodic releases can be helpful to minimize waste by avoiding releases during low-pest periods (Vreysen *et al.*, 2007). Moreover, continuous releases for a prolonged period may lead to sterile males competing with each other for mates which reduces per-male efficiency (Barclay and Hendrichs, 2014; Lance and McInnis, 2021). Periodic pulses ensure high sterile-to-wild male ratios during critical windows, maximizing mating disruption (Dyck *et al.*, 2021; Knipling, 1955). Thus, although both of the two release strategies discussed in this study are proven to be effective, the periodic release of sterile males (instead of continuous release) in SIT programs for Jatropha plantations is highly recommended for efficiency, cost-effectiveness, ecological alignment and crop phenology. This outcome is also supported previously by Shanker & Dhyani et al. (Shanker and Dhyani, 2006) where the authors outlined the importance of periodic strategy.

In conclusion, implementation of SIT through the proposed mathematical frameworks proves to be a robust, eco-friendly, sustainable method for mitigating pest-induced crop damage and promoting the ecological recovery of Jatropha plantations and should necessarily be considered in future trials and experiments in Jatropha pest management. Aligning with the foliar flush cycle of Jatropha and peak infestation period, such as post-pruning or after the first rains, the impulsive release strategy should be applied as the most suitable control method. Depending on the pest outbreak scenario, the release intensity and release intervals should be adjusted after carefully monitoring and assessing the severity of the situation. Investigations

suggest that in extreme situations, the release intensity should be maximized as $\pi = 50$ and the intervals should be decreased to $T = 5$ or $T = 10$ for achieving the most beneficial outcomes. Although constant outputs indicate high waste in low-pest periods, continuous release strategy can be helpful in varying conditions in highly persistent pest hotspots such as infested wild Jatropha stands and in those particular cases where systematic and consistent monitoring is not a feasible option. Futuristic works, depending on the proposed models, should focus on evaluating the cost-effective analysis, optimization of SIT and exploring the in-depth relation of seasonal dynamics of Jatropha fruiting with pest life cycles.

7 Future Directions - An Outline

- **For Biodiesel Production:** We compared two effective mixing techniques, mechanical stirring and ultrasound, for biodiesel production in Chapter 3, and demonstrated that ultrasound is superior to mechanical stirring in reducing mass transfer resistance during the transesterification reaction. These observations also open the scope for exploring hybrid mixing approaches, where mechanical stirring (MS) and ultrasound (US) are applied together to potentially enhance biodiesel production. While MS primarily enhances bulk circulation and increases interfacial area, US induces cavitation and intense micro-mixing. These mechanisms are complementary and can be represented mathematically by combining their individual mass-transfer rate expressions, $K_c(f)$ for MS and $M_c(H)$ for US. Several functional forms for the effective mass-transfer coefficient $K_{\text{eff}}(f, H)$ may be explored. An additive model,

$$K_{\text{eff}} = K_c(f) + M_c(H),$$

assumes independent contributions, whereas a multiplicative form,

$$K_{\text{eff}} = K_c(f)\big(1 + \alpha M_c(H)\big),$$

introduces a synergy parameter $\alpha \geq 0$. Alternatively, saturating or bounded functions may be used to prevent unrealistically large values at high control inputs. In all cases, K_{eff} would replace the single term M_c in the logistic growth component of the biodiesel production equation, thereby capturing the joint influence of f and H.

The proposed hybrid model allows for direct inclusion of energy consumption into the process optimisation framework. Future research should also address the problem of optimal operating conditions when both f and H are treated as control variables. By introducing the power consumption functions $P_{\mathrm{MS}}(f)$ and $P_{\mathrm{US}}(H)$, an optimal control problem can be formulated to maximize biodiesel yield while penalizing total energy usage. This can be expressed through an objective functional of the form

$$\mathcal{J} = Y_B(T_f) - \lambda \int_0^{T_f} \left[P_{\mathrm{MS}}(f(t)) + P_{\mathrm{US}}(H(t))\right] dt,$$

where λ is a weighting factor and T_f is the final reaction time. Pontryagin's Maximum Principle or forward–backward sweep algorithms can then be applied to determine optimal time-dependent strategies for $f(t)$ and $H(t)$. Such an approach will identify the most energy-efficient operating points for a given yield target.

Finally, the hybrid approach can be generalised to other feedstocks (e.g., rapeseed oil or waste cooking oil) to assess robustness, or adapted to enzymatic transesterification where MS and US may influence enzyme activity and stability. Such studies will provide a physically grounded and experimentally validated framework for optimising biodiesel production under combined mixing strategies.

- **For Pest Management:** The work presented in Chapter 6 can be extended using chemical pesticides along with sterile male release, both impulsively. Sterile males are released at discrete times t_k ($k \in \mathbb{N}$), while chemical pesticides are applied at discrete times τ_m ($m \in \mathbb{N}$). Let $C(t)$ denote the pesticide residue in the environment (e.g., on foliage or within the field), subject to natural decay at rate $\delta_C > 0$. Pesticide imposes additional mortality on pest compartments via stage-specific Holling type-II kill functions:

$$k_X(C) = \alpha_X \frac{C}{K_C + C}, \qquad X \in \{I, F, R, M, S\},$$

where $\alpha_X > 0$ are maximal kill rates and $K_C > 0$ is the half-saturation constant. Optional phytotoxicity is represented by $\theta\, C\, J$ in the plant equation, with $\theta \geq 0$ (set $\theta = 0$ for non-phytotoxic doses).

The corresponding impulsive model can be written as: when $t \neq t_k$ and $t \neq \tau_m$,

$$\begin{cases} \dfrac{dJ}{dt} = r_J J\left(1 - \dfrac{J}{K_J}\right) - \beta_J J P_I - \theta\, C\, J, \\ \dfrac{dP_I}{dt} = r_1 P_R - d_1 P_I - \beta'_J J P_I - k_I(C) P_I, \\ \dfrac{dP_F}{dt} = d\,\beta'_J J P_I - \gamma_1 P_F\left(\dfrac{P_M}{P_M + P_S}\right) - \gamma_2 P_F\left(\dfrac{P_S}{P_M + P_S}\right) + r_2 P_R - d_2 P_F - k_F(C) P_F, \\ \dfrac{dP_R}{dt} = \gamma_1 P_F\left(\dfrac{P_M}{P_M + P_S}\right) - r_2 P_R - d_3 P_R - k_R(C) P_R, \\ \dfrac{dP_M}{dt} = (1-d)\,\beta'_J J P_I - d_4 P_M - k_M(C) P_M, \\ \dfrac{dP_S}{dt} = -d_5 P_S - k_S(C) P_S, \\ \dfrac{dC}{dt} = -\delta_C\, C. \end{cases} \tag{7.1}$$

Impulsive release of sterile males and pesticide application:
At sterile-male release times $t = t_k$,

$$P_S(t_k^+) = P_S(t_k^-) + \pi, \qquad \pi > 0,$$

where π is the number of sterile males introduced per release.

At pesticide application times $t = \tau_m$,

$$C(\tau_m^+) = C(\tau_m^-) + c_p, \qquad c_p > 0,$$

where c_p represents the immediate increase in environmental pesticide residue due to application. All other parameters used in the above model are described in Chapter 6.

Objectives: The impulsive SIT–pesticide model aims to assess the relative performance of biological and chemical controls, optimize release and application schedules, explore timing synergies, maintain pesticide residues within safe limits, and evaluate robustness and sensitivity of the model parameters.

List of Publications

1. Xianbing Cao, **Sk Mosaraf Ahammed**, Siddhartha Datta, Jahangir Chowdhury, and Priti Kumar Roy. Enhancement of biodiesel production via ultrasound technology: a mathematical study,
   ACS omega 9, no. 18 (2024): 20502-20511.

2. **Sk Mosaraf Ahammed**, Priti Kumar Roy, and Shu Wang. Effect of Ultrasound Technique for Production of Biodiesel Using Enzyme as Catalyst: A Mathematical Study,
   International Conference on Mathematical Analysis and Application in Modeling, pp. 251-261. Singapore: Springer Nature Singapore, 2023.

3. **Sk Mosaraf Ahammed**, Oluwole Daniel Makinde, Tushar Ghosh & Priti Kumar Roy. Exploring Fractional-Order Nonlinear Dynamics in Biodiesel Production with Optimal Control,
   CSIAM Transactions on Applied Mathematics, (2025)

4. Lakshmi Narayan Guin, **Sk Mosaraf Ahammed**, Muniyagounder Sambath. Effect of prey refuge in a tri-trophic food chain model with Monod-Haldane type response function.
   International Journal of Ecological Economics & Statistics, 41, no. 4 (2020): 30-44.

List of Communicated Works

1. **Sk Mosaraf Ahammed**, Amit Kumar Roy, Xue-Zhi Li, Oluwole Daniel Makinde, Lu-Bin Cui, Xin-Guang Yang, Fahad Al Basir, Priti Kumar Roy. Optimization of Biodiesel Synthesis using US (Ultrasound) and MS (Mechanical Stirring) Methods: A Comparative Study.

2. **Sk Mosaraf Ahammed**, Salil Ghosh, Priti Kumar Roy. Mathematical Modeling of Pest Control on *Jatropha curcas* using Sterile Insect Technique.

3. Sanju Sardar, Priti Kumar Roy, **Sk Mosaraf Ahammed**, Tushar Ghosh, David Greenhalgh. Treatment of Methanol toxicity through Ethanol and Folinic Acid: a mathematical study

Bibliography

Achten, W. M. *et al.* (2008). Jatropha bio-diesel production and use. *Biomass and Bioenergy* **32**(12): 1063–1084.

Adepoju, T. and Okunola, A. A. (2015). Modeling and optimization of transesterification of beniseed oil to beniseed methylester: A case of artificial neural network versus response surface methodology. *International Journal of Chemical and Process Engineering Research* **2**(3): 30–43.

Al Basir, F. and Roy, P. K. (2014). Production of biodiesel using enzymatic transesterification of Jatropha curcas oil: a mathematical study. *Mathematics in Engineering, Science and Aerospace* **5**(2): 175–184.

— (2017). Optimization of Biodiesel Production through Enzymatic Transesterification of Jatropha curcas Oil. *Int. J. Syst. Appl. Eng. & Dev* **11**.

Al Basir, F. *et al.* (2015). Studies on biodiesel production from Jatropha curcas oil using chemical and biochemical methods–A mathematical approach. *Fuel* **158**: 503–511.

Al Basir, F. *et al.* (2017). A fractional order mathematical model for enzymatic biodiesel synthesis and its optimization. *Int. J. Math. Models Methods Appl. Sci.* **11**: 170–177.

Al-Basir, F. *et al.* (2017). Impact of roguing and insecticide spraying on mosaic disease in Jatropha curcas. *Control and Cybernetics* **46**(4).

Al Basir, F. *et al.* (2018). Modelling the effects of awareness-based interventions to control the mosaic disease of Jatropha curcas. *Ecological complexity* **36**: 92–100.

Al Basir, F. *et al.* (2023). Dynamics of a double-impulsive control model of integrated pest management using perturbation methods and floquet theory. *Axioms* **12**(4): 391.

Al-Zuhair, S. *et al.* (2007). Proposed kinetic mechanism of the production of biodiesel from palm oil using lipase. *Process Biochemistry* **42**(6): 951–960.

Anitha, K and Varaprasad, K. (2012). Jatropha pests and diseases: an overview. *Jatropha, Challenges for a New Energy Crop: Volume 1: Farming, Economics and Biofuel*: 175–218.

Atadashi, I. *et al.* (2013). The effects of catalysts in biodiesel production: A review. *Journal of industrial and engineering chemistry* **19**(1): 14–26.

Atangana, A. and Baleanu, D. (2016). New fractional derivatives with nonlocal and non-singular kernel: theory and application to heat transfer model. *arXiv Preprint arXiv:1602.03408*.

Badday, A. S. *et al.* (2014). Artificial neural network approach for modeling of ultrasound-assisted transesterification process of crude Jatropha oil catalyzed by heteropoly-acid based catalyst. *Chemical Engineering and Processing: Process Intensification* **75**: 31–37.

Barclay, H. J. (1987). Models for pest control: complementary effects of periodic releases of sterile pests and parasitoids. *Theoretical Population Biology* **32**(1): 76–89.

Barclay, H. J. and Hendrichs, J. (2014). Models for assessing the male annihilation of Bactrocera spp. with methyl eugenol baits. *Annals of the Entomological Society of America* **107**(1): 81–96.

Benavides, P. T. and Diwekar, U. (2012). Optimal control of biodiesel production in a batch reactor: Part I: Deterministic control. *Fuel* **94**: 211–217.

Berlan, J *et al.* (1994). Oxidative degradation of phenol in aqueous media using ultrasound. *Ultrasonics Sonochemistry* **1**(2): S97–S102.

Bertsekas, D. (2012). *Dynamic programming and optimal control: Volume I*. Vol. 4. Athena scientific.

Bhattacharyya, S and Bhattacharya, D. (2006). Pest control through viral disease: mathematical modeling and analysis. *Journal of Theoretical Biology* **238**(1): 177–197.

Bourtzis, K. and Vreysen, M. J. (2021). *Sterile insect technique (SIT) and its applications*.

Cao, X. *et al.* (2024). Enhancement of Biodiesel Production via Ultrasound Technology: A Mathematical Study. *ACS Omega* **9**(18): 20502–20511.

Caputo, M. (1969). *Elasticita e dissipazione*. Zanichelli.

Caputo, M. and Fabrizio, M. (2015). A new definition of fractional derivative without singular kernel. *Progress in Fractional Differentiation & Applications* **1**(2): 73–85.

Chowdhury, J. *et al.* (2016). Pest control for Jatropha curcas plant through viral disease: a mathematical approach. *Nonlinear Stud* **23**(4): 517–532.

Chowdhury, J. *et al.* (2017). Effect of mass transfer and reaction kinetics in transesterification of Jatropha curcas oil. *International Journal of Mathematical Models and Methods in Applied Sciences* **11**: 130–138.

Chowdhury, J. *et al.* (2019). A mathematical model for pest management in Jatropha curcas with integrated pesticides-An optimal control approach. *Ecological Complexity* **37**: 24–31.

Chowdhury, J. *et al.* (2020). Comparative study on biodiesel production from Jatropha Curcas oil by supercritical and chemical catalytic method: a mathematical approach. *Energy Sources, Part A: Recovery, Utilization, and Environmental Effects* **42**(12): 1449–1463.

Colucci, J. A. *et al.* (2005). Biodiesel from an alkaline transesterification reaction of soybean oil using ultrasonic mixing. *Journal of the American Oil Chemists' Society* **82**(7): 525–530.

Contran, N. *et al.* (2013). State-of-the-art of the Jatropha curcas productive chain: from sowing to biodiesel and by-products. *Industrial crops and products* **42**: 202–215.

Cum, G. *et al.* (1988). Effect of static pressure on the ultrasonic activation of chemical reactions. Selective oxidation at benzylic carbon in the liquid phase. *Journal of the Chemical Society, Perkin Transactions 2* (3): 375–383.

Dame, D. A. (1984). Control of insects of veterinary importance by genetic techniques. *Preventive Veterinary Medicine* **2**(1-4): 515–522.

Dembilio, Ó. and Jaques, J. A. (2015). "Biology and management of red palm weevil". *Sustainable pest management in date palm: current status and emerging challenges*. Springer, 13–36.

Dharma, S. *et al.* (2017). Optimization of biodiesel production from mixed jatropha curcas-ceiba pentandra using artificial neural network-genetic algorithm: Evaluation of reaction kinetic models. *Chem. Eng. Trans*.

Dittus, F. and Boelter, L. (1985). Heat transfer in automobile radiators of the tubular type. *International communications in heat and mass transfer* **12**(1): 3–22.

Diwekar, U and Benavides, P (2012). Optimal control of biodiesel production in a batch reactor Part I: Deterministic control. *Fuel* **94**: 211–217.

Dutta, P. *et al.* (2024). Nipah virus transmission dynamics: equilibrium states, sensitivity and uncertainty analysis. *Nonlinear Dynamics*: 1–41.

Dyck, V. A. *et al.* (2021). *Sterile insect technique: principles and practice in area-wide integrated pest management*. Taylor & Francis.

Edessa, G. K. (2022). Existence and uniqueness solution of the model of enzyme kinetics in the sense of caputo–fabrizio fractional derivative. *International Journal of Differential Equations* **2022**(1): 1345919.

Freedman, B. *et al.* (1986). Transesterification kinetics of soybean oil 1. *Journal of the American Oil Chemists' Society* **63**(10): 1375–1380.

Gato, R. *et al.* (2021). Sterile insect technique: successful suppression of an Aedes aegypti field population in Cuba. *Insects* **12**(5): 469.

Georgogianni, K. *et al.* (2007). Biodiesel production: reaction and process parameters of alkali-catalyzed transesterification of waste frying oils. *Energy & Fuels* **21**(5): 3023–3027.

Georgogianni, K. *et al.* (2008). Conventional and in situ transesterification of sunflower seed oil for the production of biodiesel. *Fuel processing technology* **89**(5): 503–509.

Georgogianni, K. *et al.* (2009). Transesterification of soybean frying oil to biodiesel using heterogeneous catalysts. *Fuel Processing Technology* **90**(5): 671–676.

Ghosh, S and Bhattacharya, D. (2010). Optimization in microbial pest control: an integrated approach. *Applied Mathematical Modelling* **34**(5): 1382–1395.

Grass, D. *et al.* (2008). Optimal control of nonlinear processes. *Berlino: Springer*.

Jie, M. S. L. K. and Lam, C. (1995). Ultrasound-assisted epoxidation reaction of long-chain unsaturated fatty esters. *Ultrasonics Sonochemistry* **2**(1): S11–S14.

Juan, J. C. *et al.* (2011). Biodiesel production from jatropha oil by catalytic and non-catalytic approaches: an overview. *Bioresource technology* **102**(2): 452–460.

Khan, A. *et al.* (2017). Atangana–Baleanu and Caputo Fabrizio analysis of fractional derivatives for heat and mass transfer of second grade fluids over a vertical plate: a comparative study. *Entropy* **19**(8): 279.

Klausmeier, C. A. (2008). Floquet theory: a useful tool for understanding nonequilibrium dynamics. *Theoretical Ecology* **1**: 153–161.

Knipling, E. F. (1955). Possibilities of insect control or eradication through the use of sexually sterile males. *Journal of Economic Entomology* **48**(4): 459–462.

Knipling, E. F. (1979). *The basic principles of insect population suppression and management*. 512. US Department of Agriculture.

Komers, K. *et al.* (2001). Biodiesel from rapeseed oil, methanol and KOH. 3. Analysis of composition of actual reaction mixture. *European Journal of Lipid Science and Technology* **103**(6): 363–371.

Kotze, A. and James, P. (2022). Control of sheep flystrike: what's been tried in the past and where to from here. *Australian veterinary journal* **100**(1-2): 1–19.

Kusumo, F *et al.* (2017). Optimization of transesterification process for Ceiba pentandra oil: A comparative study between kernel-based extreme learning machine and artificial neural networks. *Energy* **134**: 24–34.

Lance, D. and McInnis, D. (2021). Biological basis of the sterile insect technique. *Sterile insect technique*: 113–142.

Lanouette, G. *et al.* (2017). The sterile insect technique for the management of the spotted wing drosophila, Drosophila suzukii: establishing the optimum irradiation dose. *Plos one* **12**(9): e0180821.

Lebl, J. (2018). *Introduction to Real Analysis, Volume I*.

Leung, D. Y. *et al.* (2010). A review on biodiesel production using catalyzed transesterification. *Applied Energy* **87**(4): 1083–1095.

Lifka, J and Ondruschka, B (2004). Influence of the transport of substances on the production of biodiesel. *Chemie Ingenieur Technik* **76**: 168–171.

Likozar, B and Levec, J (2014). Effect of process conditions on equilibrium, reaction kinetics and mass transfer for triglyceride transesterification to biodiesel: experimental and modeling based on fatty acid composition. *Fuel Processing Technology* **122**: 30–41.

Liu, Q.-X. *et al.* (2021). The Effect of gut bacteria on the physiology of red palm weevil, Rhynchophorus ferrugineus Olivier and their potential for the control of this pest. *Insects* **12**(7): 594.

Liu, S. *et al.* (2014). Kinetic study on lipase-catalyzed biodiesel production from waste cooking oil. *Journal of Molecular Catalysis B: Enzymatic* **99**: 43–50.

Luche, J.-L. (1994). Effect of ultrasound on heterogeneous systems. *Ultrasonics Sonochemistry* **1**(2): S111–S118.

Ma, F. and Hanna, M. A. (1999). Biodiesel production: a review. *Bioresource technology* **70**(1): 1–15.

Maran, J. P. and Priya, B (2015). Modeling of ultrasound assisted intensification of biodiesel production from neem (Azadirachta indica) oil using response surface methodology and artificial neural network. *Fuel* **143**: 262–267.

Marino, S. *et al.* (2008). A methodology for performing global uncertainty and sensitivity analysis in systems biology. *Journal of theoretical biology* **254**(1): 178–196.

Moradi, G. *et al.* (2013). The optimized operational conditions for biodiesel production from soybean oil and application of artificial neural networks for estimation of the biodiesel yield. *Renewable energy* **50**: 915–920.

Musa, I. A. (2016). The effects of alcohol to oil molar ratios and the type of alcohol on biodiesel production using transesterification process. *Egyptian journal of petroleum* **25**(1): 21–31.

Ogunkunle, O. and Ahmed, N. A. (2021). Overview of biodiesel combustion in mitigating the adverse impacts of engine emissions on the sustainable human–environment scenario. *Sustainability* **13**(10): 5465.

Patinvoh, R. J. and Susu, A. A. (2014). Mathematical modelling of sterile insect technology for mosquito control. *Advances in Entomology* **2**(4): 180–193.

Patnaik, S. *et al.* (2020). Applications of variable-order fractional operators: a review. *Proceedings of the Royal Society A* **476**(2234): 20190498.

Pontryagin, L. S. (1987). *Mathematical theory of optimal processes*. CRC Press.

Pontryagin, L. S. (2018). *Mathematical theory of optimal processes*. Routledge.

Posom, J. and Sirisomboon, P. (2014). Evaluation of the thermal properties of Jatropha curcas L. kernels using near-infrared spectroscopy. *Biosystems Engineering* **125**: 45–53.

Pramanik, K. (2003). Properties and use of Jatropha curcas oil and diesel fuel blends in compression ignition engine. *Renewable energy* **28**(2): 239–248.

Rajković, K. M. *et al.* (2013). Optimization of ultrasound-assisted base-catalyzed methanolysis of sunflower oil using response surface and artifical neural network methodologies. *Chemical Engineering Journal* **215**: 82–89.

Ranga Rao, G. *et al.* (2010). Insect pests of Jatropha curcas., L and their management. Information Bulletin.

Ross, I. M. (2015). *A primer on Pontryagin's principle in optimal control*. Collegiate Publishers.

Roy, P. K. *et al.* (2014). Effect of mass transfer kinetics for maximum production of biodiesel from Jatropha Curcas oil: A mathematical approach. *Fuel* **134**: 39–44.

Roy, P. K. *et al.* (2015). Effect of insecticide spraying on Jatropha curcas plant to control mosaic virus: a mathematical study. *Commun. Math. Biol. Neurosci.* **2015**: Article–ID.

Sabi-Sabi, M. O., Nacro, S., *et al.* (2016). Some Biology Features of Pempelia spp.(Lepidoptera: Pyralidae): An Insect Pest of Jatropha curcas. *Advances in Entomology* **4**(04): 240.

Sajjadi, B. *et al.* (2017). Hybrid nero-fuzzy methods for estimation of ultrasound and mechanically stirring Influences on biodiesel synthesis through transesterification. *Measurement* **103**: 62–76.

Šánek, L. *et al.* (2019). "Mathematical modeling of transesterification process kinetics of triglycerides catalyzed by TMAH". *MATEC Web of Conferences*. Vol. 292. EDP Sciences, 01027.

Santos, F. F. *et al.* (2010). Production of biodiesel by ultrasound assisted esterification of Oreochromis niloticus oil. *Fuel* **89**(2): 275–279.

Sassù, F. *et al.* (2019). Mass-rearing of Drosophila suzukii for sterile insect technique application: evaluation of two oviposition systems. *Insects* **10**(12): 448.

Sengupta, A. *et al.* (2019). Effect of temperature and molar ratio on biodiesel production in supercritical-carbon dioxide medium. *Nonlinear Studies* **26**(2): 327–341.

Shanker, C. and Dhyani, S. (2006). Insect pests of Jatropha curcas L. and the potential for their management. *Current Science* **91**(2): 162–163.

Shenbaga Vinayaga Moorthi, N *et al.* (2015). Application of design of experiments and artificial neural network in optimization of ultrasonic energy-assisted transesterification of Sardinella longiceps fish oil to biodiesel. *Journal of the Chinese Institute of Engineers* **38**(6): 731–741.

Singh, J. *et al.* (2017). On the analysis of chemical kinetics system pertaining to a fractional derivative with Mittag-Leffler type kernel. *Chaos: An Interdisciplinary Journal of Nonlinear Science* **27**(10).

Smith, R. F. (1962). Integration of biological and chemical control: introduction and principles. *Bulletin of the ESA* **8**(4): 188–189.

Stavarache, C. *et al.* (2003). Conversion of vegetable oil to biodiesel using ultrasonic irradiation. *Chemistry Letters* **32**(8): 716–717.

Su, F. and Guo, Y. (2014). Advancements in solid acid catalysts for biodiesel production. *Green Chemistry* **16**(6): 2934–2957.

Subramanian, R. S. (2014). *Convective Mass Transfer*.

Takase, M. (2022). Biodiesel yield and conversion percentage from waste frying oil using fish shell at elmina as a heterogeneous catalyst and the kinetics of the reaction. *International Journal of Chemical Engineering* **2022**(1): 8718638.

Tan, S. X. *et al.* (2019). Two-step catalytic reactive extraction and transesterification process via ultrasonic irradiation for biodiesel production from solid Jatropha oil seeds. *Chemical Engineering and Processing-Process Intensification* **146**: 107687.

Terren, M. *et al.* (2012). Principal disease and insect pests of Jatropha curcas L. in the lower valley of the Senegal river. *Tropicultura* **30**(4).

Uchaikin, V. V. (2013). *Fractional derivatives for physicists and engineers*. Vol. 2. Springer.

Venturino, E. *et al.* (2016). A model for the control of the mosaic virus disease in Jatropha curcas plantations. *Energy, Ecology and Environment* **1**(6): 360–369.

Vreysen, M. J. *et al.* (2007). *Area-wide control of insect pests: from research to field implementation*. Springer.

Xu, Y. *et al.* (2005). Study on the kinetics of enzymatic interesterification of triglycerides for biodiesel production with methyl acetate as the acyl acceptor. *Journal of Molecular Catalysis B: Enzymatic* **32**(5-6): 241–245.

Yan, Y. *et al.* (2020). Using moderate transgene expression to improve the genetic sexing system of the Australian sheep blow fly Lucilia cuprina. *Insects* **11**(11): 797.

Yin, X. *et al.* (2012). Comparison of four different enhancing methods for preparing biodiesel through transesterification of sunflower oil. *Applied Energy* **91**(1): 320–325.

Zhang, Y. *et al.* (2009). Rapid transesterification of soybean oil with phase transfer catalysts. *Applied Catalysis A: General* **366**(1): 176–183.

Zhou, Y. (2023). *Basic theory of fractional differential equations*. World scientific.

Zongo, A. S. *et al.* (2018). Temperature dependence of density, viscosity, thermal conductivity and heat capacity of vegetable oils for their use as biofuel in internal combustion engines. *Advances in Chemical Engineering and Science* **9**(1): 44–64.